



IFS DOCUMENTATION CY28R1 (Operational implementation 9 March 2004)

PART II: DATA ASSIMILATION

Table of contents

Chapter 1 ‘Overview’

Chapter 2 ‘4D Variational Assimilation’

Chapter 3 ‘3D variational assimilation (with the first-guess at appropriate time)’

Chapter 4 ‘Background term’

Chapter 5 ‘Observation operators and the observation cost function (J_o)’

Chapter 6 ‘Background, analysis and forecast errors’

Chapter 7 ‘Gravity-wave control’

Chapter 8 ‘Diagnostics.’

Chapter 9 ‘Observation processing’

Chapter 10 ‘Observation screening’

Chapter 11 ‘Analysis of snow’

Chapter 12 ‘Land-surface analysis’

Chapter 13 ‘Analysis of sea-ice concentration and sea surface temperature’

Chapter 14 ‘Data Flow’



Part II: DATA ASSIMILATION

CHAPTER 1 Overview

Table of contents

- 1.1 Introduction
- 1.2 Scientific publications
- 1.3 Brief history of 3D and 4D-Var in ECMWF operations
- 1.4 Incremental Formulation of variational data assimilation

1.1 INTRODUCTION

This documentation of 4D-Var and 3D-FGAT serves as a scientific guide to the data assimilation codes within ECMWF's Integrated Forecasting System (IFS). The documentation is divided into a number of chapters. This, the first chapter provides an overview of ECMWF's data assimilation system, a brief history of its evolution and a description of the basic scientific formulation.

The second chapter describes the practical implementation of the multi-resolution incremental method for 4D-Var data assimilation (used operationally since January 2003, CY25r3), and the solution algorithm including minimization and preconditioning. The 3D-FGAT configuration as used in the production of ERA-40 (*Uppala et al. 2005*) and operationally in the so-called Boundary-Condition suite is described in [Chapter 3](#). Thereafter follows a description of the background term ([Chapter 4](#)) and a chapter on observation operators and the organisation of observation cost-function calculations for conventional and satellite data ([Chapter 5](#)). [Chapter 6](#) deals with the computation and cycling of background and analysis errors and [Chapter 7](#) is on initialization and control of gravity waves. Diagnostic tools for investigation of the performance of the assimilation system are described in [Chapter 8](#). The modules for observation selection, quality control and screening are described in [Chapter 9](#) and [Chapter 10](#). [Chapter 11](#) outlines the snow analysis, [Chapter 12](#) describes the Soil analysis, [Chapter 13](#) describes the sea surface temperature and sea-ice analysis. The final chapter [Chapter 14](#) provides summary information about the main unix-scripts and important files, and a schematic of the data flow between the various jobs steps that constitute a data assimilation cycle.

1.2 SCIENTIFIC PUBLICATIONS

The scientific description of 3D/4D-Var has been published in a series of papers in QJRMS, in ECMWF workshop proceedings and Technical Memoranda over the years. The incremental formulation was introduced by *Courtier et al. (1994)*. The ECMWF implementation of 3D-Var was published in a three-part paper by *Courtier et al. (1998)*, *Rabier et al. (1998)* and *Andersson et al. (1998)*. The original observation operators for conventional data can be found in *Vasiljevic et al. (1992)*. The methods for assimilation of TOVS radiance data and ERS scatterometer data were developed by *Andersson et al. (1994)* and *Stoffelen and Anderson (1997)*, respectively. The pre-operational experimentation with 4D-Var has been documented in three papers by *Rabier et al. (2000)*, *Mahfouf and Rabier (2000)* and *Klinker et al. (2000)*. The background term has been published by *Derber and Bouttier (1999)*, with more recent developments described by *Fisher (2003)*.

Papers of data usage and impact include a study of commercial aircraft data (*Cardinali et al. 2003*), scatterometer impact (*Isaksen 1997; Isaksen and Stoffelen, 2000; Isaksen and Janssen, 2004*), conventional and satellite humidity data (*Andersson et al. 2004*), ozone analysis (*Dethof and Holm 2004*), time series of frequent data (*Andersson et al. 2001*), wind profiler data (*Bouttier 2001b; Andersson and Garcia-Mendez 2002*), TOVS radiance data (*McNally et al. 1999*), water-vapour radiances from geostationary satellites (*Munro et al. 2004; Kopken et al. 2004*), and the use of high-volume satellite data in general (*Thepaut and Andersson, 2003*).

1.3 BRIEF HISTORY OF 3D AND 4D-VAR IN ECMWF OPERATIONS

3D-Var was implemented in ECMWF operations on 30 January 1996, and was replaced on 25 November 1997 by 4D-Var. The two three-part series of QJRMS papers mentioned above basically describe the two schemes as they were at the time of their implementation. However, there have been very significant developments of the variational data assimilation system during its time in operations. Major code-upgrades have taken place in connection with migrations to new computers. 3D-Var was first implemented on a CRAY C90 shared-memory parallel computer system and was migrated to a distributed-memory Fujitsu VPP700 machine in September 1996. Further migrations of the codes took place in May 2000 to a Fujitsu VPP5000, and in March 2003 to an IBM P690, and later in 2004 to an IBM P690+. A history of the evolution of ECMWF super-computing is available at www.ecmwf.int. The current IBM implementation of the assimilation system utilizes both shared-memory (OpenMP) and distributed-memory (MPI) parallelism. A general list of changes to the operational forecasting system is available at http://www.ecmwf.int/products/data/technical/model_id/index.html.

The observation handling and data screening modules have also developed rapidly to keep pace with the changing computer environment, and the arrival of new observational data sets. The codes inherited from OI were replaced with new codes at the time of the migration to Fujitsu in 1996. The need for improved parallelism and rapidly increasing data volumes lead to the development of the Observation DataBase (ODB) software (see ODB documentation), facilitating in March 2003 the move to the IBM computers and the introduction of high-spectral resolution satellite data (e.g. AIRS). The quality control, data selection and screening algorithms are described in the paper by *Järvinen and Undén (1997)*, and variational quality control of observations in *Andersson and Järvinen (1999)*.

One of the most important aspects of a variational assimilation is the specification of background errors. The original formulation of *Courtier et al. (1998)* was replaced in May 1997 by that of *Derber and Bouttier (1999)*. The latter formulation is still used as described here in Chapter 4, including more recent improvements (e.g. non-linear balance January 2003, CY25r3) introduced by *Fisher (2003)*, introduction of ozone as an analysis variable (*Dethof and Holm, 2004*) in October 1999 (CY21r4), and the new humidity analysis (*Holm et al. 2002*) in October 2003 (CY26r3). The cycling algorithms for analysis and background errors (*Fisher and Courtier 1995*, and Chapter 6) were introduced in 1996. The calibration of background error statistics is since October 1999 based on an ensemble of 3D-Var data assimilations, updated in January 2003 to statistics based on a 4D-Var ensemble (*Fisher 2003*).

On the 25th November 1997 6-hourly 4D-Var was introduced operationally, at resolution T213L31, with two iterations of the outer loop: the first at T63L31 with 50 iterations (simplified physics) and the second with 20 iterations (with tangent-linear physics, at same resolution). In April 1998 the resolution was changed to T_L319 and in June 1998 we revised the radiosonde/pilot usage (significant levels, temperature instead of geopotential) and we started using time-sequences of data (*Järvinen et al. 1999*), so-called 4D-screening. The data assimilation scheme was extended higher into the atmosphere on 10 March 1999, when the T_L319L50 model was introduced, which in turn enabled the introduction in May 1999 of ATOVS radiance data (*McNally et al. 1999*). In October 1999 the vertical resolution of the boundary layer was enhanced taking the number of model levels to a total of L60. In summer 2000 the 4D-Var period was extended from 6 to 12 hours (*Bouttier 2001a*), whereas the ERA-40 configuration (*Uppala et al. 2005*) was built as an FGAT (first guess at the appropriate time) of 3D-Var with a period of 6 hours (Chapter

3). In November 2000 the horizontal resolution of 4D-Var was increased to T_L511L60, with inner loop resolution enhanced from T63L60 to T_L159L60 using the linearized semi-Lagrangian scheme.

In January 2003 the 4D-Var solution algorithm was comprehensively revised (in cy25r4, *Andersson et al. 2003*) to take advantage of the efficiency of conjugate gradient minimisation (with pre-conditioning, as introduced one year earlier) and a multi-resolution incremental technique. This is the 4D-Var solution algorithm that is presented here in [Chapter 2](#).

1.4 INCREMENTAL FORMULATION OF VARIATIONAL DATA ASSIMILATION

In 3D/4D-Var an objective function J is minimized. The cost function consists of three terms:

$$J = J_b + J_o + J_c \quad (1.1)$$

measuring, respectively, the discrepancy with the background (a short-range forecast started from the previous analysis), J_b , with the observations, J_o and with the slow character of the atmosphere, J_c . The J_c -term controls the amplitude of fast waves in the analysis and is described in [Chapter 7](#). It is omitted from the subsequent derivations in this section.

In its incremental formulation (*Courtier et al. 1994*), we write

$$J(\delta\mathbf{x}) = \frac{1}{2}\delta\mathbf{x}^T\mathbf{B}^{-1}\delta\mathbf{x} + \frac{1}{2}(\mathbf{H}\delta\mathbf{x} - \mathbf{d})^T\mathbf{R}^{-1}(\mathbf{H}\delta\mathbf{x} - \mathbf{d}) \quad (1.2)$$

$\delta\mathbf{x}$ is the increment and at the minimum the resulting analysis increment $\delta\mathbf{x}^a$ is added to the background \mathbf{x}^b in order to provide the analysis \mathbf{x}^a :

$$\mathbf{x}^a = \mathbf{x}^b + \delta\mathbf{x}^a \quad (1.3)$$

\mathbf{B} is the covariance matrix of background error while \mathbf{d} is the innovation vector,

$$\mathbf{d} = \mathbf{y}^o - \mathbf{H}\mathbf{x}^b \quad (1.4)$$

where \mathbf{y}^o is the observation vector. \mathbf{H} is a suitable low-resolution linear approximation of the observation operator H in the vicinity of \mathbf{x}^b , and \mathbf{R} is the covariance matrix of observation errors. The incremental formulation of 3D/4D-Var consists therefore of solving for $\delta\mathbf{x}$ the inverse problem defined by the (direct) observation operator \mathbf{H} , given the innovation vector \mathbf{d} and the background constraint. The gradient of J is obtained by differentiating [Eq. \(1.2\)](#) with respect to $\delta\mathbf{x}$,

$$\nabla J = (\mathbf{B}^{-1} + \mathbf{H}^T\mathbf{R}^{-1}\mathbf{H})\delta\mathbf{x} - \mathbf{H}^T\mathbf{R}^{-1}\mathbf{d} \quad (1.5)$$

At the minimum, the gradient of the objective function vanishes, thus from [Eq. \(1.5\)](#) we obtain the classical result that minimizing the objective function defined by [Eq. \(1.2\)](#) is a way of computing the following equivalent matrix-vector products:

$$\delta\mathbf{x}^a = (\mathbf{B}^{-1} + \mathbf{H}^T\mathbf{R}^{-1}\mathbf{H})^{-1}\mathbf{H}^T\mathbf{R}^{-1}\mathbf{d} = \mathbf{B}\mathbf{H}^T(\mathbf{H}\mathbf{B}\mathbf{H}^T + \mathbf{R})^{-1}\mathbf{d} \quad (1.6)$$

where \mathbf{B} and \mathbf{R} are positive definite, see e.g. *Lorenz (1986)* for this standard result. $\mathbf{H}\mathbf{B}\mathbf{H}^T$ may be interpreted as the square matrix of the covariances of background errors in observation space while $\mathbf{B}\mathbf{H}^T$ is the rectangular



matrix of the covariances between the background errors in model space and the background errors in observation space. 3D-Var uses the observation operator \mathbf{H} explicitly and statistical models (\mathbf{B} and \mathbf{R}) are required only for describing the statistics of the background errors in model space and the observation error in observation space. Consequently, in 3D/4D-Var it is easy, from an algorithmic point of view, to make use of observations such as TOVS radiances (*Andersson et al. 1994*), which have a quite complex dependence on the basic analysis variables. The background term and background error covariance modelling (i.e. \mathbf{B}) are described in [Chapter 4](#) and observation operators \mathbf{H} are described in [Chapter 5](#).



Part II: DATA ASSIMILATION**CHAPTER 2 4D Variational Assimilation****Table of contents**

- 2.1 Introduction
- 2.2 Solution algorithm
 - 2.2.1 The incremental method
 - 2.2.2 The job-steps
 - 2.2.3 Interpolation of trajectory and increments
 - 2.2.4 Pre-conditioning and control variable
 - 2.2.5 Minimization
- 2.3 Top-level controls
 - 2.3.1 Last simulation
- 2.4 A simulation
 - 2.4.1 The cost function and its gradient
 - 2.4.2 Interface between control variable and model arrays
- 2.5 The assimilation window
- 2.6 Tangent linear physics
 - 2.6.1 Set-up
 - 2.6.2 Mixed-phase thermodynamics
 - 2.6.3 Vertical diffusion
 - 2.6.4 Subgrid scale orographic effects
 - 2.6.5 Radiation
 - 2.6.6 Cloud scheme
 - 2.6.7 Large-scale condensation
 - 2.6.8 Deep moist convection
 - 2.6.9 Trajectory management

2.1 INTRODUCTION

This part of the documentation covers the top level controls of 4D-Var. It gives a detailed description of the solution algorithm, and the various steps that are performed during a 4D-Var simulation (**SIM4D**). The procedure consists of nested iterations, called inner and outer loops, which communicate through files that either contain meteorological fields, observations, or parameters. The data flow and is documented in [Chapter 14](#). All of this chapter also

applies to 3D-Var with some exceptions which will be detailed in Chapter 3. The interpolation of model fields to observation points (OBSSHOR) and the organization of the data in memory (yomsp, yommvo) is described in Chapter 5. The structure of the computation of the observation cost function and its gradient, managed by the routines OBSV and TASKOB can also be found in Chapter 5. The background term and the 'change-of-variable' operators are explained in Chapter 4.

2.2 SOLUTION ALGORITHM

2.2.1 The incremental method

The adopted solution algorithm is incremental (Courtier et al. 1994), which allows for considerable flexibility with respect to the computer expense of the various job-steps of the 4D-Var minimisation. In the incremental approach the highest possible resolution is used for the computation of the model trajectory, and for calculating the departures between observations and model, whereas a lower-resolution model (its adjoint and tangent linear) are used for the iterative and relatively costly computation of analysis increments (Tremolet 2004). The lower-resolution iterations (the inner-loops) can optionally be nested within a set of outer-loop iterations at full resolution. Apart from the resolution, the cost of the inner-loops will depend also upon the complexity of the inner-loop model, e.g. the use of simpler or more complete representations of the physical processes (Janiskova et al. 2002).

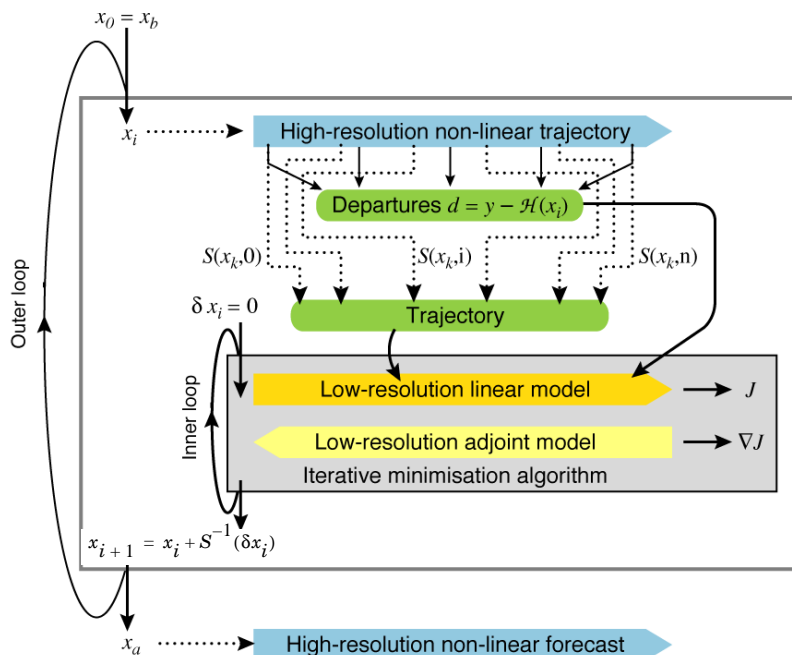


Figure 2.1 Schematic of the revised 4D-Var solution algorithm implemented in January 2003 (cy25r4). Outer loops are performed at high resolution (T511) using the full non-linear model. Inner iterations are performed at lower resolution (first T95, then T159) using the tangent-linear forecast model, linearised around a 12-hour succession of model states ('the trajectory') obtained through interpolation from high resolution (S denotes the truncation operator, J the cost function and x the atmospheric state vector).

In a further 'multi-resolution' extension to the incremental method (Veerse and Thepaut 1998) the inner-loop resolution is increased with each iteration of the outer-loop. A schematic is shown in Fig. 2.1. In particular, the in-

formation about the shape of the cost-function obtained during the early low-resolution iterations provides a very effective pre-conditioner (Chapter 6) for subsequent iterations at higher-resolution, thus reducing the number of costly iterations. The inner-loops can be particularly efficiently minimised using the conjugate gradient method, provided the cost-function is purely quadratic (Fisher 1998, ECMWF Seminar), i.e. the operators involved in the definition of the cost function (the model and the observation operators) are purely linear. For this reason, the inner-loops have been made entirely linear, with the non-linear effects gathered at the outer-loop level.

2.2.2 The job-steps

In the 28r1 operational configurations the assimilation window is 12-hours long, running from 03-15 UTC to produce the 12 UTC analysis and forecast products, and from 15-03 UTC for the 00 UTC production. Several different job steps are performed.

- 1) Comparison of the observations with the background at high resolution to compute the innovation vectors. These are stored in the NCMIFC1-word of the ODB (the observation database) for later use in the minimization. This job step also performs **screening** (i.e. blacklisting, thinning and quality control against the background) of observations (see Chapter 10). The screening determines which observations will be passed for use in the main minimisation. Very large volumes of data are present during the screening run only, for the purpose of data monitoring. The model trajectory is interpolated to the resolution of the next job step and written out,
- 2) First minimization at low resolution to produce preliminary low-resolution analysis increments, using simplified tangent-linear physics, and tangent-linear observation operators. The eigenvectors of the analysis Hessian are computed and these will be used to precondition subsequent inner-loop iterations. The analysis and background errors required for the cycling of error variances are calculated, as described in Chapter 6.
- 3) Update of the high-resolution trajectory to take non-linear effects partly into account. Observed departures from this new atmospheric state are stored in the ODB and the analysis problem is re-linearized around the updated model state. Variational quality control is computed, and the resulting QC weights will be used in the subsequent minimisation. The updated model trajectory is interpolated to the resolution of the next job step and written out,
- 4) Second main minimization at increased resolution with more complete representation of tangent-linear physics,
- 5) Formation of the high-resolution analysis (described below) and a comparison of the analysis with all observations (including those not used by the analysis, for diagnostic purposes).

Each of the job steps is carried out by a different configuration of IFS. They are commonly called:

- (i) **The first trajectory run**, which includes a model integration, comparison to observations, and observation screening (quality control and data selection) and is sometimes called **the screening run**. – NCONF=2, LSCREEN=.T.
- (ii) **The first minimization**, simplified physics, typically run at low resolution. This job step includes estimation of analysis and forecast error variances (required for cycling), and calculation of Hessian eigenvectors for pre-conditioning of subsequent minimisation(s). NCONF=131, LSPHLC=.T., LAVCGL=.T.
- (iii) **The first trajectory update**, applies the analysis increments obtained in the first minimisations and performs another forecast integration with comparison to observations. This provides a new linearisation state for the next minimisation. NCONF=1, LOBS=.T.,
- (iv) **The second minimization**, with more complete tangent-linear physics, typically higher resolution increments, NCONF=131, LSPHLC=.F.,

- (v) **Late 4D-start runs**, If LATE4DSTART (default), the analyses (type=an) at the main synoptic hours (00, 06, 12, 18), that fall within the assimilation window, are formed in separate quick job-steps by adding the low-resolution increment to the penultimate high-resolution trajectory of the corresponding time (no forecast integration). See also schematic in [Chapter 14](#).
- (vi) **The final trajectory runs**, NCONF=1, LOBS=T., NUPTRA=NRESUPD, with verification screening - that is comparison between observations and final analysis. In the final trajectory job-steps with NUPTRA=999 the final analysis (type=4v) is formed ([Bouttier, 2001a](#)), by adding the low-resolution increment to the background (at initial time), and integrating to the analysis times.

The steps (iii) and (iv) are referred to as the second iteration of the *outer loop*, and these can optionally be iterated further to incorporate additional non-linear effects. The trajectory update is not normally done in 3D-Var. The *inner loop* takes place within the main minimization, job steps (ii) and (iv).

2.2.3 Interpolation of trajectory and increments

A truncation operator (shown as S in the schematic, [Fig. 2.1](#) above) is required to take the trajectory fields from high to low resolution. This is done using appropriate grid-point interpolations for the surface grid-point fields, whereas upper-air fields are truncated spectrally. Humidity and ozone, which are grid-point fields in the model, are first transformed to spectral representation, then truncated to the lower resolution of the inner loop. In the minimisation job-step humidity and ozone of the trajectory are read in as spectral fields and finally transformed back to grid-point fields when they are required by the model. Initial time model cloud fields are interpolated to lower resolution using the so-called 'full-pos' configuration of IFS. Trajectory cloud fields and trajectory of physical tendencies are generated in a (low resolution) model integration in which the model state is replaced by the interpolated trajectory at each time instance for which it is available. The trajectory handling is managed by the module **TRAJECTORY**.

The spectral analysis increments produced by the minimisation are read in by the routine **RDFPINC**. The spectral fields are padded with zeroes for the wave numbers not represented in the inner-loops. The increments for the spectral model variables (vorticity, divergence and logarithm of surface pressure) are added to the background fields. The temperature increments are added to the temperature of the background (after it has been converted from virtual temperature) and the resulting temperature analysis is converted back to virtual temperature. The humidity and ozone increments are inverse-transformed to grid-point fields and added to the background. Super-saturation checks are applied to the humidity, and checks for negative values are applied to humidity and ozone.

2.2.4 Pre-conditioning and control variable

In practice, it is necessary to pre-condition the minimization problem in order to obtain a quick convergence. As the Hessian (the second derivative) of the objective function is not accessible, [Lorenz \(1988\)](#) suggested the use of the Hessian of the background term J_b . The Hessian of J_b is the matrix \mathbf{B} . Such a preconditioning may be implemented either by a change of metric (i.e. a modified inner product) in the space of the control variable, or by a change of control variable. As the minimization algorithms have generally to evaluate several inner products, it was found more efficient to implement a change of variable (under **CHAVAR CHAVARIN** etc.). Algebraically, this requires the introduction of a variable χ such that

$$J_b = \chi^T \chi \quad (2.1)$$

Comparing [Eq. \(1.2\)](#) and [Eq. \(2.1\)](#) shows that $\chi = \mathbf{B}^{-1/2} \delta \mathbf{x}$ satisfies the requirement. χ thus becomes the *control variable* of the preconditioned problem. This is indeed what has been implemented, as will be explained in [Section](#)



4.2. A single-observation analysis with such preconditioning converges in one iteration.

The J_b -based pre-conditioning is sufficient when the B-term dominates over the observation term of the Hessian. With increasing amounts of observational information, and in cases with locally dense observation coverage, the observation term can be dominant over the background term in defining the shape of the cost-function (its second derivative). The combined Lanczos/conjugate gradient method allows computation of the leading eigenvectors and eigenvalues of the Hessian while solving for the analysis, essentially at no extra cost. This method is fully described in Chapter 6, and it is used for all inner-loop iterations. The Hessian eigenvector information obtained at low resolution is used as pre-conditioner at subsequent inner-loop iterations at higher resolution. This has been shown to be a very effective way of reducing the number of iterations required at higher inner-loop resolutions.

2.2.5 Minimization

The minimization problem involved in 3D/4D-Var can be considered as large-scale, since the number of degrees of freedom in the control variable is of the order of 107. In the case of purely quadratic cost-function (as in operational 4D-Var) the most efficient minimisation is provided by the conjugate gradient algorithm (**CONGRAD** called from **CVA2** and **FORECAST_ERROR**). Congrad is preconditioned with the leading Hessian eigenvectors, as described in Chapter 6. The forecast error configuration (Chapter 6, switch **LAVCGL=T**. in **yomvar**) always uses **CONGRAD**, and otherwise it is activated by the switch **LCONGRAD** in **yomvar**.

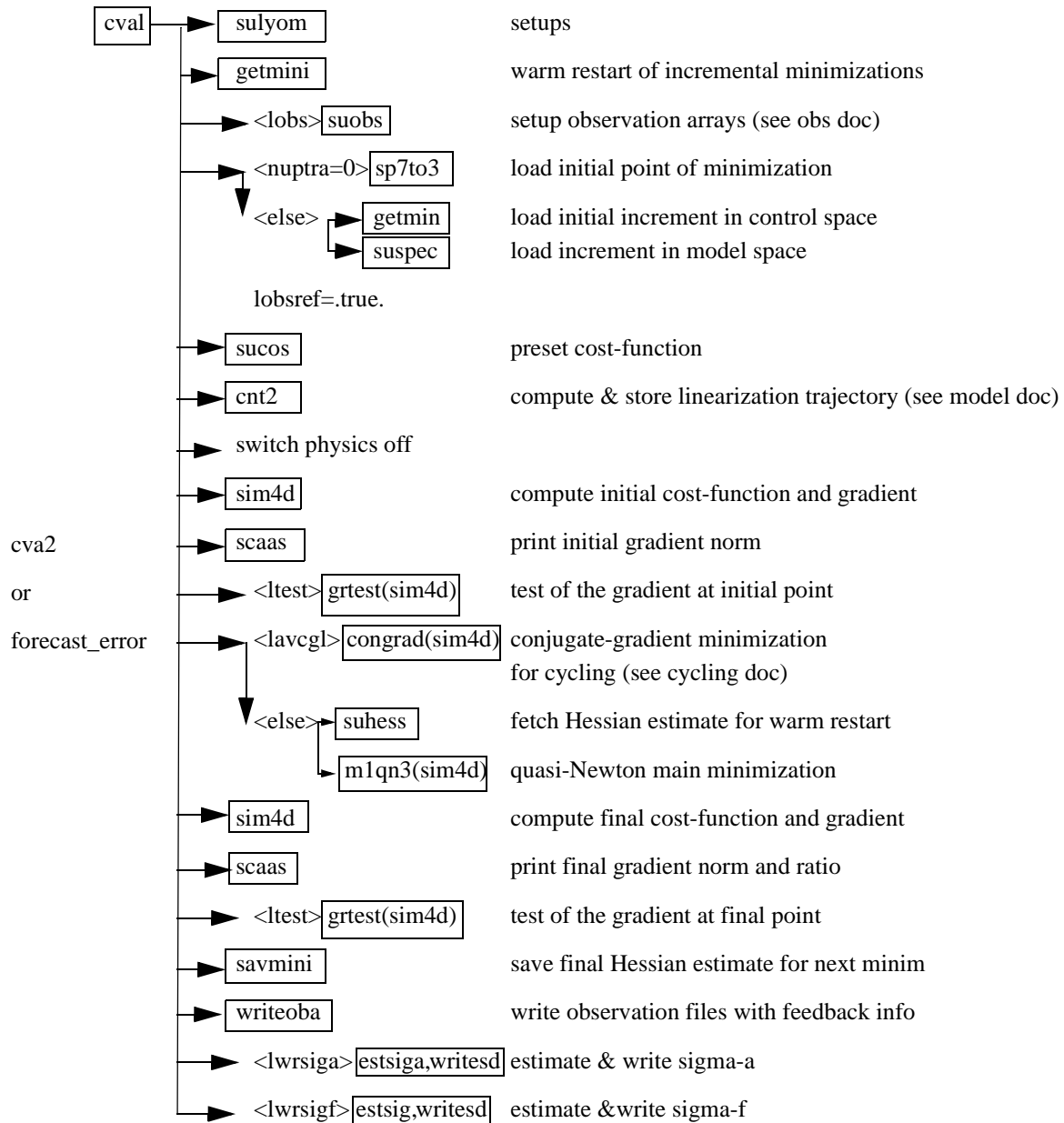
For non-quadratic problems, an efficient descent algorithm was provided by the Institut de Recherche en Informatique et Automatique (INRIA, France). It is a variable-storage quasi-Newton algorithm (**.MIQN3**) described in Gilbert and Lemaréchal (1989). **MIQN3** uses the available in-core memory to update an approximation of the Hessian of the cost function. In practice, ten updates (NMUPD, **namiom**) of this Hessian matrix were used. is currently used in the 3D-FGAT configuration, described in Chapter 3.

2.3 TOP-LEVEL CONTROLS

The routines **CVA1**, **CVA2** and **FORECAST_ERROR** control the variational configurations of IFS. The flow diagram of **CVA1/CVA2** is shown in Fig. 2.2. The first guess fields (FG) have been read in to the SP7-arrays (in **YOMSP**) by **SUECGES**, called from **SUJBSTD** within the J_b setup, see Subsection 4.3.3. At the start of **CVA1** additional setups for the variational configurations are done (**SU1YOM**). The SP3-arrays, i.e. the current model state, (in **YOMSP**) are filled by copying from SP7, using **SP7TO3**. This is done under **SUVAZX**, and only at first minimisation job-step. For subsequent minimisations SPA3 must come from the previous minimisation (**GETMINI** and **SUSPEC**). This is controlled by switches **LREADSP** and **LREADVAZX (.h)**.

2.3.1 Last simulation

After minimisation is complete one final simulation is performed in **CVA2** or **FORECAST_ERROR**. This simulation is diagnostic, and characterized by the simulation counter being set to 999, **NSIM4D=NSIM4DL**, **yomvar**. The observation departure from the low-resolution analysis, $\mathbf{y}^o - H\mathbf{x}_{LR}^a$, is computed and stored in the NCMIOMN-word of the ODB. Finally at the end of **CVA2** and **FORECAST_ERROR**., respectively, the updated ODB is written to disk, using the routine **WRITEOBA**.


 Figure 2.2 Flow diagram for subroutines **CVA1** and **CVA2**.

2.4 A SIMULATION

2.4.1 The cost function and its gradient

A simulation consists of the computation of J and ∇J . This is the task of the routine **SIM4D**, see Fig. 2.3 for the flow diagram. The input is the latest value of the control variable χ in the array **VAZX**, computed by **M1QN3**, or **CONGRAD**. First J_b and its gradient are computed (see Section 4.2):

$$\begin{aligned} J_b &= \chi^T \chi \\ \nabla_{\chi} J_b &= 2\chi \end{aligned} \quad (2.2)$$

The gradient of J_b with respect to the control variable is stored in the array VAZG (**YOMCVA**).

- Copy χ from VAZX to SP3-arrays (**YOMSP**) using the routine **CAIN**
- Compute \mathbf{x} , the physical model variables, using **CHAVARIN**:

$$\mathbf{x} = \delta\mathbf{x} + \mathbf{x}^b = L\chi + \mathbf{x}^b. \quad (2.3)$$

- If L131TL then work in terms of increments. **SUBFGS** does: $\delta\mathbf{x} = \mathbf{x} - \mathbf{x}^g$, where \mathbf{x}^g is the guess (not necessarily equal to the background).
- Perform the direct integration of the model (if 4D-Var), using the routine **CNT3** or **CNT3TL**, and compare with observations. See [Section 2.5](#).
Calculate J_o for which **OBSV** is the master routine.
- Perform the adjoint model integration (if 4D-Var) using **CNT3AD**, and observation operators' adjoint.
Calculate $\nabla_{\mathbf{x}} J_o$, and store it in SP3.
- J_c and its gradient are calculated in **COSJC** called from **CNT3AD**, if LJC is switched on (default) in **namvar**.
- Transform $\nabla_{\mathbf{x}} J_o + \nabla_{\mathbf{x}} J_c$ to control variable space by applying **CHAVARINAD**.
- Copy $\nabla_{\chi} J_o + \nabla_{\chi} J_c$ from SP3 and add to $\nabla_{\chi} J_b$, already in the array VAZG, using **CAIN**
- Add the various contributions to the cost function together, in **EVCOST**, and print to log file using **prtjo**.
- Increase the simulation counter NSIM4D by one.

The new J and $\nabla_{\chi} J$ are passed to the minimization algorithm to calculate the χ of the next iteration, and so on until convergence (or the maximum number of iterations) has been reached.

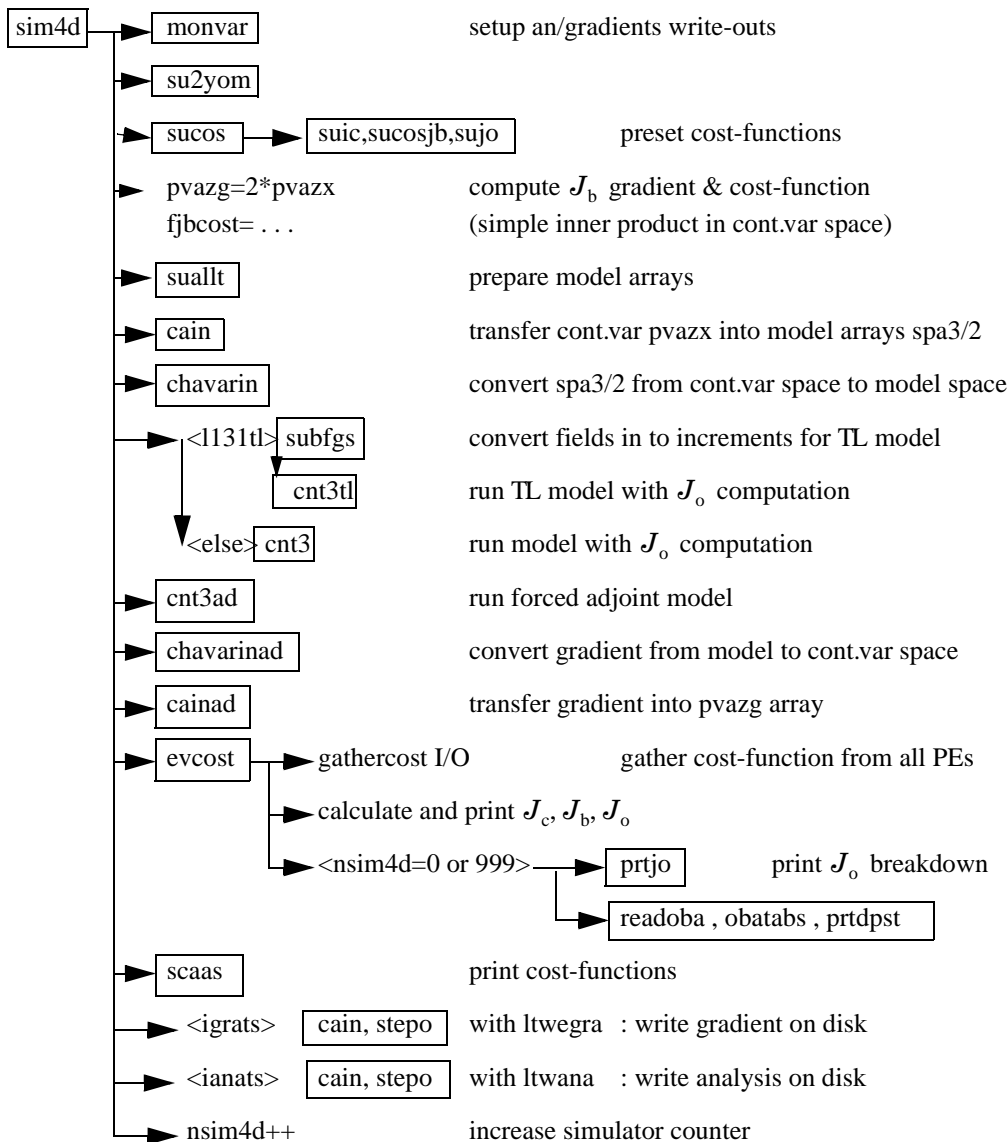
2.4.2 Interface between control variable and model arrays

The purpose of the routine **CAIN** (the canonical injection) is to identify those parts of the model state that should be included in the variational control variable. This is controlled by on/off switches such as NVA2D and NVA3D (**yomcva**) initialized in **SUALCTV**. The scalar product used is the one defined by the array SCALP (in **yomcva**, set up in the routine **SCALJGS** called from **SUSCAL**), which is 1 if $m = 0$, and 2 otherwise. This allows the compression of arrays of the type VAZX while using the L^2 norm on the sphere with real fields in spectral space.

The control vector currently consists of four parts, as defined in the module **CONTROL_VECTORS** residing in the ifsaux library. Any of the four parts can be absent. They are:

- 1) the initial-condition control-variables that define the original 4D-Var problem.
- 2) a representation of model error (for weak-constraint 4D-Var), see *Tremolet (2003)*,
- 3) the TOVS control vector (LTOVSCV), used to estimate surface skin temperature at the radiance field-of-view locations,
- 4) components for the limited-area model ALADIN,

The organisation of elements of the control-vector is now quite flexible and allows for future planned extensions, such as observation bias coefficients e.g. for radiance data, and wavelet-Jb components.


 Figure 2.3 Flow diagram for the subroutine `sim4d`.

2.5 THE ASSIMILATION WINDOW

4D-Var is a temporal extension of 3D-Var. Observations are organized in time-slots (currently half-hourly) as described in the ODB documentation. The cost-function measures the distance between a model trajectory and the available information (background, observations) over an assimilation interval or window. For a 12-hour window (in the configuration used before June 2004), it is either (03UTC–15UTC) or (15UTC–03UTC). Eq. (1.2) (see Chapter 1) is replaced by

$$J(\delta\mathbf{x}) = \frac{1}{2}\delta\mathbf{x}^T\mathbf{B}^{-1}\delta\mathbf{x} + \frac{1}{2}\sum_{i=0}^n (\mathbf{H}_i\delta\mathbf{x}(t_i) - \mathbf{d}_i)^T\mathbf{R}_i^{-1}(\mathbf{H}_i\delta\mathbf{x}(t_i) - \mathbf{d}_i) \quad (2.4)$$

with subscript i the time index. Each i corresponds to a half-hour time slot. $\delta\mathbf{x}$ is as before the increment at low resolution at initial time, and $\delta\mathbf{x}(t_i)$ the increment evolved according to the tangent linear model from the initial time to time index i . \mathbf{R}_i and \mathbf{B} are the covariance matrices of observation errors at time index i and of background errors respectively. \mathbf{H}_i is a suitable linear approximation at time index i of the observation operator H_i . The innovation vector is given at each time step by $\mathbf{d}_i = \mathbf{y}_i^o - H_i\mathbf{x}^b(t_i)$, where $\mathbf{x}^b(t_i)$ is the background propagated in time using the full non-linear model and \mathbf{y}_i^o is the observation vector at time index i . As SYNOP and DRIBU time sequences of surface pressure and height data are now used **with** serial correlation of observation error, the observation cost-function computation for those data spans all time slots. Eq. (2.4) therefore needs generalising, as has been done in the paper by *Järvinen et al. (1999)*.

The minimization is performed in the same way as in 3D-Var. However, it works fully in terms of increments, a configuration which is activated by the switches L131TI and LOBSTL, and involves running the tangent-linear and adjoint models iteratively as explained in Section 2.4 of Chapter 2, and using the tangent-linear observation operators.

A way to account in the final 4D-Var analysis for some non-linearities is to define a series of minimization problems

$$J(\delta\mathbf{x}^n) = \frac{1}{2}(\delta\mathbf{x}^n + \mathbf{x}^{n-1} - \mathbf{x}^b)^T\mathbf{B}^{-1}(\delta\mathbf{x}^n + \mathbf{x}^{n-1} - \mathbf{x}^b) + \frac{1}{2}\sum_{i=0}^n (\mathbf{H}_i\delta\mathbf{x}^n(t_i) - \mathbf{d}_i^{n-1})^T\mathbf{R}_i^{-1}(\mathbf{H}_i\delta\mathbf{x}^n(t_i) - \mathbf{d}_i^{n-1}) \quad (2.5)$$

with superscript n the minimization index.

\mathbf{x}^{n-1} is the current estimate of the atmospheric flow. It is equal to the background for the first minimization. $\mathbf{d}_i^{n-1} = \mathbf{y}_i^o - H_i\mathbf{x}^{n-1}(t_i)$ is the innovation vector, computed by integrating the model at high resolution from the current estimate.

2.6 TANGENT LINEAR PHYSICS

The linearized physics describes five processes: vertical diffusion, subgrid-scale orographic effects, radiation, large-scale condensation and deep convection. In order to prevent spurious unstable perturbations from growing, a number of simplifications have been defined for these schemes with respect to the nonlinear physical parametrization schemes (described in section IV: Physical processes) used in the forecast model.

The first minimization uses just a simple physics, which is represented by very simple vertical diffusion scheme acting mainly close to the surface and surface drag scheme. A scientific description of this simple physics is given in Buizza (1994). Note that from cycle 28R3 onwards the more detailed simplified vertical diffusion scheme described in subsection Section 2.6.3 will be used instead of Buizza’s in the first minimization.

The following minimizations use a more complete linearized physics, which is described in this section. The text is focused on brief scientific description of these linearized physical parametrization schemes and some technical

aspects. More detailed scientific issues can be found elsewhere (*Mahfouf et al. 1997; Rabier et al. 1997; Mahfouf 1999; Janiskova et al. 2002*).

2.6.1 Set-up

The simple physics used in the first minimization is activated by the switches LSPHLC, LVDFDS, LSDRDS, LVDFLC, LSDRLC, LKEXP in namelist **NAPHLC**.

In order to activate the improved linear physics, the switch LSPHLC of the simplified linear physics in **NAPHLC** should be set to FALSE. In **CVAI** when both logicals LSPHLC and LETRAJP are equal to TRUE, LSPHLC is reset to FALSE and a warning is written in the standard output (logical unit NULOUT).

The improved linearized physics is activated by the switches LETRAJP, LEVDIF2, LEGWDG2, LECOND2, LERADI2, LERADS2, LERADN2, LERADSW2, LEDCLD2, LECUMF2 in namelist **NAMTRAJP**. The following switches must be set to TRUE: LEPHYS, LAGPHY (also necessary to activate the ECMWF nonlinear physics) in namelist **NAEPHY** and LETRAJP (to activate storage of the trajectory at $t - \Delta t$). The linear physics contains a set of five physical processes: vertical diffusion (LEVDIF2), subgrid-scale orographic effects (LEGWD2), large scale condensation (LECOND2), radiation (LERADI2, LERADS2, LERADN2, LERADSW2) taking into account clouds (LEDCLD2) and deep moist convection (LECUMF2).

Tunable parameters of the improved physics (which should not in principle be modified) are defined in **SUPHLI**. The logical LPHYLIN is used to activate the simplifications and/or modifications associated with the linear package in the nonlinear physics. This variable is set to FALSE by default, but is forced to TRUE before starting the tangent-linear and adjoint computations in **CNT3TL** and **CNT3AD**. Thus this switch remains TRUE for the linear physics called in **EC_PHYS_TL** and **EC_PHYS_AD**.

2.6.2 Mixed-phase thermodynamics

The thermodynamical properties of the water mixed phase are represented by a differentiable weighting function between $T_0 = 0\text{C}$ and $T_{\text{ice}} = -23\text{C}$:

$$\alpha(T) = \frac{1}{2}[1 + \tanh\{\mu(T - T_{\text{crit}})\}] \quad (2.6)$$

with $\mu = 0.15$ (RLPALP1) and $T_{\text{crit}} = T_{\text{ice}} + \frac{T_0 - T_{\text{ice}}}{\sqrt{2}}$ (RLPTRC).

The tuning parameter μ controls the intensity of the smoothing, and the temperature T_{crit} has been chosen to give $\alpha = 0.5$ for the same temperature as in the operational quadratic formulation (see function **FCTTRE**).

This weighting function is used by the large-scale condensation and moist-convection routines.

2.6.3 Vertical diffusion

Vertical diffusion applies on wind components, dry static energy and specific humidity. The exchange coefficients in the planetary boundary layer and the drag coefficients in the surface layer are expressed as functions of the local Richardson number (*Louis et al. 1982*). They differ from the operational formulation which uses the Monin-Obukhov length as a stability parameter in stable conditions and a K -profile approach for convective boundary layers (see the documentation of the ECMWF physics). Analytical expressions are generalized to the situation of different roughness lengths for heat and momentum transfer. The mixing length profile $l(z)$ uses the formulation of Blackadar (1962) with a reduction in the free atmosphere.

For any conservative variable ψ (wind components u, v ; dry static energy s ; specific humidity q), the tendency of

its perturbation ψ' produced by vertical diffusion is:

$$\frac{\partial \psi'}{\partial t} = \frac{1}{\rho} \frac{\partial}{\partial z} \left(K(Ri) \frac{\partial \psi'}{\partial z} \right), \quad (2.7)$$

where ρ is the air density.

In the planetary boundary layer, the exchange coefficient K is given by the following expression:

$$K = l^2 \left\| \frac{\partial \mathbf{V}}{\partial z} \right\| f(Ri) \quad (2.8)$$

where $f(Ri)$ represents the coefficient of the vertical turbulent diffusion which is a function of the Richardson number. The mixing length vertical profile is defined as:

$$l_{M/H} = \frac{\kappa(z+z_0)}{1 + k \frac{(z+z_0)}{\lambda}} \left[\gamma + \frac{1-\gamma}{1 + \frac{(z+z_0)^2}{L^2}} \right] \quad (2.9)$$

The asymptotic mixing length λ_M for momentum is set to 150 m, whereas $\lambda_H = \lambda_M \sqrt{1.5d}$. The pseudo-depth of the boundary layer is defined by $L = 4$ km (RLPMIXL), and the reduction factor applied to the mixing length in the free atmosphere is $\gamma = 0.2$ (RLPBETA) [$l \rightarrow \gamma l$ when $z \gg L$]. κ is von Kármán's constant and z_0 is the roughness length.

The coefficients of the vertical turbulent diffusion for momentum are given by

$$f(Ri) = \begin{cases} \frac{1}{1 + \frac{2bRi}{\sqrt{1+dRi}}} & \text{if } Ri > 0, \text{ the stable case} \\ 1 - \frac{2bRi}{1 + 3bc \left(\frac{1}{\sqrt{27}} \right) \left(\frac{l_M}{z+z_{0M}} \right)^2 \sqrt{|Ri|}} & \text{if } Ri < 0, \text{ the unstable case} \end{cases} \quad (2.10)$$

The vertical diffusion coefficients for dry static energy and specific humidity are defined as

$$f(Ri) = \begin{cases} \frac{1}{1 + 3bRi \sqrt{1+dRi}} & \text{if } Ri > 0 \\ 1 - \frac{3bRi}{1 + 3bc \left(\frac{1}{\sqrt{27}} \right) \left(\frac{l_H}{z+z_{0H}} \right)^2 \sqrt{|Ri|}} & \text{if } Ri < 0 \end{cases} \quad (2.11)$$

where b, c, d are constants controlling the dependency of vertical exchange on the stability.

To parametrize the turbulent fluxes at the surface, the drag coefficients (i.e. the exchange coefficients between the surface and the lowest model level) are computed. The neutral coefficients C_{MN} and C_{HN} are written as

$$C_{MN} = \frac{\kappa^2}{\left[\ln\left(\frac{z+z_{0M}}{z_{0M}}\right)\right]^2} \quad \text{and} \quad C_{HN} = \frac{\kappa^2}{\left[\ln\left(\frac{z+z_{0M}}{z_{0M}}\right)\ln\left(\frac{z+z_{0M}}{z_{0H}}\right)\right]} \quad (2.12)$$

The drag coefficients for momentum are computed as

$$C_M = \begin{cases} \frac{1}{1 + \frac{2bRi}{\sqrt{1+dRi}}} C_{MN} & \text{if } Ri > 0 \\ \left(1 - \frac{2bRi}{1 + 3bcC_{MN}\sqrt{\frac{z+z_{0M}}{z_{0M}}|Ri|}}\right) C_{MN} & \text{if } Ri < 0 \end{cases} \quad (2.13)$$

The surface exchange coefficients for dry static energy and specific humidity are

$$C_H = \begin{cases} \frac{1}{1 + 3bRi\sqrt{1+dRi}} C_{HN} & \text{if } Ri > 0 \\ \left(1 - \frac{3bRi}{1 + 3bcC_{HN}\sqrt{\frac{z+z_{0M}}{z_{0H}}|Ri|}}\right) C_{HN} & \text{if } Ri < 0 \end{cases} \quad (2.14)$$

The empirical coefficients b (RLPBB), c (RLPCC) and d (RLPDD) are set to 5 in **SUPHLI**.

In Eq. (2.7), perturbations of the exchange coefficients are neglected, $K' = 0$, in order to prevent spurious unstable perturbations from growing in the linearized version of the scheme (Mahfouf 1999). This is also the case for the exchange coefficients between the surface and the lowest model level.

This modified diffusion scheme is called directly from **VDFMAIN** and makes use of all the routines from the operational vertical diffusion, except **VDFSFLX** (computation of the surface fluxes for tiles) and some diagnostic routines. However, the exchange coefficients are computed in a different way in **VDFEXCS** and **VDFEXCU**.

The linear versions of the vertical diffusion scheme are called from the drivers **VDFMAINTL** and **VDFMAINAD**. The linearization of the surface energy balance is also performed (**VDFTSKTL**, **VDFTSKAD**), but perturbations of the skin temperature are not evolved in time (in **EC_PHYS_TL** and **EC_PHYS_AD**). This simplification should be relaxed when the skin temperature becomes part of the control variable. There are tangent-linear and adjoint versions of some routines, which were not updated when introducing the surface tile scheme and are not recently used. This is secured by the logical switch **LENOPERT** set to **TRUE** in **SUPHLI** (i.e. no perturbation is required for the surface arrays). This concerns the routines for computation of: the roughness length (**VDFUPDZ0TL**, **VDFUPDZ0AD**), the surface boundary conditions for T and q (**VDFSURFTL**, **VDFSURFAD**), the surface exchange coefficients (**VDFEXCSTL**, **VDFEXCSAD**) and the equivalent evapotranspiration efficiency (**VDFEVAP-TL**, **VDFEVAPAD**).

The logical **LEKPERT** in **NAMTRAJP** controls the perturbations of the exchange and drag coefficients. When set to **FALSE** (default), the perturbations are set to 0. to prevent the growth of spurious instabilities in the tangent-

linear model.

2.6.4 Subgrid scale orographic effects

Only the low-level blocking part of the operational nonlinear scheme developed by *Lott and Miller (1997)* (see documentation on ECMWF nonlinear physics) is taken into account in the tangent-linear and adjoint calculations. The deflection of the low-level flow around orographic obstacles is supposed to occur below an altitude Z_{blk} such that

$$\int_{Z_{\text{blk}}}^{2\mu} \frac{N}{|\mathbf{U}|} dz \geq H_{n_{\text{crit}}} \quad (2.15)$$

where $H_{n_{\text{crit}}}$ is a critical non-dimensional mountain height (GFRCRIT = 0.5), μ is the standard deviation of sub-grid-scale orography, N is the vertical stability and \mathbf{U} is the wind vector.

The deceleration of the wind due to the low-level blocking is given by

$$\begin{aligned} \left(\frac{\partial \mathbf{U}}{\partial t}\right)_{\text{blk}} &= -C_d \max\left(2 - \frac{1}{r}, 0\right) \frac{\sigma}{2\mu} \left(\frac{Z_{\text{blk}} - z}{z + \mu}\right)^{0.5} (B \cos^2 \psi + C \sin^2 \psi) \frac{\mathbf{U}|\mathbf{U}|}{2} \\ &= \mathbf{A}(\mathbf{U}|\mathbf{U}|) \end{aligned} \quad (2.16)$$

where

C_d is the low-level drag coefficient (GWAKE = 1),

σ is the mean slope of the subgrid-scale orography,

γ is the anisotropy of the subgrid-scale orography,

ψ is the angle between the low-level wind and the principal axis of topography,

$$B = 1 - 0.18\gamma - 0.04\gamma^2,$$

$$C = 0.48\gamma + 0.3\gamma^2,$$

$$\text{and } r = (\cos^2 \psi + \gamma \sin^2 \psi) / (\gamma \cos^2 \psi + \sin^2 \psi).$$

Since the final wind tendency produced by the low-level drag parametrization is obtained from the following partially implicit discretization of Eq. (2.17)

$$\left(\frac{\partial \mathbf{U}}{\partial t}\right)_{\text{blk}} = -\frac{\beta}{\beta + 1} \frac{\mathbf{U}^{n-1}}{2\Delta t} \quad (2.17)$$

where $\beta = \mathbf{A}|\mathbf{U}^{n-1}|2\Delta t$, the corresponding perturbation write

$$\left(\frac{\partial \mathbf{U}}{\partial t}\right)_{\text{blk}} = -\frac{\beta'}{(\beta + 1)^2} \frac{\mathbf{U}^{n-1}}{2\Delta t} - \frac{\beta}{\beta + 1} \frac{\mathbf{U}^{n-1}}{2\Delta t} \quad (2.18)$$

Finally, the local dissipation heating is computed in the same way as in the nonlinear scheme, together with the associated perturbation.

The main tangent-linear and adjoint routines, **GWDRAGTL** and **GWDRAGAD**, are called from **CALLPARTL** and

CALLPARAD respectively. The depth of the low-level blocking layer is determined in GWSETUPTL and GWSETUPAD, while the low-level blocking effect described by Eq. (2.17) is computed at the end of GWDRAGTL and GWDRAGAD. As mentioned above, the representation of wave breaking is currently not activated in the linearized code by setting the constant RLPDRAG to zero in SUPHLI. Note that RLPDRAG is only used when logical LPHYLIN is TRUE, otherwise GKDRAG is used (set to 0.3 in SUGWD).

2.6.5 Radiation

The radiation scheme solves the radiative transfer equation in two distinct spectral regions. The computations for the longwave (LW) radiation are performed over the spectrum from 0 to 2820 cm⁻¹. The shortwave (SW) part of the scheme integrates the fluxes over the whole shortwave spectrum between 0.2 and 4.0 μm. The scheme used for data assimilation purposes must be computationally efficient to be called at each time step and at the full spatial resolution for an improved description of the cloud-radiation interactions during the assimilation period (Janiskova et al. 2002).

2.6.5 (a) *The short-wave radiation scheme.* The linearized code for the shortwave radiation scheme has been derived from the ECMWF original nonlinear scheme developed by Fouquart and Bonnel (1980) and revised by Morcrette (1991). In this scheme, the photon-path-distribution method is used to separate the parametrization of the scattering processes from that of molecular absorption. Upward $F_{sw\uparrow}$ and downward $F_{sw\downarrow}$ fluxes at a given level j are obtained from the reflectance and transmittance of the atmospheric layers as:

$$F_{sw\downarrow}(j) = F_0 \prod_{k=j}^N \tau_{bot}(k) \quad (2.19)$$

(2.20)

Computations of the transmittance at the bottom of a layer T_{bot} start at the top of atmosphere and work downward. Those of the reflectance at the top of the same layer R_{top} start at the surface and work upward. In the presence of cloud in the layer, the final fluxes are computed as a weighted average of the fluxes in the clear sky and in the cloudy fractions of the column as:

(2.21)

(2.22)

In the previous equations, f_c is the cloud fractional coverage of the layer within the cloudy fraction of the column (depending on cloud-overlap assumption).

The cloud optical properties depend on three different parameters: the optical thickness δ_c , the asymmetry factor g_c and the single scattering albedo $\overline{\omega}_c$. These parameters are derived from Fouquart (1987) for water clouds, and Ebert and Curry (1992) for ice clouds. They are functions of cloud condensate and a specified effective radius. All cloudy fluxes are computed from cloud optical thicknesses derived from the liquid and ice cloud water contents weighted by a 0.7 inhomogeneity factor following Tiedtke (1996).

The nonlinear version of the shortwave radiation scheme (described in details in section IV: Physical processes) uses six spectral intervals with transmission functions derived from a line-by-line code (Dubuisson et al. 1996).

The nonlinear scheme is reasonably fast for application in 4D-Var and has, therefore, been linearized without a pri-

ori modifications. The only modification with respect to the nonlinear model is using two spectral intervals with transmission functions (instead of six intervals used in the nonlinear model) in order to reduce the computational cost.

2.6.5 (b) *The longwave radiation scheme.* The longwave radiation scheme, operational in the ECMWF forecast model until June 2000, was a band emissivity type scheme (*Morcrette 1989*). This scheme has been replaced by the Rapid Radiation Transfer Model (RRTM: Mlawer et al. 1997) in June 2000. The scheme is based on a two-stream solution of the longwave transfer. The ECMWF version of the RRTM longwave radiation scheme (*Morcrette 1998*) also includes a maximum-random overlap assumption but keeps the cloud fraction and cloud optical thickness as two separate quantities. In RRTM, the cloud optical thickness is defined as a function of spectrally varying mass absorption coefficients and relevant cloud water and ice paths. This quantity is then used within the actual cloudy fraction of the layer.

Cloud longwave optical properties are represented by the emissivity $\varepsilon_{\text{clid}}$ related to the condensed water amount, and by the condensed water mass absorption coefficient k_{abs} obtained following *Smith and Shi (1992)* for water clouds and *Ebert and Curry (1992)* for ice clouds.

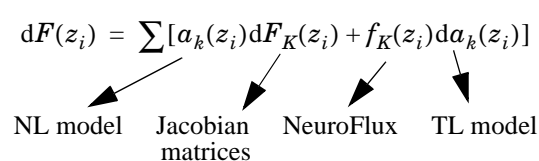
The complexity of the RRTM radiation scheme for the longwave part of the spectrum makes accurate computations expensive. In the variational assimilation framework, simplifications were made to reduce its computational cost. A combination of artificial neural networks (*Chevallier et al. 2000*) and pre-computed Jacobians of the longwave radiation flux with respect to global mean temperature and water vapour profiles (*Chevallier and Mahfouf 2001*) has been defined for the linearized longwave radiation scheme.

The longwave radiative fluxes depend upon temperature, water vapour, cloud cover and liquid and ice water contents. The design of the scheme allows the separation of the contribution of temperature and water vapour from that of cloud parameters. More precisely, the upward and downward longwave fluxes at a certain height z_i are expressed as:

$$F(z_i) = \sum_k \alpha_k(z_i) F_k(z_i) \quad (2.23)$$

where the coefficients α_k are a function of the cloudiness matrices $CC_{i,k}$ computed using some overlap assumption. Differentiating the above equation, a flux perturbation is computed as:

$$dF(z_i) = \sum [\alpha_k(z_i) dF_k(z_i) + f_k(z_i) d\alpha_k(z_i)] \quad (2.24)$$



In the proposed approach, the coefficients α_k are computed using the nonlinear (NL) model (code computing cloud optical properties). Due to the weak nonlinearities in the variations of the radiative fluxes F_k with respect to temperature and water vapour, the tangent-linear approximation can be used to compute perturbations of radiation fluxes dF_k from pre-computed mean Jacobian matrices. Perturbations of radiative fluxes with respect to cloud parameters $d\alpha_k$ are computed using a tangent-linear (TL) scheme. The trajectory of radiative fluxes required in the tangent-linear and adjoint computations are efficiently estimated from a neural network version of the ECMWF longwave radiative transfer model (called NeuroFlux) in order to avoid significant extra memory storage or

costly re-computations. The Neutroflux is significantly faster (seven times) than the operational longwave radiation code with a comparable accuracy.

2.6.5 (c) Cloud overlap assumptions. Cloud overlap assumptions must be made in atmospheric models in order to organize the cloud distribution used for radiation and precipitation/evaporation computations. A cloud overlap assumption of some sort is necessary to account for the fact that clouds often do not fill the whole grid box. The maximum-random overlap assumption (originally introduced in *Geleyn and Hollingsworth 1997*) is used operationally in the ECMWF model (*Morcrette 2000*). Adjacent layers containing cloud are combined by using maximum overlap to form a contiguous cloud and discrete layers separated by clear-sky are combined randomly as:

$$CC_{i,j} = 1 - (1 - C_i) \prod_{k=i+1}^{j-1} \left[\frac{1 - \max(C_k, C_{k-1})}{1 - C_{k-1}} \right] \quad (2.25)$$

where $CC_{i,j}$ is cloudiness encountered between any levels i and j in the atmosphere and C_k is the cloud fraction of the layer k located between levels k and $k+1$.

The tangent-linear (TL) and adjoint (AD) versions of the shortwave radiation scheme can be activated using the logical switch `LERADSW2 = TRUE` in the namelist `NAMTRAJP`. The default value is set to `FALSE`. To decrease a computational cost of the shortwave radiation in data assimilation, the number of spectral intervals is reduced to two (six intervals are used in the forecast model) during minimization. The number of spectral intervals `NSW` is changed in `CVA1`. This change also requires to read several parameters for two spectral intervals. This is done in set-up routines `SUSWN`, `SUCLOPN` and `SUAERSN`.

Due to the low impact of cloud perturbations produced by the current linearized cloud scheme and in order to decrease the computational cost, a reduced version of the linearized longwave radiation (i.e. $dF(z_i) \approx \sum_k a_k(z_i) dF_k(z_i)$) is currently used in data assimilation. This reduced version can be activated by `LERADN2 = TRUE` in the namelist `NAMTRAJP`. If the full linearized longwave radiation should be used, the logical switch `LERADFL2` must also be set to `TRUE` in the same namelist. The default values are set to `FALSE`.

The linearized radiation schemes are called from `RADINATL` and `RADINAAD`, where the computation of radiation fluxes is performed. Tendencies produced by the linearized longwave and shortwave radiation are computed in `RADHEATTL` and `RADHEATAD`. All those routines are called from `CALLPARTL` and `CALLPARAD`, respectively.

`RADLSWTL` and `RADLSWAD` are the drivers for the computation of the solar and thermal fluxes by calling specialized routines for shortwave radiation (`SWTL` and `SWAD`) and for longwave radiation (`LWPTL` and `LWPAD`).

2.6.6 Cloud scheme

The ECMWF diagnostic cloud scheme (*Slingo 1997*), used before the implementation of the current operational prognostic scheme (*Tiedtke 1993*), has been linearized to be used with the linearized radiation scheme.

The diagnostic cloud scheme allows for four cloud types: convective cloud and three types of layer clouds (high, middle and low level). The convective clouds (C_{conv}) are parametrized using the scale-averaged precipitation rate (\bar{P}) from the model convection scheme as

$$C_{\text{conv}} = 0.4 \min(0.8, 0.125 \ln \bar{P} - 1.5) \quad (2.26)$$

They can fill any number of model layers and their depth is determined by the convection scheme. The stratiform

clouds (C_{strat}) are determined from a function of the layer relative humidity (RH_e) after adjustment for the presence of convective clouds, $RH_e = RH - C_{\text{conv}}$, as:

$$C_{\text{strat}} = f(RH_e) = \left\{ \max \left(\left[\frac{RH_e - RH_{\text{crit}}}{1 - RH_{\text{crit}}}, 0 \right] \right) \right\}^2 \quad (2.27)$$

RH_{crit} is a critical relative humidity for cloud formation defined as

$$RH_{\text{crit}} = 1 - \max[0, 1.8\sigma(1 - \sigma)(1 + 0.95(\sigma - 0.5))] \quad (2.28)$$

where σ is the vertical coordinate of the pressure divided by the surface pressure.

Liquid water l_{wvc} and ice water l_{iwc} are proportional to the specific humidity at saturation q_{sat} . They are defined as

$$l_{\text{wvc}} = \alpha l_{\text{lc}} \quad (2.29)$$

$$l_{\text{iwc}} = (1 - \alpha)l_{\text{lc}} \quad (2.30)$$

where α is the fraction of condensate held as liquid water and $l_{\text{lc}} = 0.5C_{\text{cloud}}q_{\text{sat}}$ with C_{cloud} being cloud cover.

The linearized diagnostic cloud scheme has been further simplified by accounting for part of the dependencies only. The current linearized convection scheme does not provide perturbations of precipitation. This leads to a zero perturbation of convective cloudiness since it is determined from the convective precipitation rate. A modification of the linearized cloud scheme was also necessary in order to avoid the threshold problem in the parametrization of the layer clouds computed as a function of relative humidity RH_e (Eq. (2.27)). For this reason, the derivative of the function of relative humidity has been set to zero (Janiskova et al. 2000).

The linearized versions of the diagnostic cloud scheme are **CLOUDTL** and **CLOUDAD** and they are called from **CALLPARTL** and **CALLPARAD**, respectively. These linearized schemes can be activated using the logical switch **LEDCLD2 = TRUE** in the namelist **NAMTRAJP**. The default value is set to **FALSE**.

2.6.7 Large-scale condensation

The linearized version of large-scale condensation scheme is based on a local moist adjustment scheme designed to produce stratiform precipitation as described in Mahfouf (1999).

If (q, T) is an initial supersaturated state ($q > q_s(T)$), a final adjustment state (q_*, T_*) such that $q_* = q_s(T_*)$ is reached by conserving moist static energy in a given atmospheric layer. The adjusted values are obtained through an iterative method with two updates.

The equations for the nonlinear scheme are:

$$T_* - T = -\lambda(q_s(T_*) - q) \quad (2.31)$$

$$q_* - q = q_s(T_*) - q \quad (2.32)$$

with $\lambda = L/C_p$, where L is the latent heat of liquid water and C_p is the specific heat at constant pressure. They are solved using a linearization of the specific humidity at saturation: $q_s(T_*) = q_s(T) + \gamma(T_* - T)$ with $\gamma = \partial q_s / \partial T$. Then, the linearization of $q_s(T')$ as $\gamma T'$, provides the equation for the tangent-linear scheme:

$$T'_* - T' = -\frac{\lambda}{1 + \lambda\gamma}(\gamma T' - q') \quad (2.33)$$

$$q'_* - q' = -\frac{1}{1 + \lambda\gamma}(\gamma T' - q') \quad (2.34)$$

Tendencies produced by large-scale condensation are thus:

$$\frac{\partial q'}{\partial t} = -\frac{1}{\lambda} \frac{\partial T'}{\partial t} = \frac{q'_* - q'}{2\Delta t} \quad (2.35)$$

where Δt is the model time step.

This scheme also accounts for melting of snow whenever the temperature of a given layer exceeds 2\deg C. Evaporation of precipitation in subsaturated layer is neglected to avoid the growth of spurious unstable modes (*Mahfouf 1999*).

Linearized versions of the large-scale condensation scheme are **CONDTL** and **CONDAD**. Local supersaturation is removed through a local moist-adjustment scheme (CUADJTQTL, CUADJTQAD). Supersaturation produces precipitation instantaneously (without a cloud stage). The effect of rainfall evaporation in sub-saturated layers is disregarded in the linearized versions of the scheme by setting the constant RLPEVAP to 0., instead of 0.95 in the nonlinear parametrization.

2.6.8 Deep moist convection

The physical tendencies produced by convection on any conservative variable ψ (wind components, specific humidity, dry static energy) can be written in a mass-flux formulation as (*Betts 1997*):

$$\frac{\partial \psi}{\partial t} = \frac{1}{\rho} \left[(M_{\text{up}} + M_{\text{down}}) \frac{\partial \psi}{\partial z} + D_{\text{up}}(\psi_{\text{up}} - \psi) + D_{\text{down}}(\psi_{\text{down}} - \psi) \right] \quad (2.36)$$

The first term on the right hand side represents the compensating subsidence induced by cumulus convection on the environment through the mass flux M . The other terms accounts for the detrainment of cloud properties in the environment with a detrainment rate D . The subscripts 'up' and 'down' refer to the updrafts and downdrafts properties respectively. Evaporation of cloud water and precipitation should also be added in Eq. (2.36) for the dry static energy s and specific humidity q . Mass-flux theory predicts that the effect of convection on large-scale temperature and moisture structures is dominated by compensating subsidence, as shown in the study of Gregory and Miller (1989). Therefore, nonlinear tendencies produced by convection can be approximated by:

$$\frac{\partial \psi}{\partial t} \approx \frac{1}{\rho} \left[(M_{\text{up}} + M_{\text{down}}) \frac{\partial \psi}{\partial z} \right] \quad (2.37)$$

This approach is better for the heat budget than for the moisture budget (*Betts 1997*). As a consequence, a partial linearization of Eq. (2.37) is performed, where the vertical transport by the mean mass flux is applied to the perturbations. From a nonlinear integration of the convection scheme mass-flux profiles $M(z)$ are used to estimate the vertical transport of perturbed fields ψ' :

$$\frac{\partial \psi'}{\partial t} = \frac{1}{\rho} \left[(M_{\text{up}} + M_{\text{down}}) \frac{\partial \psi'}{\partial z} \right] \quad (2.38)$$

This linearized equation only applies to deep convection. The underlying assumption of Eq. (2.38) is that perturbations of cloud properties can be neglected.

The mass-flux profiles associated with the updrafts M_{up} and the downdrafts M_{down} are recomputed in the tangent-linear and adjoint integrations from the stored basic state. This partial linearization implies that all the nonlinear routines for the convection scheme have their tangent-linear and adjoint counterparts (starting from the driving routines **CUCALLNTL** and **CUCALLNAD**). However, most of them are only used to recompute the trajectory. The only routines which contain linear statements are **CUININTL** (mean thermodynamical properties at half model levels), **CUDUDVTL** (tendencies for the wind components) and **CUDTDQNTL** (tendencies for dry static energy and specific humidity). Eq. (2.38) is solved numerically in the following form (see *Tiedtke 1989*):

$$\frac{\partial \Psi'}{\partial t} = \frac{1}{\rho} \left[\frac{\partial(M_{\text{up}} \Psi')}{\partial z} + \frac{\partial(M_{\text{down}} \Psi')}{\partial z} + (D_{\text{up}} - E_{\text{up}} + D_{\text{down}} - E_{\text{down}}) \Psi' \right] \quad (2.39)$$

which requires extra local storage of the profiles of entrainment E and detrainment D rates computed in **CUASCN** and in **CUDDRAFN** (variables PDMFEN and PDMFDE). Eq. (2.39) is only applied when deep convection is diagnosed from the basic state.

2.6.9 Trajectory management

The ECMWF physics uses the tendencies from the dynamics, and variables at $t - \Delta t$ as input to compute the tendencies of a given process (represented by the operator P) for a prognostic variable ψ :

$$\frac{\Psi_u^{n+1} - \Psi_u^{n-1}}{2\Delta t} = P(\Psi_u^{n-1}) \quad (2.40)$$

where the variable Ψ_u has already been updated by the dynamics and by the previous physical processes (which are called in the following order: radiation; vertical diffusion; subgrid-scale orographic effects; moist convection; large-scale condensation).

Thus:

$$\Psi_u^{n-1} = \Psi_u^{n-1} + \left(\frac{\partial \Psi}{\partial t} \right)_{\text{dyn}} + \left(\frac{\partial \Psi}{\partial t} \right)_{\text{phys}} \quad (2.41)$$

In Eq. (2.40), if the operator P is nonlinear, its linearization around the basic state Ψ_u^{n-1} , will require to store the model state at time step $n - 1$ (trajectory at $t - \Delta t$) as well as the tendencies produced by the dynamics $(\partial \Psi / \partial t)_{\text{dyn}}$. The physical tendencies from the previous processes $(\partial \Psi / \partial t)_{\text{phys}}$, require an additional call to the nonlinear routines in the adjoint computations (**CALLPARAD**) and a local storage of the partial tendencies.

The storage of the trajectory at $t - \Delta t$ is performed in **EC_PHYS** by the routine **STORE_TRAJ_PHYS** called before the driver of the ECMWF physics **CALLPAR**. Fields are stored in grid-point space in an array **TRAJ_PHYS**. This array is allocated in the module **TRAJ_PHYSICS**, where also the number of the fields to be stored is defined.

The following three-dimensional fields are stored :

- **for the atmosphere:** the prognostic variables (wind components, temperature, specific humidity) and their tendencies produced by adiabatic processes, the vertical velocity, the long-wave fluxes and the solar transmissivity;
- **for the soil:** the prognostic variables for temperature and moisture content (used to compute the surface fluxes from the trajectory in the linear vertical-diffusion scheme);

- **for the tiles**, i.e. vegetation (surface cover) types: u- and v-stress, surface sensible heat flux, surface evaporation and skin temperature.

A number of two-dimensional fields used at time step $t - \Delta t$ need to be stored: surface pressure, surface fluxes, skin temperature, skin reservoir, snow reservoir, roughness lengths (mainly for the vertical diffusion).

The preliminary computations (pressure and geopotential at full and half model levels, astronomy parameters) are performed in `EC_PHYS_TL` and `EC_PHYS_AD` before calling the driver of the tangent-linear physics `CALLPARTL` or the driver of the adjoint physics `CALLPARAD`, and after reading the trajectory fields from `GET_TRAJ_PHYS`.

Part II: DATA ASSIMILATION**CHAPTER 3 3D variational assimilation (with the first-guess at appropriate time)****Table of contents**

3.1. Introduction

3.2. 3D-FGAT

3.2.1. Solution algorithm

3.2.2. Main differences with respect to 4D-Var

3.2.3. Data selection

3.1 INTRODUCTION

3D-Var is a temporal simplification of 4D-Var. The simplest way to implement a 3D-Var within the context of an existing 4D-Var scheme is to replace the tangent-linear (and its adjoint) model integration within the inner loops (as defined in the previous section) by the identity operator (LIDMODEL=.T. in `yomtnewt.F90`). This approach has indeed been adopted, as it saves on maintenance of scripts and codes. It is this 3D-Var version that was used for the production of the ERA-40 re-analysis (*Uppala et al. 2005*) and it is used in ECMWF operations within the so called BC-suite to generate timely boundary conditions for the participating member states.

In this version of 3D-Var as much as possible of the 4D-Var structure is maintained. The available observations, typically over the period of a 6-hour assimilation window, are compared with a model integration at high resolution. The comparison between observation and model is thus performed at the appropriate time: therefore the abbreviation 3D-FGAT (first-guess at appropriate time). This configuration is activated via the switch `LFGAT=.T.` in `namvar.h`.

3.2 3D-FGAT**3.2.1 Solution algorithm**

The tangent-linear model in 4D-Var evolves the analysis increment over time, within the assimilation window. In 3D-FGAT no such evolution takes place: one static increment is produced. The valid time of this increment is not at the initial time of the window as in 4D-Var, but at the central time. The increment is added to the background field, which forms the analysis at the central time. This has the consequence that a trajectory update from the start of the assimilation window cannot be performed. The 3D-FGAT configuration is therefore based on one single outer-loop without iteration. There are nevertheless two minimisation steps. The first provides analysis error and background error estimates required for cycling, and also pre-conditioning vectors (Hessian eigenvectors) that are used in the second minimisation job-step. The resolution of the first minimisation is typically lower (T42) than for the main one (e.g. T159).

Scatterometer de-aliasing is active and variational quality control is activated approximately halfway into the min-

imisation, rendering the problem non-linear (and the cost function non-quadratic). The use of conjugate-gradient minimisation is thus prevented. The **MIQN3** algorithm is used instead.

3.2.2 Main differences with respect to 4D-Var

The main differences with respect to the standard operational 4D-Var configuration are thus

- Variational quality control is carried out within the inner-loop iterations (LQVARQC=F.)
- The scatterometer de-aliasing is performed within the inner-loop iterations (LQSCAT=F.)
- Use of **MIQN3** instead of conjugate gradient minimisation, due to the cost-function being quadratic
- The Jc term relies on NMI (normal mode initialisation) rather than DFI (Digital filter initialisation), LJCDFI=F., LJCNMI=T..
- No iteration at outer-loop level.
- LTRAJHR=F., which means that the observation operators are linearized around the low-resolution trajectory, which is generated through an integration by the full non-linear model (at the resolution of the minimisation) at the beginning of the minimisation job-step. **CVA1** calls **CNT2** to do this.

3.2.3 Data selection

The observational data are stored in time-slots within the ODB (just as in 4D-Var). The data selection criteria are applied in identically the same way as in 4D-Var, allowing time sequences of data to be used also in 3D-FGAT. The 3D scheme is however unable to extract temporal information from the data, and produces an analysis of the temporal average of the FGAT departures. Optionally the screening data selection rules can be applied once for the entire (6-hour) assimilation window, which would pick only the data closes to the analysis centre time. This is called '3D-screening' and was the practice in the original operational 3D-Var configuration.

Part II: DATA ASSIMILATION

CHAPTER 4 Background term

Table of contents

- 4.1 Introduction
- 4.2 Description of the algorithm
- 4.3 Technical implementation
 - 4.3.1 Input files
 - 4.3.2 Namelist parameters of
 - 4.3.3 IFS routines
 - 4.3.4 Background error

4.1 INTRODUCTION

The background term described in *Courtier et al. (1998)* was in May 1997 replaced by a new formulation by *Bouttier et al. (1997)*, available online as newjb.ps. The old code is still part of the IFS but will not be described in this documentation.

4.2 DESCRIPTION OF THE ALGORITHM

We use the following notation:

- $\delta\mathbf{x}$ is the low-resolution analysis increment, i.e. model field departures from the background,
- \mathbf{B} is the assumed background error covariance matrix,
- ζ , η , (T, p_{surf}) and q are increments of vorticity, divergence, temperature and surface pressure, and specific humidity, respectively, on model levels.
- η_b and $(T, p_{\text{surf}})_{\text{bal}}$ are the *balanced* parts of the η and (T, p_{surf}) increments. The concept of balance will be defined below, and
- η_u and $(T, p_{\text{surf}})_{\text{unbal}}$ are the *unbalanced* parts of η and (T, p_{surf}) , i.e. $\eta - \eta_b$ and $[(T, p_{\text{surf}}) - (T, p_{\text{surf}})_{\text{bal}}]$, respectively.

The incremental variational analysis problem, Eq. (1.2) of Chapter 1, is rewritten in the space defined by the change of variable $\delta\mathbf{x} = \mathbf{L}\chi$ (Section 1.4) where \mathbf{L} satisfies $\mathbf{L}\mathbf{L}^T = \mathbf{B}$ so that J_b takes a simple form. In operational practice, the initial point of the minimization is the background, so that initially $\delta\mathbf{x} = \chi = 0$. The minimization can be carried out in the space of χ , where J_b is the euclidean inner product. At the end of the minimization, the analysis increments are reconstructed in model space by $\delta\mathbf{x} = \mathbf{L}\chi$. In order to compare with observations \mathbf{x} is reconstructed using Eq. (2.4), in each simulation. Thus the variational analysis can be done with L , the inverse change of variable from minimization space to model space (`chavarin`), without ever using `CHAVAR`.

The background-error covariance matrix \mathbf{B} is implied by the design of \mathbf{L} , which currently has the form

$$\mathbf{L} = \mathbf{K}\mathbf{B}_u^{1/2} \quad (4.1)$$

where \mathbf{K} is a balance operator going from the set of variables $\zeta, \eta_u, (T, p_{\text{surf}})_u$ and q , to the model variables $\zeta, \eta, (T, p_{\text{surf}})$ and q . The $\mathbf{B}_u^{1/2}$ operator is the right-hand symmetric square root of the background-error covariances \mathbf{B}_u of $\zeta, \eta_u, (T, p_{\text{surf}})_u$ and q , so that

$$\mathbf{B}_u = (\mathbf{B}_u^{1/2})^T \mathbf{B}_u^{1/2} \quad (4.2)$$

So far, the formulation is perfectly general. Now, we restrict \mathbf{B}_u to a simple form and choose a particular balance operator \mathbf{K} .

The covariance matrix \mathbf{B}_u is assumed to be block-diagonal, with no correlation between the parameters:

$$\mathbf{B}_u = \begin{bmatrix} \mathbf{C}_\zeta & 0 & 0 & 0 \\ 0 & \mathbf{C}_{\eta_u} & 0 & 0 \\ 0 & 0 & \mathbf{C}_{(T, p_{\text{surf}})_u} & 0 \\ 0 & 0 & 0 & \mathbf{C}_q \end{bmatrix} \quad (4.3)$$

It implies that the q analysis is independent from the other variables. However, assuming that the unbalanced variables are uncorrelated is not too restrictive because, as we shall see below, the design of the balance implies significant multivariate correlations between the meteorological variables.

Each autocovariance block in the above matrix is itself assumed to be block-diagonal in spectral space, with no correlation between different spectral coefficients, but a full vertical autocovariance matrix for each spectral coefficient. The vertical covariance matrices are assumed to depend only on the total wavenumber n . The resulting autocovariance model is homogeneous, isotropic and non-separable in grid-point space: the correlation structures do not depend on the geographical location, but they depend on the scale. The shape of the horizontal correlations is determined by the covariance spectra. The same representation was used in the previous J_b formulation (*Rabier and McNally 1993, Courtier et al. 1998*). The covariance coefficients are computed statistically using the NMC method (*Parrish and Derber 1992, Rabier et al. 1998*) on 24/48-hour forecast differences to estimate the total covariances for each total wavenumber n , and assuming an equipartition of errors between the $2n + 1$ associated spectral coefficients.

The balance relationship is arbitrarily restricted to the following form:

$$\begin{aligned} \eta_b &= \mathbf{M}\zeta \\ (T, p_{\text{surf}})_b &= \mathbf{N}\zeta + \mathbf{P}\eta_u \end{aligned} \quad (4.4)$$

So that the complete balance operator \mathbf{K} is defined by:

$$\begin{aligned} \zeta &= \zeta \\ \eta &= \mathbf{M}\zeta + \eta_u \\ (T, p_{\text{surf}}) &= \mathbf{N}\zeta + \mathbf{P}\eta_u + (T, p_{\text{surf}})_u \\ q &= q \end{aligned} \quad (4.5)$$

or equivalently, in matrix form:



$$\mathbf{K} = \begin{bmatrix} \mathbf{I} & 0 & 0 & 0 \\ \mathbf{M} & \mathbf{I} & 0 & 0 \\ \mathbf{N} & \mathbf{P} & \mathbf{I} & 0 \\ 0 & 0 & 0 & \mathbf{I} \end{bmatrix} \quad (4.6)$$

The matrix blocks \mathbf{M} , \mathbf{N} and \mathbf{P} are, in general, not invertible, but \mathbf{K} is. As explained above, the inverse of \mathbf{K} is not actually used in the variational analysis, because the initial point of the minimization is the background.

The matrix multiplication of \mathbf{B}_u by \mathbf{K} allows one to write explicitly the implied background error covariance matrix \mathbf{B} in terms of the meteorological variables ζ , η , (T, p_{surf}) and q :

$$\mathbf{B} = \mathbf{K}\mathbf{B}_u\mathbf{K}^T = \begin{bmatrix} \mathbf{C}_\zeta & \mathbf{C}_\zeta\mathbf{M}^T & \mathbf{C}_\zeta\mathbf{N}^T & 0 \\ \mathbf{M}\mathbf{C}_\zeta & \mathbf{M}\mathbf{C}_\zeta\mathbf{M}^T + \mathbf{C}_{\eta_u} & \mathbf{M}\mathbf{C}_\zeta\mathbf{N}^T + \mathbf{C}_{\eta_u}\mathbf{P}^T & 0 \\ \mathbf{N}\mathbf{C}_\zeta & \mathbf{N}\mathbf{C}_\zeta\mathbf{M}^T + \mathbf{P}\mathbf{C}_{\eta_u} & \mathbf{N}\mathbf{C}_\zeta\mathbf{N}^T + \mathbf{P}\mathbf{C}_{\eta_u}\mathbf{P}^T + \mathbf{C}_{(T, p_{\text{surf}})_u} & 0 \\ 0 & 0 & 0 & \mathbf{C}_q \end{bmatrix} \quad (4.7)$$

The blocks implied by \mathbf{C}_ζ and its transforms by the balance operator blocks \mathbf{M} , \mathbf{N} and \mathbf{P} are the *balanced* parts of the covariances. For instance, the vorticity covariances \mathbf{C}_ζ and the unbalanced temperature covariances $\mathbf{C}_{(T, p_{\text{surf}})_u}$ are both homogeneous and isotropic, whereas the $\mathbf{N}\mathbf{C}_\zeta\mathbf{N}^T$ ‘vorticity-balanced’ (T, p_{surf}) matrix term depends on latitude—it is predominant in the extratropics, negligible near the equator. The $\mathbf{N}\mathbf{C}_\zeta$ term is responsible for the geostrophic mass/wind coupling.

The \mathbf{M} , \mathbf{N} and \mathbf{P} operators used to define the balance have a restricted algebraic structure. \mathbf{M} and \mathbf{N} are both the product of a so-called horizontal balance operator \mathcal{H} by vertical balance operators \mathcal{M} , \mathcal{N} :

$$\begin{aligned} \mathbf{M} &= \mathcal{M}\mathcal{H} \\ \mathbf{N} &= \mathcal{N}\mathcal{H} \end{aligned} \quad (4.8)$$

The \mathcal{H} operator is a block–diagonal matrix of identical horizontal operators transforming the spectral coefficients of vorticity, independently at each level, into an intermediate variable P_b which is a kind of linearized mass variable defined below. The horizontal operators in \mathcal{H} have exactly the same algebraic structure as the standard analytical linear balance on the sphere, and this is where the latitudinal variations of the J_b structures come from: in spectral space,

$$P_b(n, m) = \beta_1(n, m)\zeta(n, m + 1) + \beta_2(n, m)\zeta(n, m - 1) \quad (4.9)$$

The \mathcal{M} , \mathcal{N} and \mathbf{P} operators all have the same structure: block-diagonal, with one full vertical matrix per spectral component. The vertical matrices depend only on the total wavenumber n .

The actual calibration of the J_b operator requires the following 4 steps; each one uses a set of 24/48-hour-range forecast differences as surrogates to background error patterns in order to calculate the statistics:

- 1) **\mathcal{H} operator.** The horizontal balance coefficients (β_1, β_2) of \mathcal{H} are computed by a linear regression between the errors in vorticity and in linearized total mass P_{tot} , assuming the functional relationship defined by the above equation, and building P_{tot} from (T, p_{surf}) using the linearized hydrostatic relationship at level l ,

$$P_{\text{tot}}(l) = \sum_{i=L}^l RT_i \Delta \ln p_i + RT_{\text{ref}} \ln p_{\text{surf}} \quad (4.10)$$

which relies on the definition of the model vertical geometry and of reference values for (T, p_{surf}) . We use (270 K, 800 hPa) currently. The sensitivity to the somewhat arbitrary choice of these parameters has been tested and it is negligible. Unlike in the previous J_b formulation, P_b is just an intermediate variable in the linear regression. Modifying the reference values, e.g. to (300 K, 1000 hPa), does change the scaling of \mathcal{H} , but it is compensated by corresponding changes in the \mathcal{M} and \mathcal{N} operators, so that the effective covariances are virtually unchanged.

- 2) **\mathcal{M} operator.** The vertical blocks $\mathcal{M}(n)$ of this operator are computed for each wavenumber n by a linear regression between the spectral vertical profiles $[P_b]_n^m$ and $[\eta]_n^m$, respectively, of balanced mass P_b (defined as \mathcal{H} times the vorticity error patterns) and divergence. The relationship is assumed to be

$$[\eta]_n^m = \mathcal{M}(n)[P_b]_n^m \quad (4.11)$$

so that the statistical sampling is better for the small scales than for the large scales because there are $2n + 1$ spectral profiles to be used per total wavenumber in each forecast error pattern. At least as many independent error patterns as number of model levels are needed in order to have a well-posed regression problem for the very large scales.

- 3) **\mathcal{N} and \mathbf{P} operators.** The vertical blocks are computed for each wavenumber exactly like \mathcal{M} , except that now the linear regression goes from the vertical spectral profiles of $P_b = \mathcal{H}\zeta$ and $\eta_u = \eta - M\zeta$ to the profiles of temperature concatenated with surface pressure:

$$[(T, p_{\text{surf}})]_n^m = \mathcal{N}_n[P_b]_n^m + P_n[\eta_u]_n^m \quad (4.12)$$

One notes that the \mathcal{N}_n matrix is not square (the output is larger than the input because there is a kernel in the hydrostatic relationship) but the resulting (T, p_{surf}) covariances are still positive definite by construction thanks to the $C_{(T, p_{\text{surf}})_u}$ term in the expression of \mathbf{B} .

- 4) **Error covariances.** The vertical autocovariances of the ζ , η_u , $(T, p_{\text{surf}})_u$ and q , difference patterns are computed for each total wavenumber n . Again, since there are $2n + 1$ wavenumbers for each n and each error pattern, at least as many linearly independent error patterns as model levels (plus one for p_{surf}) *must* be used in order to ensure that the autocovariances are positive definite at the very large scales. It is strongly advised to use several times more in order to reduce the sampling noise at large scales; this is important for the performance of the resulting assimilation/forecast system. In the May 1997 implementation of the 3D-Var system, about 180 forecast-difference patterns have been used for 31 levels.

In addition to these 4 steps, some minor preprocessing is performed on the covariances. The vertical correlations of humidity are set to zero above 100 hPa in order to avoid spurious stratospheric humidity increments because of the tropospheric observations. The ζ , η_u and $(T, p_{\text{surf}})_u$ vertical profiles of total variance are rescaled by an arbitrary factor of 0.9 in order to account for the mismatch between the amplitudes of the 24/48-hour-forecast differences and of the 6-hour forecast errors. In the future this factor will be recalculated more precisely using observation departures from the background in the assimilation, similarly to [Hollingsworth and Lönnerberg \(1986\)](#). It may be different for 3D-Var than for 4D-Var. The variance spectra are slightly modified in order to ensure that



the horizontal error correlations of ζ , η_u and $(T, p_{\text{surf}})_u$ are compactly supported (they are set to zero beyond 6000 km). This operation removes the residual sampling noise in the error covariances. No other processing is performed except for a spectral truncation if the analysis resolution is lower than the statistics resolution (currently T106). It would be easy to extrapolate the statistics to higher resolutions, but it would be very hazardous to alter the vertical geometry of the covariances and balance operators. Instead, it is recommended to run a set of forecasts using a model with the right vertical resolution, and recompute all the statistics from scratch.

4.3 TECHNICAL IMPLEMENTATION

The statistical calibration is done using dedicated scripts outside the IFS code. First, the 24/48-hour forecast error differences for a set of dates are constructed in terms of spectral ζ , η , $(T, p_{\text{surf}})_u$ and q . This involves running a set of MARS requests and building the required GRIB files. Then, the forecast-error differences are read and processed by a Fortran statistics program that finally writes two files in GSA format: one with the coefficients of the balance operator, one with the error covariances of ζ , η_u , $(T, p_{\text{surf}})_u$ and q . These files take up a couple of megabytes. They are computed for a given triangular truncation and number of levels (currently T106L31). In the covariance file there are 4 sets of vertical covariance matrices. The balance files contain one set of coefficients for the \mathcal{H} operator, and three sets of vertical balance matrices for \mathcal{M} , \mathcal{N} and \mathbf{P} .

4.3.1 Input files

The IFS needs these two GSA files to use \mathcal{J}_b in e.g. the incremental analysis jobs. The \mathcal{J}_b configuration described here corresponds to namelist switch LSTABAL=.true. (NAMJG), and it is identified in the \mathcal{J}_b code by the string CDJBTYPE='STABAL96'. LSTABAL=.false. would give the old \mathcal{J}_b formulation. The input files must be named **stabal96.cv** and **stabal96.bal**. They are read in by **subjdat** and **subjbal**, respectively.

4.3.2 Namelist parameters of \mathcal{J}_b

Some other important namelist options in NAMJG are LCFCE (to enforce uniform background errors), L3DBGERR (to have a 3D distribution vorticity background errors), and LCORCOSU (to enforce compactly supported horizontal correlations). The switch LGUESS in NAMCT0 can be used to switch \mathcal{J}_b off altogether. The default is LGUESS=.true., i.e. \mathcal{J}_b switched on.

(This is the J_b setup code tree in IFS cy16r3, option stabal96)
 (namelist namjg has already been read into yomjg in routine subj below su0yoma)

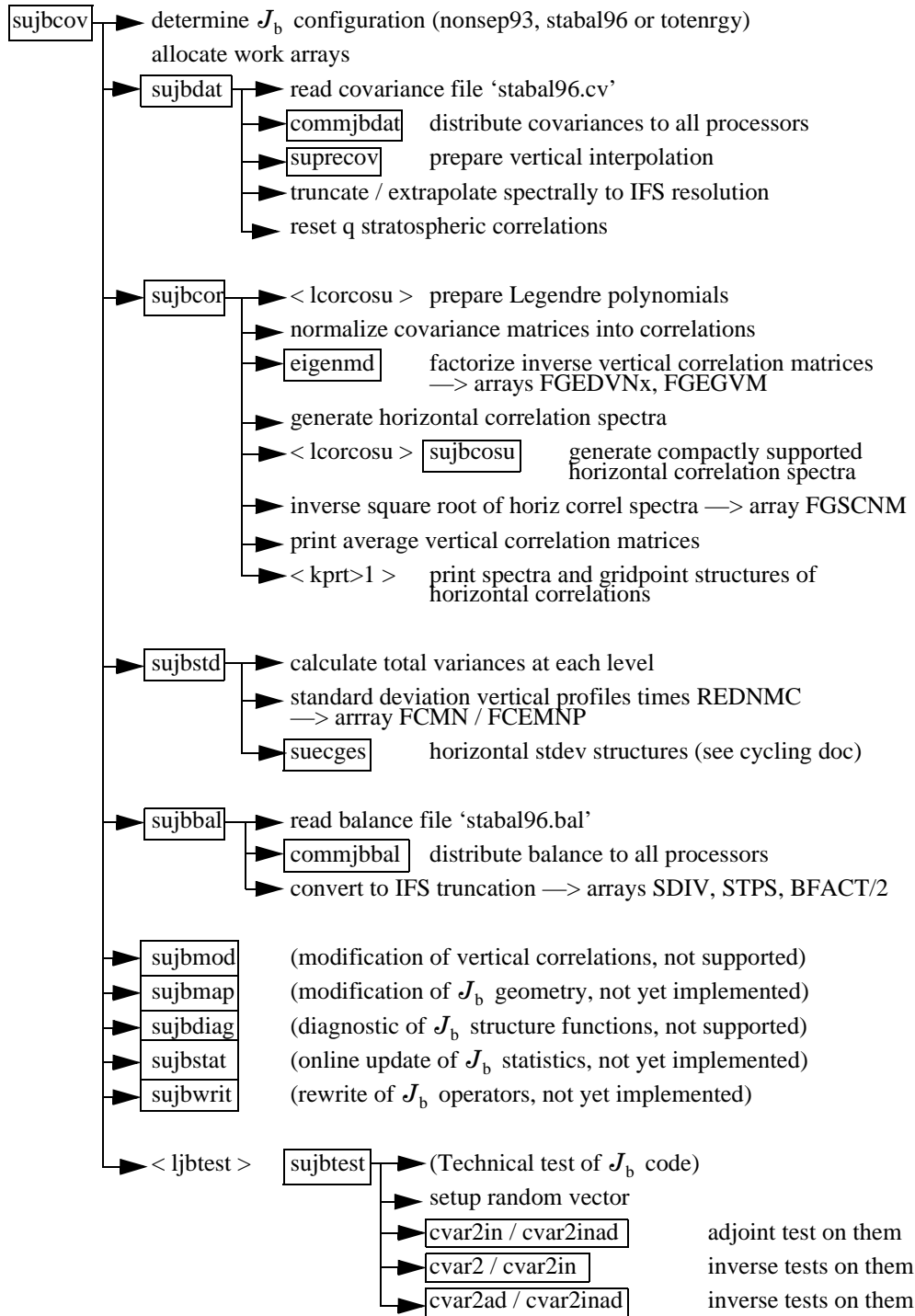


Figure 4.1 Calling tree for subroutine `subjcov`.

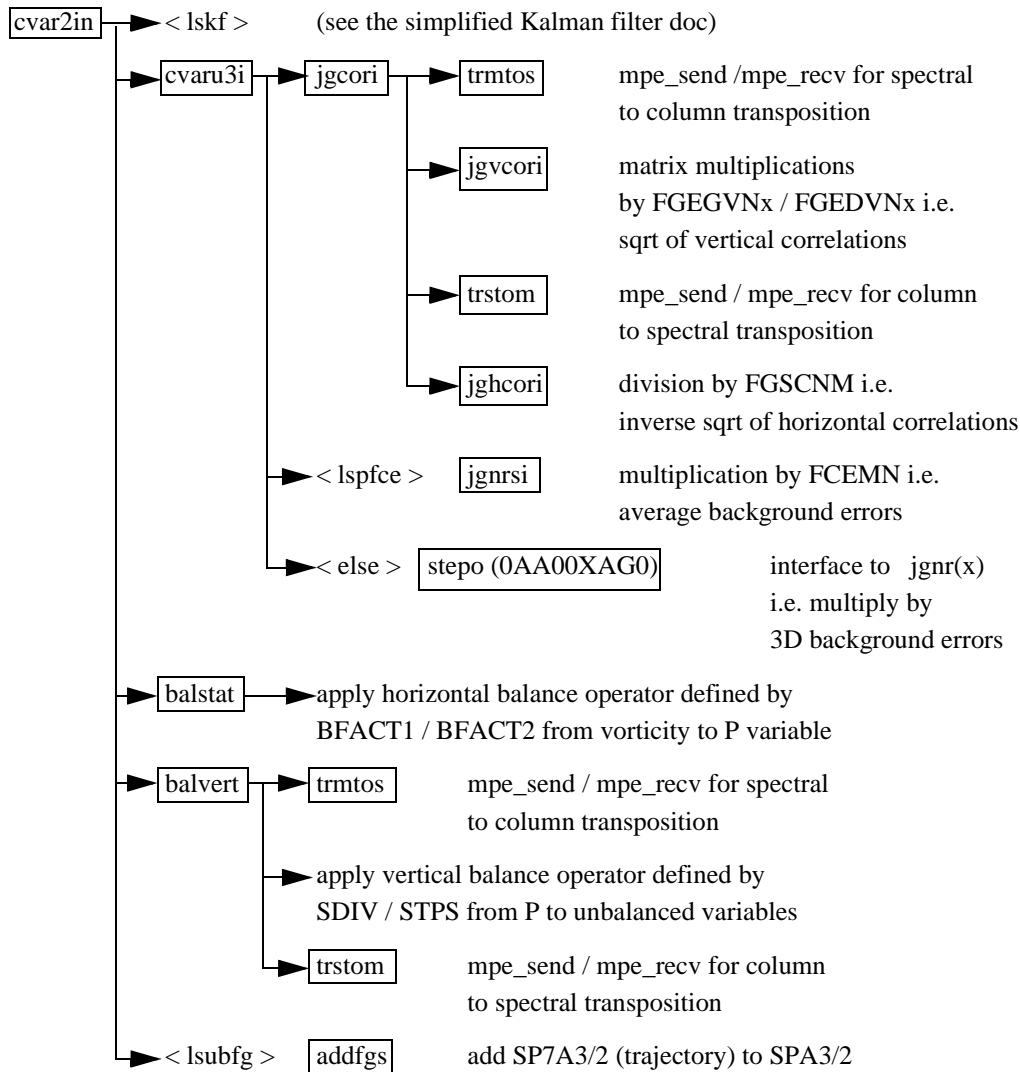
4.3.3 IFS J_b routines

Inside the IFS code, J_b is localized in the setups below subroutine `sujbcov` and in the inverse change of variable `cvar2in` (and its adjoint and their inverses, `CVAR2INAD`, `CVAR2` and `CVAR2AD`). Calling trees are shown in Fig. 4.1 and Fig. 4.2. The computation of the cost function and its adjoint is done in `sim4d` (Section 2.3 in Chapter 2) --it is planned to move it to a dedicated subroutine. The sequence within the set-up routine is the following:

- (i) **SUJBDAT**: Reads covariances from file `stabal96.cv`,
Interpolates in the vertical to the model's vertical levels (if necessary)
Sets humidity correlations to 0, for pressures less than 100 hPa.
- (ii) **SUJBCOR**: Sets up spectral correlation operator
Covariance matrices (one per n) are converted to vertical correlation matrices and horizontal autocorrelation spectra. The eigenvectors and the eigenvalues of vertical correlations matrices are computed using `EIGENMD` and stored in `FGEDVNS` and `FGEGVNS`-arrays (`yomjg`), respectively, for later use in `JGVCOR`, `JGVCORI`, `JGVCORAD` and `JGVCORIAD`. The horizontal autocorrelation spectra are stored in the `FGSCNM`-array (`yomjg`), for later use in `JGHCOR` and `JGHCORI`.
- (iii) **SUJBSTD**: Set up background error standard deviations, see Subsection 4.3.4.
- (iv) **SUJBBAL**: Set up balance constraint. Read the file `stabal96.bal` and store in `yomjg`, for later use in `balstat`, `balstatad`, `balvert`, `balvertad`, `balverti` and `balvertiad` as part of the change of variable operator.
- (v) **SUJBTEST**: Test of the adjoint of the change of variable, if `LJBTEST=.true`.

The distributed memory affects the setups below `sujbdat` and `sujbbal` when the data files are read in (by the master processor only). First, the resolution of the files is read, then the relevant arrays are allocated and the actual data is read, truncated if necessary, and broadcast. The code is designed to work at any resolution.

In the change of variable, there is a transposition of the fields between the horizontal and vertical balance operators, `balstat` and `balvert`, respectively. Note that the operator L is performed by calling `cvar2in`, so in IFS parlance L corresponds to the *inverse* change of variable.


 Figure 4.2 Calling tree for subroutine `cvar2in`.

4.3.4 Background error σ_b

The background standard errors are set up below `subjstd` (in `SUINFCE`, called from `SUECGES`) and used in `jgnr` or `jgnrs` (and their adjoint and inverses, `jgnrad` and `jgnrsi`). In addition to the covariance files, they use a gridpoint GRIB file called `errgrib` in order to specify the three-dimensional error patterns. The data from the file is converted to the appropriate parameters and resolution if needed. The background error fields for some parameters (wind, height, temperature and surface pressure) are built for the screening job although they are not needed in the analysis itself. For more information, refer to the chapter on the cycling of background errors, [Chapter 6](#).

4.3.4 (a) Humidity. The humidity background errors are currently not cycled – they are computed (in `SUSHFCE` under `JGNR`) by a simple empirical formulation as a function of the temperature T^b and relative humidity U^b of the background:

$$\sigma_b = -0.002T^b - 0.0033|T^b - 273| + 0.25U^b - 0.35|U^b - 0.4| + 0.70 \quad (4.13)$$

$$\sigma_b = \min[0.18, \max(0.06, \sigma_b)] \quad (4.14)$$

The standard deviation in terms of relative humidity is then converted to specific humidity, taking the variation of q of the equation

$$q = \frac{Ue_{\text{sat}}}{\frac{1}{\varepsilon}p - U\left(\frac{1}{\varepsilon} - 1\right)e_{\text{sat}}} \quad (4.15)$$

where U is the relative humidity, $\varepsilon = R_{\text{dry}}/R_{\text{vap}}$, e_{sat} is the saturation water-vapour pressure at the temperature in question (Tetens' formula, Eq. (5.11) in Chapter 5) and p is pressure.

Humidity increments are forced to be negligibly small above the tropopause to avoid a systematic drift of stratospheric humidity over extended periods of data assimilation. This is achieved by setting a very low value of 10^{-8} for σ_b everywhere the pressure is lower than 70hPa, and at any other point where the pressure is lower than 500hPa and the background temperature and pressure fields are such that the square of the buoyancy frequency exceeds $2 \times 10^{-4} \text{ s}^{-2}$ everywhere between that level and the 70hPa level.

More specifically, for each grid column σ_b is set to 10^{-8} for model levels k such that $k \leq K$, where the level K is determined by requiring either that it is the highest level with $p_K^b \geq 70$ hPa for which

$$\frac{p_{K+1}^b(T_{K+2}^b - T_K^b)}{T_{K+1}^b(p_{K+2}^b - p_K^b)} + \frac{R_{\text{dry}}T_{K+1}^b}{g^2}(2.5 \times 10^{-4}) > \kappa \quad (4.16)$$

or, if no such level can be found for p_K^b in the range from 500 to 70hPa, that it is the lowest level for which

$$p_K^b \leq 500 \text{ hPa}.$$

Here T_K^b and p_K^b are the background temperature and pressure at level K of the grid-column.

In addition, any values of σ_b lower than 10^{-8} are reset to 10^{-8} .

For pressures less than $p_0 = 800$ hPa, and over the sea, the model of background errors above is modified by

$$\sigma_{\text{mod}} = \sigma_b \left\{ 1 - \alpha + \alpha \exp \left[- \left(\frac{p^b - p_0}{b} \right)^2 \right] \right\} \quad (4.17)$$

where $\alpha = 0.5(1 - \text{LSM})$ (where LSM = land-sea mask) and $b = 12500$.





Part II: DATA ASSIMILATION

CHAPTER 5 Observation operators and the observation cost function (J_o)

Table of contents

- 5.1 Introduction
 - 5.1.1 Data selection controls, and the interface to the blacklist
- 5.2 Horizontal interpolation to observation points
 - 5.2.1 Method
 - 5.2.2 Storage in GOM-arrays
- 5.3 Computation of the observation cost function
 - 5.3.1 Variable numbers and association with observation operators
 - 5.3.2 Organization in observation sets
 - 5.3.3 Cost function
 - 5.3.4 J_o tables
 - 5.3.5 Correlation of observation error
- 5.4 Variational quality control
 - 5.4.1 Description of the method
 - 5.4.2 Implementation
- 5.5 observation operators - General
- 5.6 The observation operator for conventional data
- 5.7 Satellite observation operators
 - 5.6.1 Geopotential height
 - 5.6.2 Wind
 - 5.6.3 Humidity
 - 5.6.4 Temperature
- 5.7 Satellite observation operators
 - 5.7.1 Set-up of the radiative-transfer code
 - 5.7.2 Radiances
 - 5.7.3 Thicknesses
 - 5.7.4 Precipitable water from SATEM and SSM/I
 - 5.7.5 Ozone-layer retrievals from satellites
 - 5.7.6 Scatterometer winds

5.8 Surface observation operators

5.8.1 Mathematical formulation

5.8.2 Surface values of dry static energy

5.8.3 Transfer coefficients

5.8.4 Two-metre relative humidity

5.1 INTRODUCTION

The observation operators provide the link between the analysis variables and the observations (*Lorenc, 1986, Pailleux, 1990*). The observation operator is applied to components of the model state to obtain the model equivalent of the observation, so that the model and observation can be compared. The operator H in Eq. (1.4) signifies the ensemble of operators transforming the control variable \mathbf{x} into the equivalent of each observed quantity, \mathbf{y}^o , at observation locations. The 3D/4D-Var implementation allows H to be (weakly) non-linear, which is an advantage for the use of satellite radiance data, scatterometer data with aliased wind direction, cloud and precipitation data, for example. In this chapter we define the content of each of the IFS observation operators and the associated controls for all data used in 3D/4D-Var. The calculation of departures and the J_o costfunction are also described.

The IFS observation operators are generic in the sense that the same routine is often used for several different data types. For example, the radiance operator (RTTOV) simulates measurements from a large number of satellite radiometers (microwave and infrared), and the temperature operator (PPT) is used for TEMP, AIREP, and other data types and it is also used to provide input to RTTOV. Similarly the routine PPQ is used for interpolation of specific humidity to given pressures, but it can also be used for any other atmospheric mixing ratio constituents, such as ozone and carbon dioxide. Note that many of the PP-routines were developed for the model's pressure-level post-processing package and are used also in that context.

In Table 10.3 there is a list of the observing systems currently used by 4D-Var in ECMWF's operational data assimilation suite. The table also indicates important restrictions on data usage and thinning of data. The observation errors are also given in Chapter 10. In 4D-Var, the evolving model state is compared to the available observations at the correct time, currently at half-hourly intervals. These intervals are called *time-slots*. The Observation Data Base (see ODB documentation) holds the observations organized by time slots. If there are multiple reports from the same fixed observing station within a time slot then the data nearest the analysis time are selected for use in the analysis. Some thinning is applied for satellite data and other moving platforms reporting frequently. The thinning rules are applied to each time slot, separately. The thinning, quality control and data selection tasks are performed in the *screening* job step of 4D-Var - it is described in Chapter 10.

5.1.1 Data selection controls, and the interface to the blacklist

Most data selection criteria are coded in so called *blacklist files*, written in a convenient, readable blacklist language (see the Blacklist Documentation, *Jarvinen et al. 1996*). The blacklist mechanism is very flexible and allows nearly complete control of which data to use/not use in the assimilation. The 'monthly blacklist' is the part of the blacklist that is based on operational data monitoring results, and it is maintained by the Meteorological Operations Section. The blacklist is consulted in the screening job. The interface is set up in BLINIT, in such a way that a number of named items from the header (Table 5.1) and body (Table 5.2) parts of the observation report can be passed to the blacklist software. Depending on the blacklisting criteria flags are communicated to the routine BLACK, and those are written to the ECMA ODB data base. Blacklist-rejected data are subsequently excluded from the CCMA ODB and will not be present in the minimisation job steps. Data selection rules should be coded in the blacklist files

whenever possible rather than in the IFS code itself. The operational blacklist history is kept in an archive.

TABLE 5.1 HEADER VARIABLES FOR THE IFS/BLACKLIST INTERFACE

Index	Name	Description
1	OBSTYP	observation type
2	STATID	station identifier
3	CODTYP	code type
4	INSTRM	instrument type
5	DATE	date
6	TIME	time
7	LAT	latitude
8	LON	longitude
9	STALT	station altitude
10	LINE_SAT	line number (atovs)
11	RETR_TYP	retrieval type
12	QI_1	quality indicator 1
13	QI_2	quality indicator 2
14	QI_3	quality indicator 3
15	MODORO	model orography
16	LSMASK	land-sea mask (integer)
17	RLSMASK	land-sea mask (real)
18	MODPS	model surface pressure
19	MODTS	model surface temperature
20	MODT2M	model 2m temperature
21	MODTOP	model top level pressure
22	SENSOR	satellite sensor indicator
23	FOV	field of view index
24	SATZA	satellite zenith angle
25	NANDAT	analysis date
26	NANTIM	analysis time
27	SOE	solar elevation
28	QR	quality of retrieval
29	CLC	cloud cover
30	CP	cloud top pressure
31	PT	product type

Classes of data can also be switched on and off using the NOTVAR array in **NAMJO**, however it is preferable to use the blacklist mechanism for this purpose. The second dimension in this array is the observation type. The first dimension is the variable number (NVAR, see below). The elements of the NOTVAR array can take either of two

values: 0, means that the data will be used; -1, means that the data will not be used.

TABLE 5.2 BODY VARIABLES FOR THE IFS/BLACKLIST INTERFACE

Index	Name	Description
1	VARIAB	variable name
2	VERT_CO	type of vertical coordinate
3	PRESS	pressure, height or channel number
4	PRESS_RL	reference level pressuer
5	PPCODE	synop pressure code
6	OBS_VALUE	observed value
7	FG_DEPARTURE	first guess departure
8	OBS-ERROR	observation error
9	FG_ERROR	first-guess error
10	WINCHAN_DEP	window channel departure
11	OBS_T	observed temperature

5.2 HORIZONTAL INTERPOLATION TO OBSERVATION POINTS

5.2.1 Method

Currently it is assumed that each observation equivalent can be computed from a single vertical profile of model data. That is, it is assumed that each observation operator can be written as $H = H_v H_h(\mathbf{x})$ where H_h is horizontal interpolation of model data to the location of the observation. H_h is performed for all observations within a time-slot directly after the corresponding model time step has been performed. The output of H_h is a vertical profile of model data for each observation location. These profiles are stored in a data structure call GOM-arrays, and used later in the vertical part of the observation operator H_v performed in HOP, called from OBSV. This organisation does not permit horizontal averaging of model data over large satellite foot prints (for example). It also does not permit horizontal integration as will be required for limb-sounding and radio-occultation data. For a future release of IFS it is planned to extend the GOM-profile concept to GOM-planes. The orientation of the planes (one vertical plane per observation) would be determined by the satellite viewing geometry. The H_v operator for those data would receive the vertical plane of model data as input.

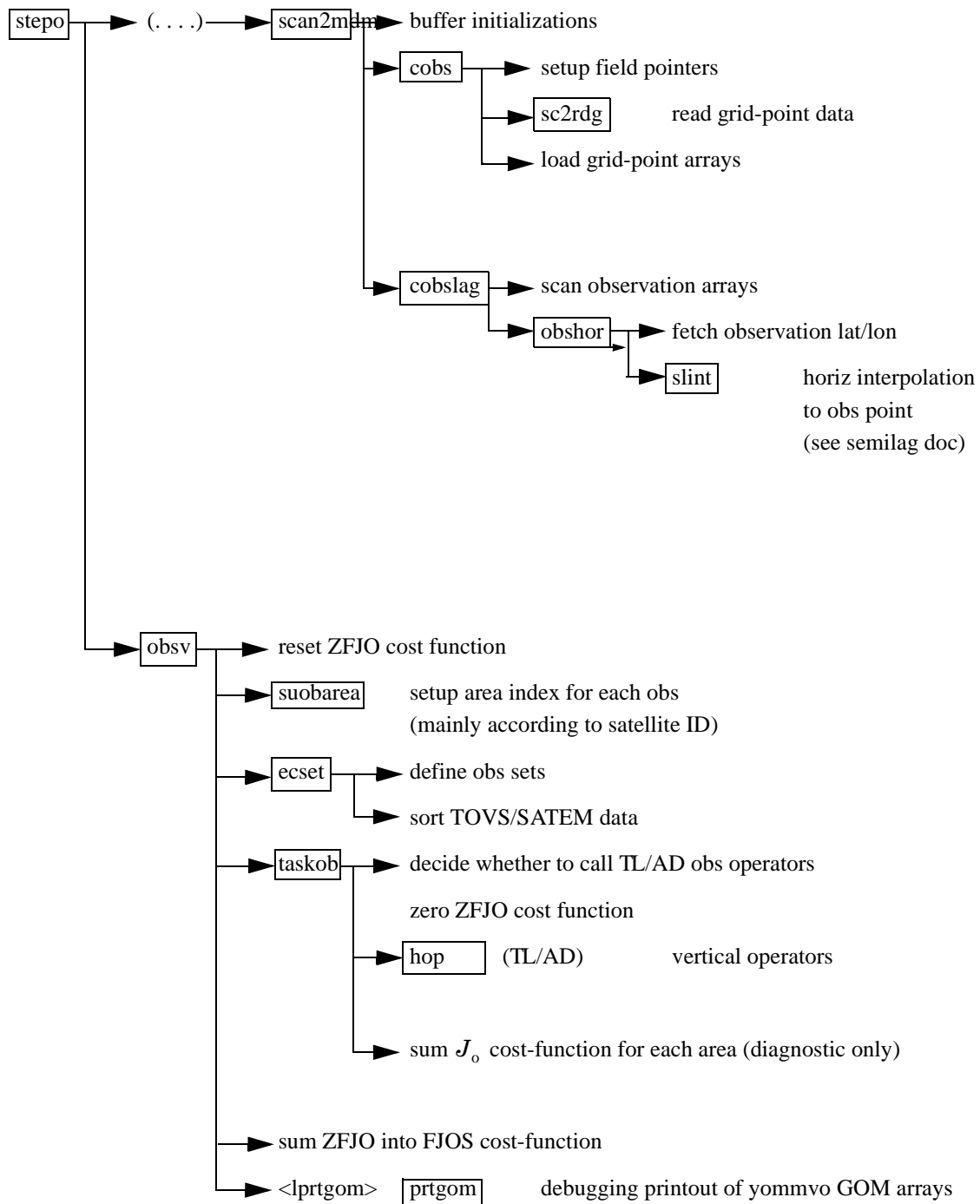


Figure 5.1 Flow diagram for subroutines `scan2mdm` and `obsv`.

COBSLAG is the master routine for the horizontal interpolation of model data to observation points. It is called after the inverse spectral transform in **SCAN2MDM**, and after the so-called *semi-Lagrangian buffers* have been prepared by **COBS** and **SLCOMM2**, see the flow diagram in Fig. 5.1. The interpolation code is shared with the semi-Lagrangian advection scheme of the dynamics. The buffers contain a *halo* of gridpoints big enough to enable

interpolation to all observations within the grid-point domain belonging to the processor. **COBSLAG** calls **OB-SHOR** which:

- Performs the interpolation, using **SLINT**
- Message-passes the result to the processors where the corresponding observations belong, and copies the model data at observation points to the so-called GOM-arrays (**yommvo**, described below) using the routine **MPOBSEQ**.

There are three methods of horizontal interpolation:

- 1) **LAIDDIOPS** 12-point bi-cubic interpolation, used for all upper-air fields (if **NOBSHOR=203**) except clouds,
- 2) **LAIDDIOPS** Bi-linear interpolation, used for surface fields, and
- 3) **LAIDLIC**: Nearest gridpoint, used for cloud parameters.

The interpolation method for the upper-air fields can be switched to bi-linear by specifying **NOBSHOR=201** in **namobs**. The default is **NOBSHOR=203** (bi-cubic) for the trajectory jobs, but **NOBSHOR=201** (bi-linear) in the minimisation jobs. Lists of interpolation points and weights are prepared by the routine **LASCAW**. In 4D-Var bi-cubic interpolation is used at high resolution (i.e. in the trajectory runs), and bi-linear is used at low resolution (i.e. in the main minimization). The interpolation is invoked once per 4D-Var time slot.

The adjoint (**OBSHORAD**) follows the same general pattern but gets further complicated by the fact that the gradient from several observations may contribute to the gradient at a given gridpoint. The summation of gradients is to done in the same order, irrespective of the number of processors, as reproducibility is desired (strictly speaking, overall 4D-Var reproducibility is only ensured if the so called reproducibility switch is ON. This adds to computational cost, and the default is OFF). Tables for managing this are prepared in **MKGLOBSTAB**.

5.2.2 Storage in GOM-arrays

The GOM arrays (**YOMMVO**) contain vertical profiles of model values at observation points. There are namelist-switches to control which upper-air model variables will appear in the GOM-arrays. There are five categories of GOM-arrays:

- **GOMx** for conventional data, containing full model profiles of optionally u , v , T , q , O_3 (ozone), CLW (cloud liquid water), CLI (cloud ice) and CC (cloud cover)
- **GOSx** for conventional data, containing surface data of p_{surf} (surface pressure), T_{skin} (skin temperature), w_s (soil water content), s_n (snow cover), z_0 (roughness length) and w_l (skin reservoir water content).
- **GSMx** for satellite radiance data, containing full model profiles similar to **GOMx**
- **GSSx** for satellite radiance data, containing surface data of p_s , T_s , w_s , s_n , z_0 , w_l , u_l and v_l , where u_l and v_l are lowest model level wind components.
- **GSCx** for SCAT data, containing lowest model level data of u_l , v_l , T_l , and q_l , and surface data of p_s , T_s and z_0 .

The reason for this split is purely to save on memory space. Model profiles of wind for example are not needed as inputs to the radiance observation operator (RTTOV), so those fields are not interpolated to the satellite radiance locations, and are not stored, unless requested. Upper-air profiles of model data at SCAT locations are also not computed. The selection of model variables to interpolate to **GOMx** and **GSMx** arrays, respectively, is flexible and is controlled through namelist switches **LGOMx** and **LGSMx** (in **namdim**). The default is that only **LGOM-U/V/T/Q** and **LGSM-T/Q/O3** are ON, with the addition of **LGSMCLW/CLI/CC** in screening run to enable computation of cloudy radiances. The addressing of the GOM-arrays is done by referring to the **MAPOMM** (**YOMOBA**) and **MABNOB** (**YOMOBSET**) tables, e.g. **ZPS(jobs) = GOSP(MAPOMM(iabnob))**, where **iabnob = MAB-**



NOB(jobs,kset) is an observation counter local to each processor.

The trajectory GOM5 arrays (identical to GOM) are allocated in the case that tangent linear observation operators are used. They are to hold the trajectory interpolated to the observation locations, and the GOM-arrays, in that case, hold the perturbations.

At the end of the adjoint observation operators the GOM-arrays are zeroed and overwritten by the gradient (in **PRE-INTAD**).

The r.m.s. of the GOM arrays is printed (by **PRTGOM**) if the switch LPRTGOM=.true., (in **YOMOBS**). The default is that the print is switched on. It can be located in the log file by searching for ‘RMS OF GOM’. The printing is done from **OBSV**, 1) when the GOM arrays contain the background interpolated to the observation points, 2) when it contains ∇J_o of the first simulation, 3) when it contains first TL perturbations after the initial call to the minimizer and 4) when it contains ∇J_o at the final simulation.

5.3 COMPUTATION OF THE OBSERVATION COST FUNCTION

The cost function computation follows the same pattern for all observational data. This common structure is described in the following section. It is assumed that all observations are independent of each other, which means that the cost function contribution from each observation station can be computed independently of others. That is to say that there is (currently) no provision for observation error correlation between reports.

5.3.1 Variable numbers and association with observation operators

In the ODB each observed value is associated with a vertical position (‘press’ with pointer MDBPPP, given in terms of pressure, height or channel number) and a variable number (‘varno’ with pointer MDBVNM). The defined variable numbers are listed in the array NVNUMB as described in the ODB documentation. The variable number indicates which physical quantity has been observed. Each observed quantity is linked to an IFS observation operator (in **HVNMTLT**). In the case there is no corresponding observation operator in IFS, no observation equivalent will be computed, and the observation will be rejected from further processing. Each available observation operator has been given a number (NVAR) and a short name (CVAR_NAME, three characters), set in **YOMCOSJO**.

There are currently JPXVAR = 25 operator names defined: U, U10, DD, FF, H, H2, T, Z, DZ, LH, T2, TS, RAD, SN, RR, PS, CC, CLW, Q, FFF, S0, X, PWC, TO3 and TCW, numbered sequentially in NVAR. Each number can be referenced by variables such as NVAR_U(=1), NVAR_U10(=2) and so on. Based on the ODB variable number for each observation, which has been associated with an observation-operator number and name, **HOP** calls the appropriate observation operator routine. For example, observations with ODB variable number = NVNUMB(8), will in **HVNMTLT** be associated with NVAR_T = 7 and CVAR_NAME(7) = ‘T’, and **HOP** will thus call the sub-routine **PPT**.

In the log file CVAR_NAME is used to label entries in the Jo-table. The Jo-table shows the Jo-values for each observation sub-type, for each observation operator (NVAR). RMS of observation error and background error are also shown. See the Section on Jo-tables below.

TABLE 5.3 ASSOCIATION BETWEEN VARIABLE NUMBERING AND OBSERVATION OPERATOR ROUTINES. THE CVAR-NAMES ALSO APPEAR IN THE PRINTED JO-TABLE IN THE LOG-FILE

NVAR	CVAR_NAME	Observation operator routine	Description
1	U	PPUV	Upper air wind components
2	U10	PPUV10M	10-metre wind components
3	DD		Wind direction
4	FF	PPUV	Wind speed
5	H	PPRH	Relative Humidity
6	H2	PPRH2M	2-metre relative humidity
7	T	PPT	Temperature
8	Z	PPGEOP	Geopotential
9	DZ	PPGEOP	Thickness
10	LH	PPRH	Layer mean RH (Meteo-France)
11	T2	PPT2M	2-metre temperature
12	TS		Surface temperature (M-France)
13	RAD	RADTR	Radiance data
14	SN		Snow (M-France)
15	RR		Rain rate (Meteo-France)
16	PS	PPPS	Surface pressure
17	CC	PPTCC	Cloud cover
18	CLW	PPCLW	Cloud liquid water
19	Q	PPQ	Specific humidity
20	FFF	PPUV10M	10-metre wind speed
21	S0		Sigma_0
22	X		Reserved
23	PWC	PPPWC	Layer water content or TCWV
24	TO3	PPPWC	Layer ozone content
25	TCW		Layer cloud water content

5.3.2 Organization in observation sets

The vertical observation operators are vectorized over NMXLLEN (yomdim0) data. To achieve this the data first have to be sorted by type and subdivided into sets of lengths not exceeding that number. NMXLLEN is currently set to 511, in **SUDIMO**. The observation sets may span several 4D-Var time slots, as the input to the observation operators is the GOM-arrays which have been pre-prepared for all time slots during the tangent linear model integration. However, in the current operational context this is not the case, as OBSV.F90 is called once per time slot. Furthermore, on the current IBM machines long vector loops are not very important for performance, our IBMs being scalar machines.

The organization of the sets is done in **ECSET** and **SMTOV** and the information about the sets is kept in **yomobset**.

Radiance observation sets (e.g. ATOVS, AIRS, SSMI) must not contain data from more than one instrument. That is to say that inside **HOP**, **HOPTL** and **HOPAD** (and routines called from there) data from several instruments are not mixed - different instrument are handled in separate calls. This is controlled by sorting according to the `area`-parameter, which for radiance data is an indicator of satellite ID and instrument, prior to forming the sets. The `area`-parameter is determined in **SUOBAREA**, and is irrelevant for the observation processing for all data other than the radiance data.

5.3.3 Cost function

The master routine controlling the calls to the individual observation operators is called **HOP**. This routine deals with all different types of observations.

The **HOP/HOPTL/HOPAD** routines are called from **TASKOB/TASKOBTL/TASKOBAD** (called from **OBSV/OBSVTL/OBSVAD**) in a loop over observation sets. The data type of each set is known from the information in tables such as **MTYPOB(KSET)** stored in `yomobset`.

The following describes **HOP/HOPTL/**. The adjoint **HOPAD** follows the reverse order.

- First prepare for vertical interpolation using the routine **PREINT**. Data on model levels are extracted from the GOM-arrays (**YOMMVO**). Pressures of model levels are computed using **GPPRE**. Height arrays for the vertical interpolation are obtained (**PPINIT**) and T^* and T_0 are computed (**CTSTAR**). T^* and T_0 are later used for extrapolation of temperature below the model’s orography, [Subsection 5.6.1 \(b\)](#). The routine **PREINTS** deals with model surface fields needed for the near-surface observation operators and **PREINTR** deals with those fields that are specific to the radiance observation operators.
- The observation array is then searched to see what data is there. The ‘body’ of each observation report is scanned for data, and the vertical coordinate and the variable-number for each datum is retained in tables (**ZVERTP** and **IVNMRQ**). These tables will later constitute the ‘request’ for model equivalents to be computed by the various observation operators. Tables of pointers to data (‘body’ start addresses) and counters are stored (arrays **IPOS** and **ICMBDY**).
- Then the forward calculations are performed. There is an outer loop over all known ‘variable numbers’. If there are any matching occurrences of the loop-variable number with the content of **IVNMRQ**, then the relevant observation operator will be called. A variable-number and an observation operator are linked by a table set up in the routine **HVNMTLT**. The interface routines **PPOBSA** (upperair) and **PPOBSAS** (surface) are used, which in turn call **PPFLEV** and the individual operator routines. For radiance data the interface is **RADTR** which calls the radiative transfer code.
- In **HDEPART**, calculate the departure \mathbf{z} as

$$\mathbf{z} = \mathbf{y}^o - H\mathbf{x} + (\mathbf{y}^o - H\mathbf{x}_{\text{HR}}^b) - (\mathbf{y}^o - H\mathbf{x}_{\text{LR}}^b), \quad (5.1)$$

where the two terms in brackets have been computed previously: the first one in the high resolution trajectory run and the second one in the **LOBSREF** call, described in [Section 2.2](#).

If **LOBSTL** then \mathbf{z} is

$$\mathbf{z} = \mathbf{y}^o - H\delta\mathbf{x} + (\mathbf{y}^o - H\mathbf{x}_{\text{HR}}^b) - \mathbf{y}^o, \quad (5.2)$$

which simplifies to what has been presented in [Section 1.4](#).

The TOVS radiance bias correction is also carried out at this point by subtracting the bias estimate (kept in the NCMTORB-word of ODB) from the calculated departure.

Finally the departure is divided by the observation error σ_o (NCMFOE in ODB) to form the *normalized departure*.

- Departures of correlated data are multiplied by \mathbf{R}^{-1} , see [Subsection 5.3.5](#). The division by σ_o has already taken place in **HDEPART**, so \mathbf{R} at this point is in fact a correlation (not a covariance) matrix.
- The cost function is computed in **HJO**, as

$$\mathbf{J}_o = \mathbf{z}^T \mathbf{z} \quad (5.3)$$

for all data, even for SCAT data when LQSCAT=T., as in current 4D-Var with quadratic cost-function. When LQSCAT=F. (as in current 3D-Var configuration) the SCAT cost function combines the two ambiguous winds (subscripts 1 and 2) in the following way (also in **HJO**,

$$\mathbf{J}_{\text{SCAT}} = \left[\frac{\mathbf{J}_1^4 \mathbf{J}_2^4}{\mathbf{J}_1^4 + \mathbf{J}_2^4} \right]^{1/4} \quad (5.4)$$

These expressions for the cost function are modified by variational quality control, see [Section 5.4](#). The cost-function values are store in two tables, as detailed in [5.3.4](#).

- **HJO**, also stores the resulting *effective departure* in the NCMIOM0-word of ODB, for reuse as the input to the adjoint. The effective departure is the normalized departure after the effects of (vertical) observation error correlation and quality control have been taken into account, $\mathbf{z}_{\text{eff}} = \mathbf{z}^T \mathbf{R}^{-1} [\mathbf{QC}_{\text{weight}}]$, where the QC-weight will be defined below, [Section 5.4](#).

5.3.3 (a) Adjoint. We have now reached the end of the forward operators. In the adjoint routine **HOPAD** some of the tasks listed above have to be repeated before the actual adjoint calculations can begin. The input to the adjoint (the effective departure) is read from the ODB. The expression for the gradient (with respect to the observed quantity) is then simply

$$\nabla_{\text{obs}} \mathbf{J}_o = -2 \mathbf{z}_{\text{eff}} / \sigma_o \quad (5.5)$$

which is calculated in **HOPAD** for all data. The gradient of \mathbf{J}_{SCAT} is much more complicated and is calculated in a separate section of **HOPAD**. The adjoint code closely follows the structure of the direct code, with the adjoint operators applied in the reverse order.

5.3.4 \mathbf{J}_o tables

There are two different tables for storing the \mathbf{J}_o values. One is purely diagnostic (JOT, yomcosjo.h), and is used for producing the printed \mathbf{J}_o tables in the log-file (**PRTJO** called rom **EVCOST**). JOT is a FORTRAN90 derived type with items containing cost function value, data count, observation error, background error and codetype, for each observation type and for each observed variable (as defined by NVAR above).

The actual \mathbf{J}_o -table is called FJOS (**yomcosjo**). FJOS is indexed by the absolute observation number, iabnob=MABNOB(jobs,kset), so that the contributions from each individual observation can be summed up in a pre-determined order (in **EVCOST**), to ensure reproducibility, irrespective of number of processors and tasks.



5.3.5 Correlation of observation error

The observation error is assumed uncorrelated (i.e. the matrix \mathbf{R} is diagonal) for all data except time-sequences of SYNOP/DRIBU surface pressure and height data (used by default in 4D-Var, *Järvinen et al. 1999*). There used to be code for vertical correlation of observation error for radiosonde geopotential data and SATEM thicknesses, but these were removed in 21r2. Similar can easily be reintroduced again in a later cycle, provided the correlation acts on data within a single report (vertical or inter-channel correlation).

The serial correlation for SYNOP and DRIBU data is modelled by a continuous correlation function $\alpha e^{-b(t_1 - t_2)^2}$ where $\alpha = \text{RTCPART} = 0.3$ and $b = \text{RTCEFT} = 6.0$ hours, under the switch LTC (namjo). The remaining fraction $1 - \alpha$ of the error variance is assumed uncorrelated (see **COMTC**).

When \mathbf{R} is non-diagonal, the ‘effective departure’ \mathbf{z}_{eff} is calculated by solving the linear system of equations $\mathbf{z}_{\text{eff}}\mathbf{R} = \mathbf{z}$ for \mathbf{z}_{eff} , using LAPACK routines SPOTRF (Choleski decomposition) and SPOTRS (backwards substitution), as is done in **COMTC**.

5.4 VARIATIONAL QUALITY CONTROL

The variational quality control, VarQC, has been described by *Andersson and Järvinen (1999)*. It is a quality control mechanism which is incorporated within the variational analysis itself. A modification of the observation cost function to take into account the non-Gaussian nature of gross errors, has the effect of reducing the analysis weight given to data with large departures from the current iterand (or preliminary analysis). Data are not irrevocably rejected, but can regain influence on the analysis during later iterations if supported by surrounding data. VarQC is a type of buddy check, in that it rejects those data that have not been fitted by the preliminary analysis (i.e. the current state vector), often because it conflicts with surrounding data.

5.4.1 Description of the method

The method is based on Bayesian formalism. First, an *a priori* estimate of the probability of gross error $P(G)_i$ is assigned to each datum, based on study of historical data. Then, at each iteration of the variational scheme, an *a posteriori* estimate of the probability of gross error $P(G)_f$ is calculated (*Ingleby and Lorenc, 1993*), given the current value of the iterand (the preliminary analysis). VarQC modifies the gradient (of the observation cost function with respect to the observed quantity) by the factor $1 - P(G)_f$ (the QC-weight), which means that data which are almost certainly wrong ($P(G)_f \approx 1$) are given near-zero weight in the analysis. Data with a $P(G)_f > 0.75$ are considered ‘rejected’ and are flagged accordingly, for the purpose of diagnostics and feedback statistics, etc.

The normal definition of a cost function is

$$J_o = -\ln p \quad (5.6)$$

where p is the probability density function. Instead of the normal assumption of Gaussian statistics, we assume that the error distribution can be modelled as a sum of two parts: one Gaussian, representing correct data and one flat distribution, representing data with gross errors. We write:

$$p_i = N_i[1 - P(G_i)] + F_i P(G_i) \quad (5.7)$$

where subscript i refers to observation number i . N and F are the Gaussian and the flat distributions, respectively:

$$N_i = \frac{1}{\sqrt{2\pi}\sigma_o} \exp\left[-\frac{1}{2}\left(\frac{y_i - Hx}{\sigma_o}\right)^2\right] \quad (5.8)$$

$$F_i = \frac{1}{L_i} = \frac{1}{2l_i\sigma_o} \quad (5.9)$$

The flat distribution is defined over an interval L_i which in Eq. (5.9) has been written as a multiple of the observation error standard deviation σ_o . Substituting Eqs. (5.7) to (5.9) into Eq. (5.6), we obtain after rearranging the terms, an expression for the QC-modified cost function J_o^{QC} and its gradient ∇J_o^{QC} , in terms of the normal cost function J_o^N

$$J_o^N = \frac{1}{2}\left(\frac{y_i - Hx}{\sigma_o}\right)^2 \quad (5.10)$$

$$J_o^{QC} = -\ln\left(\frac{\gamma_i + \exp[-J_o^N]}{\gamma_i + 1}\right) \quad (5.11)$$

$$\nabla J_o^{QC} = \nabla J_o^N \left(1 - \frac{\gamma_i}{\gamma_i + \exp[-J_o^N]}\right) \quad (5.12)$$

$$\nabla J_o^{QC} = \nabla J_o^N w_i \quad (5.13)$$

where

$$w_i = 1 - \frac{\gamma_i}{\gamma_i + \exp[-J_o^N]} \quad (5.14)$$

$$\gamma_i = \frac{P(G_i)/(2l_i)}{[1 - P(G_i)]/\sqrt{2\pi}} \quad (5.15)$$

5.4.2 Implementation

The *a priori* information i.e. $P(G)_i$ and l_i are set during the screening, in the routine **DEPART**, and stored in the NCMFGC1 and NCMFGC2-words of the ODB. Default values are set in **DEFRUN**, and can be modified by the namelist namjo. VarQC can be switched on/off for each observation type and variable individually using LVARQC, or it can be switched off all together by setting the global switch LVARQCG=F.. Since an as good as possible 'preliminary analysis' is needed before VarQC starts, it is necessary to perform part of the minimization without VarQC, and then switch it on.

HJO computes J_o^{QC} according to Eq. (5.11) and the QC-weight, w_i , according to Eq.(5.14).

The 3D-Var assimilation system (Chapter 3) can handle non-quadratic cost functions because it is using the **M1QN3** minimization routine. This allows VarQC to be activated after NITERQC (40 by default) iterations during the minimization process. The 4D-Var assimilation system (Chapter 2) by default use a conjugate gradient minimization method that requires a strictly quadratic cost function. So in 4D-Var we use a quadratic formulation of VarQC, controlled by LQVARQC (default .T.).

In the non-quadratic formulation the QC-weight, w_i , Eq.(5.14) is updated for each simulation based on the nor-



malized departure values calculated from the latest model state. However, to obtain a strictly quadratic cost function the QC-weight is not allowed to change during the minimisation process, because the cost function shape would then change. Also, when LQVARQC = .T. it is not possible to activate VarQC in the middle of the minimisation process, i.e. NITERQC MUST be zero, because this would otherwise introduce a sudden jump in the cost function. Therefore, in 4D-Var assimilations VarQC is not applied during the first outer-loop but only for the second (and possibly subsequent) outer-loop iteration(s).

The quadratic VarQC implementation satisfies the quadratic constraint by calculating the QC-weight, w_i , based on the high resolution trajectory fields and using this constant weight during the next minimisation step. The cost function value is increased/reduced for each simulation during the minimisation by a factor $w_i * (\text{norm_dep_LR} - \text{norm_dep_HR})$, linearized in the vicinity of the high resolution cost function at norm_dep_HR. For the minimisation the most important input is the modification of the gradient by the weight w_i . During the trajectory run the high resolution departure is stored in ROBODY(..,MDBIFC1(NUPTRA+1)) in HDEPART. For each simulation during the next minimisation step the high resolution departure is read and normalized by the final observation error in HJO)HJO loop 1.3.2. This is used as input to the VarQC weight calculations (loop 1.5.3-1.5.4 in HJO). It is assured that the same weight is used for each simulation in the minimisation if LLQVARQC_MIN = .T., because ZFJOS_HR(JOBS,JBODY) is constant during the minimisation. The cost function value is calculated like $\text{Jo_varqc_LR} = \text{Jo_varqc_HR} + w_i * (\text{norm_dep_LR} - \text{norm_dep_HR})$

The a posteriori probability of gross error is stored in the ODB and passed to BUFR feedback. Storing in ODB is done at the final simulation of the last minimisation if LQVARQC = .F., but done during the final trajectory run if LQVARQC=.T. in order to use the updated final trajectory for calculating the QC-weight based on final high-resolution analysis values. This is done in HJO section 1.6.

Variational quality control for time correlated observations: The same method as above is (by default) applied for time correlated observations (LTC=.T.). Here the high resolution departure values are required for all the time correlated observations. This is achieved by storing the normalized high resolution departures in the array RTCND-PHR in HJO) and reading them in COMTC. They are then copied to local array ZTCNDPHR_W and then used instead of the low resolution departures in the calculation (overwriting ZOM1DEP_W by high resolution values).

5.5 OBSERVATION OPERATORS - GENERAL

The operator H is subdivided into a sequence of operators, each one of which performs part of the transformation from control variable to observed quantity:

- (i) The inverse change of variable (CHAVARIN) converts from control variables to model variables
- (ii) The inverse spectral transforms put the model variables on the model's reduced Gaussian grid (controlled by SCAN2MDM).
- (iii) A 12-point bi-cubic or 4-point bi-linear horizontal interpolation, similar to the semi-lagrangian interpolation routines described elsewhere, gives vertical profiles of model variables at observation points (controlled by COBS, COBSLAG). The surface fields are interpolated bi-linearly to avoid spurious maxima and minima. The three steps (i) to (iii) are common to all data types. Thereafter follows:
 - (iv) Vertical integration of, for example, the hydrostatic equation to form geopotential, and of the radiative transfer equation to form radiances (if applicable), and
 - (v) vertical interpolation to the level of the observations.

The vertical operations depend on the variable. The vertical interpolation is linear in pressure for temperature (PPT) and specific humidity (PPQ), and it is linear in the logarithm of pressure for wind (PPUV). The vertical interpolation of geopotential (PPGEOP) is similar to wind (in order to preserve geostrophy) and is performed in terms of

departures from the ICAO standard atmosphere for increased accuracy (*Simmons and Chen, 1991*, see Section 5.6 below). The current geopotential vertical interpolation together with the temperature vertical interpolation are not exactly consistent with hydrostatism. A new consistent and accurate vertical interpolation has been devised by Météo-France, which may be important for intensive use of temperature information. The new routines have been tested by ECMWF and as the results were not unambiguously positive the new routines have not yet been adopted – and they are not described in this documentation. In the meantime, the old routines are still used (switch `LOLDPP=.true.` in `namct0`), under the names `PPT_OLD`, `PPGEOP_OLD` and `PPUV_OLD`, with tangent linear `PPTTL_OLD`, `PPGEOPTL_OLD` and `PPUVTL_OLD` and adjoint `PPTAD_OLD`, `PPGEOPAD_OLD` and `PPUVAD_OLD`.

The vertical interpolation operators for SYNOP 10m wind (`PPUV10M`) and 2 m temperature (`PPT2M`) match an earlier version of the model's surface layer parametrisation. The vertical gradients of the model variables vary strongly in the lowest part of the boundary layer, where flow changes are induced on very short time and space scales, due to physical factors such as turbulence and terrain characteristics. The vertical interpolation operator for those data takes this into account following Monin–Obukhov similarity theory. Results using such operators, which follow *Geleyn (1988)* have been presented by *Cardinali et al. (1994)*. It was found that 2m temperature data could not be satisfactorily used in the absence of surface skin temperature as part of the control variable, as unrealistic analysis increments appeared in the near-surface temperature gradients. The Monin–Obukhov based observation operator for 10m wind, on the other hand, is used for all 10m winds (SYNOP, DRIBU, TEMP, PILOT and SCAT).

Relative humidity is assumed constant in the lowest model layer to evaluate its 2m value (`PPRH2M`), see Section 5.8.4. The model equivalent of SSMI total column water vapour data is obtained by vertical integration of q (in `GPPWC` and `PPPWC`). Observation operators also exist for precipitable water content (also `PPPWC`) and thicknesses (`PPGEOP`).

The variational analysis procedure requires the gradient of the objective function with respect to the control variable. This computation makes use of the adjoint of the individual tangent linear operators, applied in the reverse order. The details regarding observation operators for conventional data can be found in *Vasiljevic et al. (1992)*, *Courtier et al. (1998)*, and in the following sections.

5.6 THE OBSERVATION OPERATOR FOR CONVENTIONAL DATA

5.6.1 Geopotential height

The geopotential at a given pressure p is computed by integrating the hydrostatic equation analytically using the ICAO temperature profile and vertically interpolating $\Delta\phi$, the difference between the model level geopotential and the ICAO geopotential (*Simmons and Chen, 1991*). The ICAO temperature profile is defined as

$$T_{\text{ICAO}} = T_0 - \frac{\Lambda}{g} \phi_{\text{ICAO}} \quad (5.16)$$

where T_0 is 288 K, ϕ_{ICAO} is the geopotential above 1013.25 hPa and Λ is 0.0065 K m^{-1} in the ICAO troposphere and 0 in the ICAO stratosphere (the routine `PPSTA`). The ICAO tropopause is defined by the level where the ICAO temperature has reached 216.5 K (`SUSTA`). Using this temperature profile and integrating the hydrostatic equation provides T_{ICAO} and the geopotential ϕ_{ICAO} as a function of pressure (`PPSTA`). We may then evaluate the geopotential $\phi(p)$ at any pressure p following

$$\phi(p) - \phi_{\text{surf}} = \phi_{\text{ICAO}}(p) - \phi_{\text{ICAO}}(p_{\text{surf}}) + \Delta\phi \quad (5.17)$$

where p_{surf} is the model surface pressure and ϕ_{surf} , the model orography. $\Delta\phi$ is obtained by vertical interpolation from the full model level values $\Delta\phi_k$. The interpolation is linear in $\ln(p)$ up to the second model level (**PPINTP**) and quadratic in $\ln(p)$ for levels above it (**PPITPQ**, see below). The full model level values are obtained integrating the discretized hydrostatic equation using the routine **GPGeo** of the forecast model, following *Simmons and Burridge (1981)*:

$$\Delta\phi_k = \sum_{j=L}^{k+1} R_{\text{dry}}(T_{v_j} - T_{\text{ICAO}_j}) \ln\left(\frac{p_{j+1/2}}{p_{j-1/2}}\right) + \alpha_k R_{\text{dry}}(T_{v_k} - T_{\text{ICAO}_k}) \quad (5.18)$$

with

$$\alpha_k = 1 - \frac{p_{k-1/2}}{p_{k+1/2} - p_{k-1/2}} \ln\left(\frac{p_{k+1/2}}{p_{k-1/2}}\right)$$

for $k > 1$ and $\alpha_1 = \ln(2)$.

5.6.1 (a) Quadratic vertical interpolation near the top of the model. Above the second full level of the model, the linear interpolation (**PPINTP**) is replaced by a quadratic interpolation in $\ln p$, performed in the routine **PPITPQ**:

$$z(\ln p) = a + b(\ln p) + c(\ln p)^2 \quad (5.19)$$

where a , b and c are constants determined so that the above equation fits the heights at the top levels ($k = 1, 2$ and 3). The interpolation formula is:

$$\phi(\ln p) = z_2 + \frac{(z_2 - z_1)(\ln p - \ln p_2)(\ln p - \ln p_3)}{(\ln p_2 - \ln p_1)(\ln p_1 - \ln p_3)} - \frac{(z_2 - z_3)(\ln p - \ln p_1)(\ln p - \ln p_2)}{(\ln p_2 - \ln p_3)(\ln p_1 - \ln p_3)} \quad (5.20)$$

where 1, 2 and 3 refer to levels $k = 1, 2$ and 3 , respectively.

5.6.1 (b) Below the model's orography. The extrapolation of the geopotential below the model's orography is carried out as follows: Find T^* (surface temperature) by assuming a constant lapse rate Λ , from the model level above the lowest model level (subscript $l - 1$), see the routine **CTSTAR**,

$$T^* = T_{l-1} + \Lambda \frac{R_{\text{dry}}}{g} T_{l-1} \ln \frac{p_{\text{surf}}}{p_{l-1}} \quad (5.21)$$

$$T^* = \frac{\{T^* + \max[T_y, \min(T_x, T^*)]\}}{2} \quad (5.22)$$

Find the temperature at mean sea level, T_0 (also in **CTSTAR**,

$$T_0 = T^* + \Lambda \frac{\phi_{\text{surf}}}{g} \quad (5.23)$$

$$T_0 = \min[T_0, \max(T_x, T^*)] \quad (5.24)$$

where T_x is 290.5 K and T_y is 255 K. The geopotential under the model's orography is (in **PPGEO**) calculated as:

$$\phi = \phi_{\text{surf}} - \frac{R_{\text{dry}} T^*}{\gamma} \left[\left(\frac{p}{p_{\text{surf}}} \right)^\gamma - 1 \right] \quad (5.25)$$

where $\gamma = \frac{R_{\text{dry}}}{\phi_{\text{surf}}} (T_0 - T_{\text{surf}})$.

5.6.2 Wind

In **PPUV** a linear interpolation in $\ln p$ (**PPINTP**) is used to interpolate u and v to the observed pressure levels up to the second full model level, above which a quadratic interpolation is used (**PPITPQ**, see [Subsection 5.6.1 \(a\).1](#)). Below the lowest model level wind components are assumed to be constant and equal to the values of the lowest model level.

5.6.3 Humidity

Specific humidity q , relative humidity U and precipitable water content PWC are linearly interpolated in p , in **PPQ**, **PPRH** and **PPPWC**, respectively. Upper air relative humidity data are normally not used, but could be used, if required. The use of surface relative humidity data is described in [Subsection 5.8.4](#).

5.6.3 (a) Saturation vapour pressure. The saturation vapour pressure $e_{\text{sat}}(T)$ is calculated using Tetens's formula:

$$e_{\text{sat}}(T) = a_1 \exp^{a_3 \left(\frac{T - T_3}{T - a_4} \right)} \quad (5.26)$$

using FOEEWM (mixed phases, water and ice) in the model and FOEEWMO (water only) for observations. The use of water-phase only is in accordance with the WMO rules for radiosonde and synop reporting practices. Note that these statement functions compute $(R_{\text{dry}}/R_{\text{vap}})e_{\text{sat}}(T)$, with the parameters set according to [Buck \(1981\)](#) and the AERKi formula of [Alduchov and Eskridge \(1996\)](#), i.e. $a_1 = 611.21$ hPa, $a_3 = 17.502$ and $a_4 = 32.19$ K over water, and for FOEEWM $a_3 = 22.587$ and $a_4 = -0.7$ K over ice, with $T_3 = 273.16$ K. Furthermore in FOEEWM the saturation value over water is taken for temperatures above 0°C and the value over ice is taken for temperatures below -23°C. For intermediate temperatures the saturation vapour pressure is computed as a combination of the values over water $e_{\text{sat}(\text{water})}$ and ice $e_{\text{sat}(\text{ice})}$ according to the formula

$$e_{\text{sat}}(T) = e_{\text{sat}(\text{ice})}(T) + [e_{\text{sat}(\text{water})}(T) - e_{\text{sat}(\text{ice})}(T)] \left(\frac{T - T_i}{T_3 - T_i} \right)^2 \quad (5.27)$$

with $T_3 - T_i = 23$ K.

5.6.3 (b) Relative humidity. In **GPRH** relative humidity U is computed:

$$U = \frac{pq \frac{R_{\text{vap}}}{R_{\text{dry}}}}{\left[1 + \left(\frac{R_{\text{vap}}}{R_{\text{dry}}} - 1 \right) q \right] e_{\text{sat}}(T)} \quad (5.28)$$

and then in **PPRH** interpolated to the required observed pressure levels (using **PPINTP**). Below the lowest model level and above the top of the model is U assumed to be constant. Saturation vapour pressure is calculated using FOEEWMO if **GPRH** has been called from the observation operator routines, and using FOEEWM if called from the model post processing.

5.6.3 (c) *Precipitable water.* In **GPPWC** precipitable water is calculated as a vertical summation from the top of the model:

$$PWC_k = \frac{1}{g} \sum_{i=1}^k q_i (p_i - p_{i-1}) \quad (5.29)$$

and then in **PPPWC** interpolated to the required observed pressure levels (using **PPINTP**). PWC is assumed to be zero above the top of the model. Below the model's orography PWC is extrapolated assuming a constant $q = q_l$.

5.6.3 (d) *Specific humidity.* Specific humidity q is in **PPQ** interpolated to the required observed pressure levels (using **PPINTP**). Below the lowest model level and above the top of the model is q assumed to be constant and equal to q_l and q_1 , respectively.

5.6.4 Temperature

Temperature is interpolated linearly in pressure (**PPINTP**), in the routine **PPT**. Above the highest model level the temperature is kept constant and equal to the value of the highest model level. Between the lowest model level and the model's surface the temperature is interpolated linearly, using:

$$T = \frac{(p_{\text{surf}} - p)T_l + (p - p_l)T^*}{p_{\text{surf}} - p_l} \quad (5.30)$$

Below the lowest model level the temperature is extrapolated by

$$T = T^* \left[1 + \alpha \ln \frac{p}{p_{\text{surf}}} + \frac{1}{2} \left(\alpha \ln \frac{p}{p_{\text{surf}}} \right)^2 + \frac{1}{6} \left(\alpha \ln \frac{p}{p_{\text{surf}}} \right)^3 \right] \quad (5.31)$$

with $\alpha = \Lambda R_{\text{dry}}/g$, for $\phi_{\text{sat}}/g < 2000$ m, but α is modified for high orography to $\alpha = R_{\text{dry}}(T_0' - T^*)/\phi_{\text{surf}}$, where

$$T_0' = \min(T_0, 298) \quad (5.32)$$

for $\phi_{\text{surf}}/g > 2500$ m, and

$$T_0' = 0.002[(2500 - \phi_{\text{surf}}/g)T_0 + (\phi_{\text{surf}}/g - 2000)\min(T_0, 298)] \quad (5.33)$$

for $2000 < \phi_{\text{surf}}/g < 2500$ m. If $T_0' < T^*$ then α is reset to zero. The two temperatures T^* and T_0 are computed using Eqs. (5.21) to (5.24).

5.7 SATELLITE OBSERVATION OPERATORS

The processing within 3D/4D-Var of satellite data follows the same general layout as that of conventional data. The same vertical interpolation routines are used whenever possible. The main difference in the organization is that the radiative transfer code, RTTOV-7 (*Saunders and Matricardi 1998; Matricardi et al., 2001*), currently requires the model profiles to be interpolated to NLSAT=43 fixed pressure levels from 1013.25 hPa to 0.1 hPa on which the radiative transfer coefficients are determined. Radiances are assimilated directly (*Andersson et al. 1994*) rather than retrieved products, wherever possible. The current operational configuration uses ATOVS level-1C radiances (*McNally et al. 1999*), geostationary water vapour clear-sky radiances (*Munro et al. 2004*) SCAT ambiguous surface winds (*Stoffelen and Anderson, 1997; Isaksen and Janssen 2004*) from ERS-2 and QuikSCAT, SSM/I total radiances (*Bauer et al. 2002*) and SATOB cloud motion winds of various types (*Tomassini et al. 1997; Bormann et al. 2003*). Operators also exist for SATEM thicknesses and PWC (*Kelly and Pailleux, 1988; Kelly et al. 1991*), SSM/I total-column water vapour (TCWV) and wind speed, which however are not currently in use.

5.7.1 Set-up of the radiative-transfer code

There are two set-up routines (**GETSATID** and **RTSETUP**) for the radiative transfer computations and both are called from **SURAD**. The routine **RTSETUP** calls RTTVI (in the satrad library) which reads in the transmittance coefficients to memory for the satellites present. There is a file containing these coefficients for TOVS, VTPR and other satellites and all satellites through to NOAA-17 are supported. Geostationary imager radiances (METEOSAT and GOES) follow the same path as Level-1C radiances in IFS.

5.7.1 (a) Satellite identifiers and the satellite group table. Satellite identifiers are dealt with in just one place in the IFS and that is in the routine **GETSATID**. The ODB contains the identifiers as given in the original BUFR messages. Lists of identifiers for which data exist in any given ODB are prepared in the routine **SURAD**. The routine **GETSATID** matches those BUFR satellite identifiers with the more traditional satellite numbers, used by the RT-code (e.g. 10 for NOAA-10 and 5 for METEOSAT-5). The id-conversion tables can be modified through a series of namelists: NAMTOVS; NAMDMSP; NAMMETEOSAT; NAMGOES; and NAMGMS. The satellite data are furthermore associated with a sensor number (**yomtvrad**) to be used for example as an array index in the J_o table (JOT), and with a sequence number for addressing the transmittance coefficients (rtcoef_pos) within the RT-TOVS code, for example. Note that this sequence number is universally determined across all processors, so if NOAA-12 (BUFR id=202) is satellite-1 on one processor then it will be satellite-1 on all other processors, too. The various satellite-related indices are gathered in the FORTRAN90 data structure called the 'satellite group table', satgrp_t (**yomtvrad**), containing elements: bufrid, codetype, sensor, satgroup, rtid, rtseries, rsubtype, rtcoef_pos, number of channels, and a channel number list.

5.7.1 (b) Satellite sensors. The various types of radiance data are classified by sensor. Each satellite sensor is assigned a number, in **yomtvrad**: currently HIRS = 0, MSU = 1, SSU = 2, AMSUA = 3, AMSUB = 4, SSMI = 6, VTPR1 = 7, VTPR2 = 8, METEOSAT = 20, and GOES = 21 (GOES = 22 from CY25R3 onwards). The sensor number is used as index to various tables containing observation errors, BgQC thresholds, VarQC parameters, the J_o -table JOT, et cetera. See the routine **DEFRUN**.

5.7.1 (c) Fixed pressure levels and RT validation bounds. The list of the NLSAT = 43 fixed pressure levels is passed from the RTTOV library satrad (where they have been read from the transmittance coefficients file) to **RTSETUP** and **SURAD** and copied to **yomtvrad**. **RTSETUP** also similarly obtains (from RTTOV) lists of temperature, humidities and ozone limits indicating the valid range of the RT transmittance regression. The RT code is not reliable in conditions beyond these limits. Checks are applied in **RADTR**.



5.7.1 (d) *Radiance observation errors, bias and emissivity.* Observation errors and bias corrections for 1C radiances are written to the odb in a call to **RADICOB**E (from **HRETR**). The bias correction is stored in the NCM-TORB word and later applied at each iteration of 3D/4D-Var, in the routine **HDEPART**, sd explained above. Microwave (**EMIS_MW**) and infrared (**EMIS_IR**) emissivity are computed in **RADICEMIS** and stored in the ODB for later use by RTTOV. The routine **EMIS_IR** uses the regression of ISEM-6 (*Sherlock, 1999*) to compute emissivities for the infrared channels of VTPR, HIRS, Meteosat and GOES.

5.7.2 Radiances

The routine **HOP** interpolates the model profiles of temperature, humidity and ozone (T , q and oz) to the NLSAT(=43) RT levels (\dot{T} and \dot{q}) and calls the interface **RADTR** to the RT code RTTOV. The standard routines **PPT** and **PPQ** are used to carry out the vertical interpolation, and they are called through the PPOBSA interface, as usual. Various radiance preparations have been gathered in the routine **HRADP**. In **HRADP**, the model’s pressure at the surface height of the observation location (given in the report) is calculated, using **PPPMER**.

For the purpose of radiance calculations $T_{2m} = T_l$ (the lowest model level temperature) and $q_{2m} = \dot{q}_{NLSAT}$ (specific humidity at the lowermost of the RT pressure levels). These quantities represent a very shallow layer of air near the surface and contribute little to the calculated radiances—it was not considered necessary to use **PPT2M** and **PPRH2M** (Section 5.8) in this context. In order to make the radiance cost function continuous in p_{surf} it was necessary to ensure that \dot{T} and \dot{q} approach T_{2m} and q_{2m} as the pressure on any of the RT levels approaches p_{surf} . This is done in a section of **HRADP**. More details on the radiative transfer code RTTOV can be found in *Eyre (1991)*, updated by *Saunders and Matricardi (1998)*.

The ‘sink-variable’ at satellite FOVs: In the case of 1C, or ‘raw’ radiance data, as used since May 1999 (*McNally et al. 1999*) surface skin temperature is retrieved by 3D/4D-Var at each field of view, if the switch LTOVSCV is on (default is on), in namelist NAMVAR. This is done for all infrared and microwave satellite sensors and instrument. The handling of the SST retrieval at the radiance FOVs is performed in the routine **HRADP/HRADPTL/HRADPAD**, called from **HOP/HOPTL/HOPAD**. The background SST is provided by the model trajectory integration, and a background error of 1K / 5K is assigned over sea / land, respectively (stored in TOVSCVER, module **YOMTVRAD**). The gradient with respect to SST obtained from RTTOV is temporarily store in the TOVSCVX array and later transferred to its location in the distributed control vector (Chapter 2). The next iteration of the minimisation provides updated SST increments (also stored in TOVSCVX) that are used by RTTOVTL in subsequent iterations. The outer-loop iterations result in a new linearisation state SST, stored in TOVSCVX5. All the SST-related information at FOV locations that needs to be passed between job-steps, reside in the ODB, in the satellite predictors table. This approach has more recently been adopted for CO2 retrieval at AIRS FOVs, within the COCO projects (*Engelen et al. 2004*).

In **HOP** the observation array is searched for radiance data. The compressed ODB (after screening) contains only those data to be used by the analysis. A list of existing channel numbers for each report is constructed. Model radiances for exactly those channels are then requested from the RT-code, via the interface **RADTR**. The routine **RADTR** checks that the input model profile is within the valid range of the transmittance regression. It packets the profiles into chunks of work of the appropriate maximum size for the RT-code (currently 65). The RT packet size has been communicated to IFS in the call to **RTSETUP**. The output is radiances for the channels requested.

The tangent linear **HOPTL** and the adjoint **HOPAD** follow the same pattern as **HOP**. In both the TL and the adjoint \dot{T} and \dot{q} have to be recomputed before the actual tangent linear and adjoint computations can start. The pointers to the radiance data in observation array are obtained just as it was done in the direct code.

5.7.3 Thicknesses

The pressures of layer bounds (top T, and bottom B) are found (in **HOP**) by scanning the observation array for thickness data. The geopotential for the top and the bottom of the layer are computed, using **PPGEOP** (Section 5.6), and the thickness is given by the difference $\phi_T - \phi_B$.

5.7.4 Precipitable water from SATEM and SSM/I

As for thicknesses, the pressures of layer bounds are found by scanning the observation array for TOVS PWC data. For SSMI TPW, the top pressure is set to the top of the model and the lower pressure bound is p_s . The PWC for the top and the bottom of the layer are computed, using **PPPWC** (Section 5.6.3), and the layer PWC is given by the difference $PWC_B - PWC_T$.

5.7.5 Ozone-layer retrievals from satellites

Ozone is used in the form of integrated layers bounded by a top and bottom pressure which are given as a part of the observation. The unit for ozone is kg m^{-2} . For ozone the same observation operator is used as for precipitable water (**PPPWC** (Section 5.5)). The same concept is applied to all data, whether total column data (like TOMS and GOME) or data with higher vertical resolution (like SBUV).

5.7.6 Scatterometer winds

In **HOP**, the observation array is scanned for SCAT data. Normally two ambiguous pairs of u -component and v -component observations are found at each SCAT location—with directions approximately 180 degrees apart. QuikSCAT can have 2, 3 or 4 ambiguous winds. Only the most likely wind (highest a-priori probability) and its opposing (135 to 180 apart) ambiguity are used. If there are no ambiguities in the allowed range then all ambiguities are rejected. In 3D/4D-Var both winds are used and the ambiguity removal takes place implicitly through the special SCAT cost-function, Eq. (2.14), in **HJO** (Stoffelen and Anderson, 1997). If however **LQSCATT=.true.** (**namjo**), the normal quadratic J_o will be used. In this case only the SCAT wind nearest the high resolution background will be used (which is determined in a section of **HOP**).

As **PPUV10M** (Section 5.8) is used also for SCAT data (since cy18r6), the observation operator is exactly the same as for SYNOP, SHIP and DRIBU winds. The z_0 (surface roughness) comes from the coupled wave model. The simpler logarithmic wind law can be used optionally under the switch **LSCASUR=.F.** in **NAMOBS** (true by default).

In the adjoint (SURFACAD) there is a separate section of **HOP** for the calculation of the $\nabla_{\text{obs}} J_{\text{SCAT}}$.

5.8 SURFACE OBSERVATION OPERATORS

All surface data are processed in the routine SURFACEO. Preparations for the vertical interpolation is done as for all other data in **PREINT** (see Subsection 5.6.1 (b)), and for surface data there are a few additional tasks which are performed in a separate routine, **PREINTS**. In **PREINTS**, surface roughness over sea, dry static energy (**SURBOUND**), Richardson number, drag coefficients and stability functions (**EXCHCO**), are computed, as detailed in the following.

5.8.1 Mathematical formulation

An analytical technique (Geleyn, 1988) is used to interpolate values between the lowest model level and the surface. When Monin–Obukhov theory is applied:

$$\frac{\partial u}{\partial z} = \frac{u_*}{\kappa(z+z_0)} \phi_M \left(\frac{z+z_0}{L} \right) \quad (5.34)$$

$$\frac{\partial s}{\partial z} = \frac{s_*}{\kappa(z+z_0)} \phi_H \left(\frac{z+z_0}{L} \right) \quad (5.35)$$

$$L = \frac{c_p}{g} \frac{T}{\kappa} \frac{u_*^2}{s_*} \quad (5.36)$$

where u, s are wind and energy variables, u_*, s_* are friction values and $\kappa = 0.4$ is von Kármán's constant.

The temperature is linked to the dry static energy s by:

$$s = c_p T + \phi \quad (5.37)$$

$$c_p = c_{p_{\text{dry}}} \left[1 + \left(\frac{c_{p_{\text{vap}}} - 1}{c_{p_{\text{dry}}}} \right) q \right] \quad (5.38)$$

Defining the neutral surface exchange coefficient at the height z as:

$$C_N = \left[\frac{\kappa}{\ln \left(\frac{z+z_0}{z_0} \right)} \right]^2 \quad (5.39)$$

The drag and heat coefficients as:

$$C_M = \frac{u_*^2}{[u(z)]^2} \quad (5.40)$$

$$C_H = \frac{u_* s_*}{u(z)[s(z) - \tilde{s}]} \quad (5.41)$$

we can set the following quantities:

$$B_N = \frac{\kappa}{\sqrt{C_N}}, B_M = \frac{\kappa}{\sqrt{C_M}}, B_H = \frac{\kappa \sqrt{C_M}}{C_H} \quad (5.42)$$

and considering the stability function in stable conditions as:

$$\phi_{M/H} = 1 + \beta_{M/H} \frac{z}{L} \quad (5.43)$$

we obtain integrating Eqs. (5.34) and (5.35) from 0 to z_1 (the lowest model level):

$$u(z) = \frac{u(z_1)}{B_M} \left[\ln \left(1 + \frac{z}{z_1} (e^{B_N} - 1) \right) - \frac{z}{z_1} (B_N - B_M) \right] \quad (5.44)$$

$$s(z) = \tilde{s} + \frac{s(z_1) - \tilde{s}}{B_H} \left[\ln \left(1 + \frac{z}{z_1} (e^{B_N} - 1) \right) - \frac{z}{z_1} (B_N - B_H) \right] \quad (5.45)$$

In unstable conditions the stability function can be expressed as:

$$\phi_{M/H} = \left(1 - \beta_{M/H} \frac{z}{L} \right)^{-1} \quad (5.46)$$

and the vertical profiles for wind and dry static energy are:

$$u(z) = \frac{u(z_1)}{B_M} \left[\ln \left(1 + \frac{z}{z_1} (e^{B_N} - 1) \right) - \ln \left(1 + \frac{z}{z_1} (e^{B_N - B_M} - 1) \right) \right] \quad (5.47)$$

$$s(z) = \tilde{s} + \frac{s(z_1) - \tilde{s}}{B_H} \left[\ln \left(1 + \frac{z}{z_1} (e^{B_N} - 1) \right) - \ln \left(1 + \frac{z}{z_1} (e^{B_N - B_H} - 1) \right) \right] \quad (5.48)$$

The temperature can then be obtained from s as:

$$T(z) = s(z) - \frac{zg}{c_p} \quad (5.49)$$

When z is set to the observation height, Eqs. (5.44) and (5.45) and Eqs. (5.47)–(5.49) give the postprocessed wind and temperature. To solve the problem, we have to compute the dry static energy at the surface $\tilde{s} = \tilde{s}(T_{\text{surf}}, q = 0)$ (Subsection 5.8.2), with B_M , B_N and B_H values depending on the drag and heat exchange coefficients Eq. as detailed in Subsection 5.8.3.

5.8.2 Surface values of dry static energy

To determine the dry static energy at the surface we use Eqs. (5.37) and (5.38) where the humidity at the surface is defined by:

$$\tilde{q} = q(z = 0) = h(C_{\text{snow}}, C_{\text{liq}}, C_{\text{veg}}) q_{\text{sat}}(T_{\text{surf}}, p_{\text{surf}}) \quad (5.50)$$

h is given by (Blondin, 1991):

$$h = C_{\text{snow}} + (1 - C_{\text{snow}}) [C_{\text{liq}} + (1 - C_{\text{liq}}) \bar{h}] \quad (5.51)$$

with

$$\bar{h} = \max \left\{ 0.5 \left(1 - \cos \frac{\pi \vartheta_{\text{soil}}}{\vartheta_{\text{cap}}} \right), \min \left(1, \frac{q}{q_{\text{sat}}(T_{\text{surf}}, p_{\text{surf}})} \right) \right\} \quad (5.52)$$

where ϑ_{soil} is the soil moisture content and ϑ_{cap} is the soil moisture at field capacity (2/7 in volumetric units). Eq. (5.51) assigns a value of 1 to the surface relative humidity over the snow covered and wet fraction of the grid

box. The snow-cover fraction C_{snow} depends on the snow amount W_{snow} :

$$C_{\text{snow}} = \min\left(1, \frac{W_{\text{snow}}}{W_{\text{snow}_{\text{cr}}}}\right)$$

where $W_{\text{snow}_{\text{cr}}} = 0.015$ m is a critical value. The wet skin fraction C_{liq} is derived from the skin-reservoir water content W_{liq} :

$$C_{\text{liq}} = \min\left(1, \frac{W_{\text{liq}}}{W_{\text{liq}_{\text{max}}}}\right),$$

where

$$W_{\text{liq}_{\text{max}}} = W_{\text{layer}_{\text{max}}} \{(1 - C_{\text{veg}}) + C_{\text{veg}} A_{\text{leaf}}\}$$

with $W_{\text{layer}_{\text{max}}} = 2 \times 10^{-4}$ m being the maximum amount of water that can be held on one layer of leaves, or as a film on bare soil, $A_{\text{leaf}} = 4$ is the leaf-area index, and C_{veg} is the vegetation fraction.

5.8.3 Transfer coefficients

Comparing the Eqs. (5.34) – (5.35) integrated from z_0 to $z + z_0$ with Eqs. (5.39) to (5.41), C_M and C_H can be analytically defined:

$$\frac{1}{C_M} = \frac{1}{\kappa^2} \left[\int_{z_0}^{(z+z_0)} \frac{\phi_M(z'/L)}{z'} dz' \right]^2 \quad (5.53)$$

$$\frac{1}{C_H} = \frac{1}{\kappa^2} \left[\int_{z_0}^{(z+z_0)} \frac{\phi_M(z'/L)}{z'} dz' \int_{z_0}^{(z+z_0)} \frac{\phi_H(z'/L)}{z'} dz' \right] \quad (5.54)$$

Because of the complicated form of the stability functions, the former integrals have been approximated by analytical expressions, formally given by:

$$\begin{aligned} C_M &= C_N f_M\left(Ri, \frac{z}{z_0}\right) \\ C_H &= C_N f_H\left(Ri, \frac{z}{z_0}\right) \end{aligned} \quad (5.55)$$

where C_N is given by Eq. (5.39). The bulk Richardson number Ri is defined as:

$$Ri = \frac{g \Delta z \Delta T_v}{c_p T_v |\Delta u|^2} \quad (5.56)$$

where T_v is the virtual potential temperature. The functions f_M and f_H correspond to the model instability functions and have the correct behaviour near neutrality and in the cases of high stability (Louis, 1979; Louis et al. 1982)

(a) unstable case $Ri < 0$

$$f_M = 1 - \frac{2b Ri}{1 + 3b C C_N \sqrt{\left(1 + \frac{z}{z_0}\right)(-Ri)}} \quad (5.57)$$

$$f_H = 1 - \frac{3b Ri}{1 + 3b C C_N \sqrt{\left(1 + \frac{z}{z_0}\right)(-Ri)}} \quad (5.58)$$

C=5

(b) Stable case $Ri > 0$

$$f_M = \frac{1}{1 + 2b Ri(1 + d Ri)^{1/2}} \quad (5.59)$$

$$f_H = \frac{1}{1 + 3b Ri(1 + d Ri)^{1/2}} \quad (5.60)$$

d = 5

5.8.4 Two-metre relative humidity

In **GPRH** relative humidity is computed according to Eq. (5.28). The relative humidity depends on specific humidity, temperature and pressure (q , T and p , respectively) at the lowest model level. It is constant in the surface model layer, see **PPRH2M**.



Part II: DATA ASSIMILATION**CHAPTER 6 Background, analysis and forecast errors****Table of contents**

- 6.1 Nomenclature
- 6.2 Input and ‘massaging’ of background errors
- 6.3 Diagnosis of background error variances
- 6.4 Calculation of eigenvalues and eigenvectors of the Hessian
- 6.5 The Preconditioner
- 6.6 Calculation of analysis-error variances
- 6.7 Calculation of forecast error variances

6.1 NOMENCLATURE

The calculation of standard deviations of background errors is unfortunately an area where the use of inaccurate nomenclature is widespread. For example, standard deviations of background error are almost universally referred to as ‘background errors’. Likewise, standard deviations of analysis and forecast error are referred to as ‘analysis errors’ and ‘forecast errors’. Although inaccurate, this nomenclature has been adopted in the following for the sake of brevity.

A second source of confusion is that terms ‘background error’ and ‘forecast error’ are often used interchangeably. This confusion has even crept into the code, where the buffer which contains the standard deviations of background error is called FCEBUF. Such confusion is clearly unwise when discussing the calculation of forecast errors. The following sections will describe the processing of error variances during a single analysis cycle. The term ‘background error’ will refer exclusively to the standard deviations of background error which are used in the background cost function. The background errors are an input to the analysis. The term ‘forecast error’ will refer to an estimate of the standard deviation of error in a short-term forecast made from the current analysis. The forecast errors are calculated by inflating an estimate of the standard deviation of analysis error, and are an output from the analysis system.

6.2 INPUT AND ‘MASSAGING’ OF BACKGROUND ERRORS

Background errors for use in J_b are initialised by a call to **SUINFCE**. This is part of the J_b set-up described in [Subsection 4.3.3](#). First, a call to **INQGRIB** is made. This returns a description of the data in the background error file (filename **errgrib**). **COMMFCE1** communicates the description of the data to other processors. After checking some parameters and allocating arrays to hold the background errors, a call to **READGRIB** reads the errors into a local array. The errors are communicated to the other processors by a call to **COMMFCE2**. Optionally (under the control of **LFACHR**) the errors may be increased in the tropics at this stage. (This is not done by default, and is not recommended.) The background errors may be on a regular latitude–longitude, or reduced Gaussian grid. They are interpolated bilinearly in latitude and longitude onto the reduced Gaussian analysis grid by a call to **SUINFCE**.

At this stage, all processors have complete fields of background error. Each processor now allocates a buffer (confusingly called FCEBUF) in `yomfceb` to hold background errors for those gridpoints which are local to the processor.

A large loop over variables follows. For each variable, the GRIB parameter code is examined. Depending on the setting of LSTABAL, LRDQERR, and on the presence or absence of vorticity errors in the background error file, the variable may be ignored (by cycling VARIABLE_LOOP) or an offset, IOFF, into the background error buffer is calculated.

The background errors are interpolated onto the model levels by a call to `SUVIFCE`. A number of variable-dependent things now happen. First, geopotential height errors are converted to geopotential by multiplying by g . Second, wind component errors are converted to vorticity errors by an *ad hoc* scaling. (Note that if vorticity errors are available in the file, then these will be used by preference. Wind component errors will be ignored.) Finally, if errors for the unbalanced components of temperature, divergence, ozone or surface pressure are not present in the file, the corresponding elements of the background error buffer are initialized to sensible values.

Background errors for specific humidity are read from the background-error file if the namelist variable LRDQERR is set. Currently, it is usual to calculate specific humidity errors as a function of background humidity and various other parameters. This is done by a call to `STEPO('0IB00Z000')`, which in turn calls `SUSHFCE`. The calculation of background errors for specific humidity is described in [Subsection 4.3.4](#).

Next, one of two routines is called. `SUMDFCE` calculates a vertically average 'pattern' of background error. This is required if the background errors are to be represented as a product of a vertical profile of global mean error and a horizontal pattern, and was the default with the 'old' J_b . The pattern is stored in FGMWNE. Note in particular that `SUMDFCE` is called if horizontally-constant background errors are requested by setting LCFCE. In this case, all elements of FGMWNE are set to one.

Alternatively, `SUPRFFCE` is called to calculate global mean profiles of the input background errors. This is the default. The profiles are stored in FCEIMN.

The final step in processing the background errors is to call `STEPO('00000Y000')`. This, in turn, calls `SUSEPFCE` to modify the background errors. The modification takes one of two forms. If separable background errors have been requested, the contents of the background error buffer are replaced by the product of the vertical profile stored in FCEMN and the horizontal pattern stored in FGMWNE. Otherwise, the background errors for each variable at each level are multiplied by the ratio of the corresponding elements of FCEMN and FCEIMN. The result of this operation is to adjust the global mean profiles of background error to match those stored in FCEMN.

6.3 DIAGNOSIS OF BACKGROUND ERROR VARIANCES

The analysis errors are calculated by subtracting a correction from the variances of background error. The first stage in the calculation is therefore to determine the background error variances. This is done by subroutine `BGVECS`, which is called from `CVA1`. One of two methods may be employed, depending on whether NBGVECS is equal to, or greater than, zero. In either case, the estimated variances of background error are stored in the analysis error buffer, ANEBUF (in `yomaneb`).

If NBGVECS is zero, as it is by default, then background errors for variables which are explicitly present in the background error buffer, FCEBUF, are copied into ANEBUF and squared. Errors for those variables whose background errors are defined implicitly through the change of variable are estimated using simple scaling of appropriate explicit errors. This scaling is performed by a call to `ESTSIGA`.

If NBGVECS is non-zero, then the variances of background error are estimated using randomization. This method



assumes that the change of variable transforms the background error covariance matrix into the identity matrix. A sample of NBGVECS vectors drawn from a multi-dimensional Gaussian distribution with zero mean and identity covariance matrix is generated by calls to the Gaussian random number generator GASDEV. These vectors are transformed to the space of physical variables by CHAVARIN. The transformed variables form a sample drawn from the distribution of background errors. A call to STEPO('0AA00A000') transforms each vector to gridpoint space and accumulates the sums of squares in ANEBUF. Finally, the sums of squares are divided by the number of vectors by a call to SCALEAE to provide a noisy, but unbiased estimate of the variances of background error actually used in the analysis. The noise may be filtered by a call to FLTBGERR, which transforms the variances to spectral coefficients, multiplies each coefficient by $\cos^2(\min((n/\text{NBGTRUNC}),1)\pi/2)$, and then transforms to grid space. The default is to filter with a very large value of NBGTRUNC. Effectively, the background errors are simply spectrally truncated. It is highly recommended that the filtering is performed, since it prevents a grid-scale numerical instability which occurs when the error growth model introduces spatial features which cannot be resolved by the spectral control variable.

The code allows two further configurations of the background error estimation. Neither is operational at present. The two configurations are controlled by switches LBGOBS and LBGM (namvar), respectively. If LBGOBS=.T. then the full set of tangent-linear observation operators will be applied to the NBGVECS random vectors, in model grid point space. This is done in the routine BGOBS called from VEC2GP, under SCAN2MTL. The TL routines are required as the observation operators have been linearized around the background state. The result is **background errors in observation space**. They are stored and accumulated in ANEBUF and written out as grid-fields, for geopotential, temperature, wind, humidity, total ozone, total column water vapour, TOVS and ATOVS radiance channels, 10 metre wind and 2 metre temperature. If in addition LBGM=.T. then the randomized estimate of background error will be propagated in time, using the adiabatic tangent linear model, i.e. a call to CNT3TL from BGVECS. The eigenvectors of the analysis Hessian (next section) are also propagated similarly in time, by a call to CNT3TL from XFORMEV, to obtain **flow dependent background errors**. The number of model integrations required by LBGM is NBGVECS+invtot, which is typically 50+100=150. If LBGM=.T. then the simplified error growth model (Section 6.7) is not used. In that case the routine ESTSIG is used only to limit the error growth produced by the model to within 10 and 90 % of the climate variance for vorticity.

The background errors diagnosed by BGVECS may be written out for diagnostic purposes by setting LWRISIGB. The errors are written by a call to WRITESD (called from CVA1)..

6.4 CALCULATION OF EIGENVALUES AND EIGENVECTORS OF THE HESSIAN

The second stage in the calculation of analysis errors is to determine eigenvalues and eigenvectors of the Hessian of the cost function. This is done using a combined Lanczos and conjugate-gradient algorithm, CONGRAD, called from CVA1 under the control of LAVCGL. Note that CONGRAD requires that the cost function is strictly quadratic. The tangent linear model and observation operators must be invoked by setting L131TL and LOBSTL. (L131TL should be set even in 3D-Var.) Variational quality control must be disabled by unsetting LVARQCG and LQSCATT must be set to request a quadratic cost function for scatterometer observations.

CONGRAD starts by transforming the initial control variable and gradient to a space with euclidian inner product. Typically, this transformation is simply a multiplication by SCALPSQRT, but may also involve preconditioning via calls to PRECOND. The transformed initial gradient is normalized to give the first Lanczos vector. Depending on the setting of LIOWKCGL, the Lanczos vectors are stored either on the MIO file associated with unit NWK-CGL, or in the allocated array VCGLWK.

Each iteration of the conjugate-gradient/Lanczos algorithm starts by calculating the product of the Hessian and the latest search direction. This is calculated as $J''d = \|d\|(\nabla J(x_0 + d/\|d\|) - \nabla J(x_0))$. This finite difference formula is exact, since the cost function is quadratic.

The optimal step is calculated as the point at which the gradient is orthogonal to the search direction. The control variable and gradient at the optimal point are also calculated. Once the gradient at the optimal point is known, it is orthogonalized with respect to previous gradients, and the search direction and gradient for the next iteration are calculated. The tridiagonal matrix of the Lanczos algorithm is initialized and its eigenvalues and eigenvectors are determined by a call to the NAG routine F08JEF

The leading eigenvalue of the tridiagonal system is compared against the leading converged eigenvalue of the Hessian matrix. This provides a sensitive test that the algorithm is behaving correctly. Any increase in the leading eigenvalue provides an early indication of failure (for example, due to a bad gradient) and the algorithm is immediately terminated. The calculation is not aborted, since the test detects the failure of the algorithm before the converged eigenvalues and eigenvectors become corrupted.

The new Lanczos vector is calculated by normalizing the gradient and the subroutine loops back to perform the next iteration.

After the last iteration, the converged eigenvectors of the Hessian are calculated by calling **WREVECS**. Note that the criterion used to decide which eigenvalues have converged is relaxed at this stage to $\|J''v - \lambda v\| < \varepsilon \|v\|$, where ε is given by EVBCGL. The default value for EVBCGL is 0.1. The eigenvectors are passed to **XFORMEV**, which calculates the analysis errors. This part of the calculation is described in Section 6.6.

Finally, **CONGRAD** transforms the control vector and gradient from the euclidian space used internally to the usual space of the control variable.

6.5 THE PRECONDITIONER

CONGRAD allows the use of a preconditioner. The preconditioner is a matrix which approximates the Hessian matrix of the cost function. The preconditioner used in **CONGRAD** is a matrix of the form

$$\mathbf{I} + \sum (\mu_i - 1) \mathbf{w}_i \mathbf{w}_i^T \quad (6.1)$$

where the vectors \mathbf{w}_i are orthogonal. The pairs $\{\mu_i, \mathbf{w}_i\}$ are calculated in **PREPPCM**, and are intended to approximate some of the eigenpairs (i.e. eigenvalues and associated eigenvectors) of the Hessian matrix of the cost function. They are calculated as follows.

A set of L vectors, \mathbf{u}_i , is read in using **READVEC**. These vectors are assumed to satisfy

$$\mathbf{B} - \sum \mathbf{u}_i \mathbf{u}_i^T \approx \mathbf{P}_a \quad (6.2)$$

where \mathbf{B} is the background-error covariance matrix, and \mathbf{P}_a is the analysis-error covariance matrix. Vectors which meet this criterion can be written out from an earlier forecast error calculation by setting LWRIEVEC. The vectors are transformed to the space of the control vector by calls to **CHAVAR** to give an approximation to the inverse of

the Hessian matrix

$$\mathbf{I} - \sum (\mathbf{L}\mathbf{u}_i)(\mathbf{L}\mathbf{u}_i)^T \approx (\mathbf{J}'')^{-1} \quad (6.3)$$

(Here, \mathbf{L} denotes the change-of-variable operator implemented by **CHAVAR**.)

Let us denote by \mathbf{U} the matrix whose columns are the vectors \mathbf{u}_i . A sequence of Householder transformations is now performed to transform \mathbf{LU} to upper triangular. Let us represent this sequence of Householder transformations by the matrix \mathbf{Q} . Then \mathbf{QLU} is upper triangular, which means that $(\mathbf{QLU})(\mathbf{QLU})^T$ is zero except for an $L \times L$ block in the top left hand corner.

It is clear that $(\mathbf{QLU})(\mathbf{QLU})^T$ has only L non-zero eigenvalues. Moreover, the non-zero eigenvalues are the eigenvalues of the $L \times L$ block matrix, and the eigenvectors of $(\mathbf{QLU})(\mathbf{QLU})^T$ are the eigenvectors of the block matrix, appended by zeroes. These eigenvalues and eigenvectors are calculated by a call to the NAG routine F02FAF.

Now, since \mathbf{Q} is an orthogonal matrix, we have $\mathbf{Q}\mathbf{Q}^T = \mathbf{I}$. So, we may write Eq. (6.3) as

$$\mathbf{I} - \mathbf{Q}^T(\mathbf{QLU})(\mathbf{QLU})^T\mathbf{Q} \approx (\mathbf{J}'')^{-1} \quad (6.4)$$

Let us denote the eigenpairs of $(\mathbf{QLU})(\mathbf{QLU})^T$ by $\{\rho_i, \mathbf{v}_i\}$. Then we may write Eq. (6.4) as

$$\mathbf{I} - \sum \rho_i(\mathbf{Q}^T\mathbf{v}_i)(\mathbf{Q}^T\mathbf{v}_i)^T \approx (\mathbf{J}'')^{-1} \quad (6.5)$$

The orthogonality of \mathbf{Q} and the orthonormality of the eigenvectors \mathbf{v}_i , means that the vectors $\mathbf{Q}^T\mathbf{v}_i$ are orthonormal. They are, in fact, the required vectors, \mathbf{w}_i of the preconditioner matrix.

Inverting Eq. (6.5) gives

$$\mathbf{I} - \sum \frac{1}{\rho_i} \mathbf{w}_i \mathbf{w}_i^T \approx \mathbf{J}'' \quad (6.6)$$

Defining $\mu_i = 1 - 1/\rho_i$ gives the required approximation to the Hessian matrix.

The preconditioner vectors are sorted in decreasing order of μ_i , and all vectors for which $\mu_i < 1$ are rejected. These vectors cannot be good approximations to eigenvectors of the Hessian matrix, since the eigenvalues of the Hessian matrix are all greater than or equal to one. A final refinement to the calculation is to reduce large values of μ_i to a maximum of 10. This was found to be necessary in practice to avoid ill-conditioning the minimization.

The numbers μ_i are stored in RCGLPC. The vectors, \mathbf{w}_i are stored in VCGLPC.

Application of the preconditioner is straightforward, and is performed by subroutine **PRECOND**. This routine can also apply the inverse, the symmetric square root, or the inverse of the symmetric square root of the preconditioner matrix. Application of the latter matrices relies on the observation that if

$$\mathbf{M} = \mathbf{I} + \sum (\mu_i - 1) \mathbf{w}_i \mathbf{w}_i^T \quad (6.7)$$

with orthonormal \mathbf{w}_i , then the expressions for \mathbf{M}^{-1} , $\mathbf{M}^{1/2}$ and $\mathbf{M}^{-1/2}$ result from replacing μ_i in Eq. (6.7) by $1/\mu_i$, $\sqrt{\mu_i}$ and $1/(\sqrt{\mu_i})$ respectively.

6.6 CALCULATION OF ANALYSIS-ERROR VARIANCES

The eigenvectors and eigenvalues of the Hessian matrix calculated by **CONGRAD** are passed to **XFORMEV**, which uses them to estimate the analysis error variances. If preconditioning has been employed, then the eigenvectors and eigenvalues provide an approximation to the preconditioned Hessian, $\mathbf{M}^{-1/2} \mathbf{J}'' \mathbf{M}^{-1/2}$, of the form

$$\mathbf{M}^{-1/2} \mathbf{J}'' \mathbf{M}^{-1/2} \approx \mathbf{I} + \sum (\lambda_i - 1) \mathbf{v}_i \mathbf{v}_i^T \quad (6.8)$$

The approximation is equivalent to setting to one all but the leading K eigenvalues of the preconditioned Hessian.

The first step is to undo the preconditioning. Multiplying to the left and right by $\mathbf{M}^{1/2}$, gives

$$\mathbf{J}'' \approx \mathbf{M} + \sum (\lambda_i - 1) (\mathbf{M}^{1/2} \mathbf{v}_i) (\mathbf{M}^{1/2} \mathbf{v}_i)^T \quad (6.9)$$

Substituting for the preconditioner matrix from Eq. (6.7), gives the following

$$\mathbf{J}'' \approx \mathbf{I} + \sum \mathbf{s}_i \mathbf{s}_i^T \quad (6.10)$$

where

$$\mathbf{s}_i = \begin{cases} (\mu_i - 1)^{1/2} \mathbf{w}_i & \text{for } i = 1 \dots L \\ (\lambda_{i-L} - 1)^{1/2} \mathbf{M}^{1/2} \mathbf{v}_{i-L} & \text{for } i = L + 1 \dots L + K \end{cases} \quad (6.11)$$

Operationally, preconditioning is not used. However **XFORMEV** makes no particular use of this fact. It simply sets L to zero in Eqs. (6.10) and (6.11).

The first step in **XFORMEV** is to calculate the vectors \mathbf{s}_i . They are stored in **VCGLWK**.

The next step is to invert the approximate Hessian matrix defined by Eq. (6.10). Let \mathbf{S} be the matrix whose columns are the vectors \mathbf{s}_i . Then, applying the Sherman–Morrison–Woodbury formula, the inverse of the approximate Hessian matrix is

$$(\mathcal{J}'')^{-1} \approx \mathbf{I} - \mathbf{S}(\mathbf{I} + \mathbf{S}^T \mathbf{S})^{-1} \mathbf{S}^T \quad (6.12)$$

The matrix $(\mathbf{I} + \mathbf{S}^T \mathbf{S})$ is formed and its Cholesky decomposition is calculated using the NAG routine F07FDF. This gives a lower triangular matrix \mathbf{C} such that

$$(\mathcal{J}'')^{-1} \approx \mathbf{I} - (\mathbf{S}\mathbf{C}^{-1})(\mathbf{S}\mathbf{C}^{-1})^T \quad (6.13)$$

The matrix $(\mathbf{S}\mathbf{C}^{-1})$ is calculated by back-substitution.

The final stage in the calculation of the analysis errors is to transform the columns of the matrix $(\mathbf{S}\mathbf{C}^{-1})$ to the space of model variables by applying the inverse change of variable, **CHAVARIN**. This gives the required approximation to the analysis error covariance matrix

$$\mathbf{P}_a \approx \mathbf{B} - \mathbf{V}\mathbf{V}^T \quad (6.14)$$

where $\mathbf{V} = \mathbf{L}^{-1} \mathbf{S}\mathbf{C}^{-1}$, and where \mathbf{L}^{-1} represents the inverse of the change of variable. The columns of \mathbf{V} may be written out (e.g. for diagnostic purposes, or to form the preconditioner for a subsequent minimization) by setting **LWRIEVEC**. The columns of \mathbf{V} are then transformed to gridpoint space, and their sums of squares (i.e. the diagonal elements of $\mathbf{V}\mathbf{V}^T$ in gridpoint space) are subtracted from the variances of background error which were stored in **ANEBUF** before the minimization by **BGVECS**.

The analysis errors are calculated as the difference between the background errors and a correction derived from the eigenvectors of the Hessian. If the background errors are underestimated, there is a danger that the correction will be larger than the background error, giving negative variances of analysis error. This is unlikely to happen if the background errors are estimated using randomization, or for variables whose background errors are explicitly specified in the background cost function, but is possible for variables such as temperature whose background errors are not explicitly specified. To guard against this eventuality, if **NBGVECS** is zero, then the variances of analysis error for variables whose background errors are not explicit are estimated by applying a scaling to the explicit variables by a call to **ESTSIGA** from **CVA1**. The variances are then converted to standard deviations and written out by a call to **WRITESD**.

6.7 CALCULATION OF FORECAST ERROR VARIANCES

The analysis errors are inflated according to the error growth model of *Savijärvi (1995)* to provide estimates of short term forecast error. This is done by a call to **ESTSIG**. There is also an option to advect the background errors for vorticity as if they were a passive tracer. The advection is performed by **ADVSIGA**.

The error growth model is

$$\frac{d\sigma}{dt} = (a + b\sigma) \left(1 - \frac{\sigma}{\sigma_\infty}\right) \quad (6.15)$$

Here, a represents growth due to model errors, b represents the exponential growth rate of small errors, and σ_∞ represents the standard deviation of saturated forecast errors.

The saturation standard deviations are calculated as $\sqrt{2}$ times the standard deviation of each field. The standard deviations have been calculated for each month from the re-analysis dataset. **ESTSIG** reads these climatological error fields from file 'stdev_of_climate' by calling **READGRIB**, and interpolates them in the horizontal and verti-



cal using **SUHIFCE** and **SUVIFCE**. The climatological errors may also be artificially increased in the tropics under the control of **LFACHRO**. This is the default, and is recommended in preference to using **LFACHR**, since it means that the forecast errors that are archived, and are used to screen observations, are closer to those used to formulate the background cost function. If climate standard deviations are not available for any field, they are estimated as 10 times the global mean background error for the field.

The growth due to model error is set to 0.1 times the global mean background error per day. The exponential growth rate, b , is set to 0.4 per day.

The error growth model is integrated for a period of **NFGFLEN** hours. The integration is done analytically using the expression given by *Savijärvi (1995)*. Two precautions are taken in integrating the error growth model. First, negative analysis error variances are set to zero. Second, the growth rate due to model error is limited to a sensible value with respect to the saturation errors. This was found to be necessary to prevent numerical problems when calculating specific humidity errors for the upper levels of the model.

ESTSIG overwrites the contents of **ANEBUF** with the estimated variances of forecast error. The variances are converted to standard deviations and written out by **WRITESD**.

**Part II: DATA ASSIMILATION****CHAPTER 7 Gravity-wave control****Table of contents**

- 7.1 Introduction
- 7.2 Normal-mode initialization
- 7.3 Computation of normal modes
 - 7.3.1 Vertical modes
 - 7.3.2 Horizontal modes and help arrays
- 7.4 Implementation of NMI
- 7.5 Computation of BASED ON NMI
- 7.6 Digital filter initialization
- 7.7 Implementation of DFI as a weak constraint in 4D-Var

7.1 INTRODUCTION

In 3D-Var, gravity-wave control is achieved via the techniques of normal-mode initialization (NMI), in 4D-Var a weak constraint digital filter is used

[Section 7.2](#) provides a brief overview of NMI techniques, together with references to scientific papers in which further details can be found. [Section 7.3](#) describes the computation of normal modes and related arrays. [Section 7.4](#) documents the implementation of nonlinear NMI in 3D- and 4D-Var, while [Section 7.5](#) describes the computation of J_c based on NMI. [Section 7.6](#) gives an overview of digital filter initialization techniques while [Section 7.7](#) describes its implementation as it is used in the 4D-Var assimilation system.

7.2 NORMAL-MODE INITIALIZATION

If the model equations are linearized about a state of rest, the solutions can (with a certain amount of arbitrariness) be classified into ‘slow’ (Rossby) and ‘fast’ (gravity) modes. This classification defines two mutually orthogonal subspaces of the finite-dimensional vector space containing the model state \mathbf{x} . Thus, the model state can be written as

$$\mathbf{x} = \mathbf{x}_R + \mathbf{x}_G \quad (7.1)$$

where \mathbf{x}_R is the ‘slow’ component and \mathbf{x}_G the ‘fast’ component. *Linear* NMI consists of removing the fast component altogether ($\mathbf{x}_G = 0$). Since the model is nonlinear, a much better balance is obtained by setting the *tendency* of the fast component to zero ($\dot{\mathbf{x}}_G = 0$); it is this balance condition which *nonlinear* NMI seeks to impose.

Nonlinear NMI was first demonstrated by [Machenhauer](#) (1977), in the context of a spectral shallow-water model. For a multi-level model, the first stage in the modal decomposition is a vertical transform; each vertical mode then

has its own set of horizontal slow and fast modes (for the shallower vertical modes, all the corresponding horizontal modes can be considered as 'slow'). In the case of a multi-level spectral model using the ECMWF hybrid vertical coordinate the details may be found in the report by *Wergen* (1987), which also describes techniques for taking into account forcing by physical (non-adiabatic) processes and the diurnal and semi-diurnal tidal signals. Although these options are still coded in the IFS, they are no longer used operationally at ECMWF and will not be described in this documentation.

Implicit normal mode initialization (*Temperton* 1988) is based on the observation that, except at the largest horizontal scales, the results of NMI can be reproduced almost exactly without computing the horizontal normal modes at all. The calculation reduces to solving sets of elliptic equations. In the case of a spectral model (*Temperton* 1989), these sets of equations are tridiagonal in spectral space. The IFS code includes the option of 'partially implicit NMI', in which the initialization increments are computed using the full 'explicit' NMI procedure for large horizontal scales while the remaining increments at smaller horizontal scales are computed using the simpler implicit procedure.

7.3 COMPUTATION OF NORMAL MODES

7.3.1 Vertical modes

The vertical normal modes depend on the number of levels in the model and on their vertical distribution. They also depend on the choice of reference temperature SITR (assumed isothermal) and reference surface pressure (SIPR). The vertical modes used by the initialization routines are also used in the semi-implicit scheme for the forward integration of the model. The computation of J_b and J_c also uses the vertical normal modes, but for these purposes different values of SITR and SIPR may be selected. Thus the vertical modes are computed both in **SUDYN** and **SUSINMI**, the latter being used especially in 4D-Var where it is necessary to alternate between applications using different choices of SITR and SIPR. The vertical modes are computed by first calling **SUBMAT** to set up a vertical structure matrix and then calling an eigenvalue/eigenvector routine EIGSOL (at the end of SUDYN, it calls routine RG in the auxiliary library). After reordering and normalization, the eigenvectors (vertical modes) are stored in the matrix SIMO, while the corresponding eigenvalues (equivalent depths) are stored in the array SIVP. The inverse of SIMO is computed and stored in SIMI.

7.3.2 Horizontal modes and help arrays

The horizontal normal modes depend on the equivalent depths (see above) and the chosen spectral truncation NXMAX. For 'explicit' NMI, NXMAX is equal to the model's spectral truncation NSMAX. Normally, 'partially implicit NMI' is chosen by setting the switch LRPIMP to .TRUE. In this case the explicit NMI increments are used only up to spectral truncation NLEX (21 by default) but in order to blend the explicit and implicit increments smoothly, explicit increments are computed up to a slightly higher resolution. By default, $NXMAX = NLEX + 5$.

For most applications of the NMI procedure in the operational suite, it is considered that the larger horizontal scales are best left uninitialized (they include, for example, atmospheric tidal signals and large-scale tropical circulations driven by diabatic processes). To cater for this option there is another logical switch, LASSI ('adiabatic small-scale initialization'), which sets to zero all the initialization increments for total wavenumbers up to NFILTM (= 19 by default). Since only the small-scale increments are used, the NMI can be completely implicit: NLEX is set to 0 and there is no need to calculate the 'explicit' horizontal normal modes.

All the horizontal-normal-mode computations are carried out only for the first NVMOD vertical modes. By default,

NVMOD = 5.

The horizontal modes are computed by calling **SUMODE3**. In turn, **SUMODE3E** computes the explicit modes and their frequencies while **SUMODE3I** computes the ‘help’ arrays required to invert the tridiagonal systems encountered in implicit NMI.

7.4 IMPLEMENTATION OF NMI

Nonlinear NMI is invoked by calling **NNMI3**. Model tendencies are computed by calling **STEPO** to perform one (forward) timestep. The tendencies are then supplied to **MO3DPRJ** which computes the required increments, using the ‘explicit’ (Machenauer) or the ‘implicit’ scheme (or both, after which the results are merged). The increments are added to the original spectral fields and the process is iterated NITNMI (by default 2) times.

7.5 COMPUTATION OF J_c BASED ON NMI

In the notation of Eq. (7.1), the penalty term J_c is defined by

$$J_c = \varepsilon \left\| (\dot{\mathbf{x}} - \dot{\mathbf{x}}_b)_G \right\|^2 \quad (7.2)$$

where ε is an empirically chosen weighting factor, \mathbf{x} is the current state of the control variable and \mathbf{x}_b is the background. The norm $\| \cdot \|^2$ is based on a weighted sum of squares of spectral coefficients. Only the first NVMOD vertical modes are included in the evaluation of (7.2).

J_c is computed by calling the routine **COSJC**. Control passes through **JCCOMP** to **NMIJCTL**, where J_c is evaluated by calling **STEPO** twice, then projecting the differences in the tendencies on to the gravity modes via **MO3DPRJ**, and finally computing J_c in **NMICOST**.

7.6 DIGITAL FILTER INITIALIZATION

Digital filter initialization consists in removing high frequency oscillations from the temporal signal represented by the meteorological fields. A general description of digital filter initialization can be found in Lynch (1993). It can be implemented as a strong constraint by filtering the model fields at the beginning of each forecast or as a weak constraint as described in Gustaffson (1992) and Gauthier and Thepaut (2001).

Time oscillations exceeding a cut-off frequency $\omega_c = (2\pi)/T_c$ can be filtered by applying a digital filter to a time series $f_k = f(t_k)$ for $t_k = k\Delta t$, Δt being the timestep. This proceeds by doing a convolution of $f(t)$ with a step function $h(t)$ so that

$$f \bullet h(t_N) = \sum h_k f_{N-k}$$

The step function h_k is found to be

$$h_k = \frac{\sin(\omega_c k \Delta t)}{k \pi}$$

In practice, the convolution is restricted to a finite time interval of time span T_s . We can write $T_s = 2M\Delta t$ and

$$f \bullet h(t_0) = \sum_{k=-M}^M \alpha_k f_k$$

with $\alpha_k = -h_{-k}$. This truncation introduces Gibbs oscillations which can be attenuated by introducing a Lanczos window which implies that the weights α_k are defined as $\alpha_k = -h_{-k} W_k$ with

$$W_k = \frac{\sin((k\pi)/(M+1))}{(k\pi)/(M+1)}$$

An alternative which is used at ECMWF has been proposed by Lynch(1997) to use a Dolph-Chebyshev window in which case

$$W_k = \frac{1}{2M+1} \left[1 + 2r \sum_{m=0}^M T_{2M}(x_0 \cos \theta_m / 2) \cos m \theta_k \right]$$

where $1/x_0 = \cos(\pi\Delta t)/\tau_s$, $1/r = \cosh(2M \operatorname{acosh} x_0)$, $\theta_k = (k2\pi)/M$ and T_{2M} is the Chebyshev polynomial of degree $2M$. The time span of the window is chosen so that $\tau_s = M\Delta t$.

7.7 IMPLEMENTATION OF DFI AS A WEAK CONSTRAINT IN 4D-VAR

In the context of 4D-Var data assimilation, the digital filter is used as a weak constraint. A penalty term is added to the cost function and replaces the NMI based penalty term. The implementation is based on Gauthier and Thépaut (2001). The filtered increments are calculated as:

$$\overline{\delta\mathbf{X}}(t_{N/2}) = \sum_{k=0}^N \alpha_k \delta\mathbf{X}(t_k)$$

Where N is the number of time steps in the minimisation and delta represents increments.

During each integration of the tangent linear model in the inner loop of the 4D-Var, the digital filter is applied to the increments and the partial sum accumulated by **EDIGFIL**. This gives a filtered increment valid at the mid-point of the assimilation window (arrays RACCSPA2 and RACCSPA3). The value of the non-filtered increment valid at the same time is also stored by **ECOPSP** in arrays RSTOSPA2 and RSTOSPA3. These routines are called in **CNT4TL** each time-step.

The adjoint model integration calculates the gradient in **EDIGFILAD**. The gradient is obtained by a single backward integration of the adjoint model. The adjoint calculations associated with the digital filter is a virtually cost free addition to the adjoint observation cost function calculations.

The filtering weights used by the digital filter are calculated in once during the setup phase by **SUEFW**. The default is to use a Dolph-Chebyshev non-recursive filter (NTPDFI=4).



The weak constraint term which is added to the cost function is the moist energy norm of the departure between those two states times a weight factor. All these computations are conducted in spectral space and applied to the spectral fields. The default mode at ECMWF is to redefine the norm so the digital filter is only applied to divergence (LDIVONLY=.true.). A larger weight factor (ALPHAG=100.) is in that case used in the weak constraint term.

The norm of the departure is computed in two steps. In **EVJCDFI**, the difference between RACCSPA2/RACCSPA3 and RSTOSPA2/RSTOSPA3 is computed and multiplied with alphag for the subset of wave numbers and vertical levels associated with each processor. The cost contribution is calculated for each wavenumber and vertical level using the specified norm. The contributions for all wavenumbers, levels and variables are gathered on each processor by **GATHERCOST2** and the total cost contribution is summed in array RSUMJCDFI for each variable and level. Finally, in **EVCOST**, the contributions from each variable and level are added to obtain the value of the penalty term.





Part II: DATA ASSIMILATION

CHAPTER 8 Diagnostics.

8.1. Introduction

8.1.1. Influence matrix diagnostic in 4D-Var

8.1.2. How to compute Self-Sensitivity

8.2. Observational influence and self-sensitivity for a DA scheme

8.2.1. Linear statistical estimation in numerical weather prediction

8.2.2. Approximate calculation of self-sensitivity in a large variational analysis system

8.3. The Gradient test

8.1 INTRODUCTION

8.1.1 Influence matrix diagnostic in 4D-Var

The influence matrix is used in ordinary least-squares applications for monitoring statistical multiple-regression analyses. Concepts related to the influence matrix provide diagnostics on the influence of individual data on the analysis, the analysis change that would occur by leaving one observation out, and the effective information content (degrees of freedom for signal) in any sub-set of the analysed data. The corresponding concepts have been derived in the context of linear statistical data assimilation in numerical weather prediction. An approximate method to compute the diagonal elements of the influence matrix (the self-sensitivities) has been developed for a large-dimension variational data assimilation system (the 4D-Var system of the European Centre for Medium-Range Weather Forecasts).

8.1.2 How to compute Self-Sensitivity

From clear-case branch: in /scripts/gen/ifsmin, namelist **NAMVAR** for the forecast error calculation (fce) must have LANOBS=.true.

In directory /vol/verify/sms/userID/exp/include, namelist **NAMVAR** in ifsmin (for forecast error calculation) must have LANOBS=.true.

Self-Sensitivities are stored in ODB (CCMA) in the word *an_sens_obs*. The final Self-Sensitivities are computed by dividing the content in *an_sens_obs* to (the content of) *final_obs_error* for every observation assimilated

A Fortran program is available (the program has been developed by Carla Cardinali, work is in progress to provide a user-version) to unload Self-Sensitivity from ODB and visual it with Metview.

8.2 OBSERVATIONAL INFLUENCE AND SELF-SENSITIVITY FOR A DA SCHEME

8.2.1 Linear statistical estimation in numerical weather prediction

Data assimilation systems for NWP provide estimates of the atmospheric state \mathbf{x} by combining meteorological observations \mathbf{y} with prior (or background) information \mathbf{x}_b . A simple Bayesian Normal model provides the solution as

the posterior expectation for \mathbf{x} , given \mathbf{y} and \mathbf{x}_b . The same solution can be achieved from a classical *frequentist* approach, based on a statistical linear analysis scheme providing the best linear unbiased estimate (*Talagrand, 1997*) of \mathbf{x} , given \mathbf{y} and \mathbf{x}_b . The optimal GLS solution to the analysis problem (see *Lorenc, 1986*) can be written

$$\mathbf{x}_a = \mathbf{K}\mathbf{y} + (\mathbf{I}_n - \mathbf{K}\mathbf{H})\mathbf{x}_b \quad (8.1)$$

The vector \mathbf{x}_a is the 'analysis'. The gain matrix \mathbf{K} ($n \times p$) takes into account the respective accuracies of the background vector \mathbf{x}_b and the observation vector \mathbf{y} as defined by the $n \times n$ covariance matrix \mathbf{B} and the $p \times p$ covariance matrix \mathbf{R} , with

$$\mathbf{K} = (\mathbf{B}^{-1} + \mathbf{H}^T \mathbf{R}^{-1} \mathbf{H})^{-1} \mathbf{H}^T \mathbf{R}^{-1} \quad (8.2)$$

Here, \mathbf{H} is a $p \times n$ matrix interpolating the background fields to the observation locations, and transforming the model variables to observed quantities (e.g. radiative transfer calculations transforming the models temperature, humidity and ozone into brightness temperatures as observed by several satellite instruments). In the 4D-Var context introduced below, \mathbf{H} is defined to include also the propagation in time of the atmospheric state vector to the observation times using a forecast model.

Substituting (8.2) into (8.1) and projecting the analysis estimate onto the observation space, the estimate becomes

$$\hat{\mathbf{y}} = \mathbf{H}\mathbf{x}_a = \mathbf{H}\mathbf{K}\mathbf{y} + (\mathbf{I}_p - \mathbf{H}\mathbf{K})\mathbf{H}\mathbf{x}_b \quad (8.3)$$

It can be seen that the analysis state in observation space ($\mathbf{H}\mathbf{x}_a$) is defined as a sum of the background (in observation space, $\mathbf{H}\mathbf{x}_b$) and the observations \mathbf{y} , weighted by the $p \times p$ square matrices $\mathbf{I} - \mathbf{H}\mathbf{K}$ and $\mathbf{H}\mathbf{K}$, respectively.

In this case, for each unknown component of $\mathbf{H}\mathbf{x}$, there are two data values: a real and a 'pseudo' observation. The additional term in (8.3) includes these pseudo-observations, representing prior knowledge provided by the observation-space background $\mathbf{H}\mathbf{x}_b$. From (8.3), the analysis sensitivity with respect to the observations is obtained

$$\mathbf{S} = \frac{\partial \hat{\mathbf{y}}}{\partial \mathbf{y}} = \mathbf{K}^T \mathbf{H}^T \quad (8.4)$$

Similarly, the analysis sensitivity with respect to the background (in observation space) is given by

$$\frac{\partial \hat{\mathbf{y}}}{\partial (\mathbf{H}\mathbf{x}_b)} = \mathbf{I} - \mathbf{K}^T \mathbf{H}^T = \mathbf{I}_p - \mathbf{S} \quad (8.5)$$

We focus here on the expressions (8.4) and (8.5). The influence matrix for the weighted regression DA scheme is actually more complex (see Appendix 1), but it obscures the dichotomy of the sensitivities between data and model in observation space.

The (projected) background influence is complementary to the observation influence. For example, if the self-sensitivity with respect to the i th observation is S_{ii} , the sensitivity with respect the background projected at the same variable, location and time will be simply $1 - S_{ii}$. It also follows that the complementary trace, $\text{tr}(\mathbf{I} - \mathbf{S}) = p - \text{tr}(\mathbf{S})$, is not the df for noise but for background, instead. That is the weight given to prior information, to be compared to the observational weight $\text{tr}(\mathbf{S})$. These are the main differences with respect to standard LS regression. Note that the different observations can have different units, so that the units of the cross-sensitivities are the corresponding unit

ratios. Self-sensitivities, however, are pure numbers (no units) as in standard regression. Finally, as long as \mathbf{R} is diagonal, (2.6) is assured, but for more general non-diagonal \mathbf{R} -matrices it is easy to find counter-examples to that property.

Inserting (8.1) into (8.4), we obtain

$$\mathbf{S} = \mathbf{R}^{-1} \mathbf{H} (\mathbf{B}^{-1} + \mathbf{H}^T \mathbf{R}^{-1} \mathbf{H})^{-1} \mathbf{H}^T \quad (8.6)$$

As $(\mathbf{B}^{-1} + \mathbf{H}^T \mathbf{R}^{-1} \mathbf{H})^{-1}$ is equal to the analysis error covariance matrix \mathbf{A} , we can also write $\mathbf{S} = \mathbf{R}^{-1} \mathbf{H} \mathbf{A} \mathbf{H}^T$.

8.2.2 Approximate calculation of self-sensitivity in a large variational analysis system

In an optimal variational analysis scheme, the analysis error covariance matrix \mathbf{A} is approximately the inverse of the matrix of second derivatives (the Hessian) of the cost function J , i.e. $\mathbf{A} = (\mathbf{J})^{-1}$ (Rabier and Courtier, 1992). Given the large dimension of the matrices involved, \mathbf{J} and its inverse cannot be computed explicitly. Following Fisher and Courtier (1995) we use an approximate representation of the Hessian based on a truncated eigen-vector expansion with vectors obtained through the Lanczos algorithm. The calculations are performed in terms of a transformed variable $\boldsymbol{\chi}$, $\boldsymbol{\chi} = \mathbf{L}^{-1}(\mathbf{x} - \mathbf{x}_b)$, with \mathbf{L} chosen such that $\mathbf{B}^{-1} = \mathbf{L}^T \mathbf{L}$. The transformation \mathbf{L} thus reduces the covariance of the prior to the identity matrix. In variational assimilation \mathbf{L} is referred to as the change-of-variable operator (Courtier et al. 1998).

$$\mathbf{J}^{-1} \simeq \mathbf{B} - \sum_{i=1}^M \frac{1 - \lambda_i}{\lambda_i} (\mathbf{L} \mathbf{v}_i) (\mathbf{L} \mathbf{v}_i)^T \quad (8.7)$$

The summation in (8.7) approximates the variance reduction $\mathbf{B} - \mathbf{A}$ due to the use of observations in the analysis. $(\lambda_i, \mathbf{v}_i)$ are the eigen-pairs of \mathbf{A} . In ECMWF's operational data assimilation system, the variances of analysis error are computed according to this method. The variances are inflated to provide estimates of short-term forecast (background) error variances to be used as background errors in the next analysis cycle (Fisher, 1996). The Hessian eigen-vectors are also used to precondition the minimization (Fisher and Andersson, 2001). The computed eigen-values are not used to minimize the cost function but only to estimate the analysis covariance matrix. It is well known, otherwise, that the minimization algorithm is analogous to the conjugate-gradient algorithm. Because the minimum is found within an iterative method, the operational number of iterations is sufficient to find the solution (with required accuracy) but does not provide a sufficient number of eigen-pairs to estimate the analysis error variances.

The diagonal of the background error covariance matrix \mathbf{B} in (8.7) is also computed approximately, using the randomisation method proposed by Fisher and Courtier (1995). From a sample of N random vectors \mathbf{u}_i (in the space of the control-vector), drawn from a population with zero mean and unit Gaussian variance, a low-rank representation of \mathbf{B} (in terms of the atmospheric state variables \mathbf{x}) is obtained by

$$\mathbf{B} = \frac{1}{N} \sum_{i=1}^N (\mathbf{L} \mathbf{u}_i) (\mathbf{L} \mathbf{u}_i)^T \quad (8.8)$$

This approximate representation of \mathbf{B} has previously been used by Andersson et al. (2000) to diagnose background errors in terms of observable quantities, i.e. $\mathbf{H} \mathbf{B} \mathbf{H}^T$.

Inserting (8.7) and (8.8) into (8.6) we arrive at an approximate method for calculating \mathbf{S} , that is practical for a large

dimension variational assimilation (both 3D and 4D-Var):

$$\mathbf{S} = \mathbf{R}^{-1} \mathbf{H} \left[\frac{1}{N} \sum_{i=1}^N (\mathbf{L}u_i)(\mathbf{L}u_i)^T + \sum_{i=1}^M \frac{1-\lambda_i}{\lambda_i} (\mathbf{L}v_i)(\mathbf{L}v_i)^T \right] \mathbf{H}^T \quad (8.9)$$

Only the diagonal elements of \mathbf{S} are computed and stored in ODB - that is, the analysis sensitivities with respect to the observations, or self-sensitivities S_{ii} . The cross-sensitivity S_{ij} for $i \neq j$, that represents the influence of the j th observation to the analysis at the i th location, is not computed. Note that the approximation of the first term is unbiased, whereas the second term is truncated such that variances are underestimated. For small M the approximate S_{ii} will tend to be over-estimates. For the extreme case $M=0$ Eq. (8.9) gives $\mathbf{S}=\mathbf{R}^{-1}\mathbf{H}\mathbf{B}\mathbf{H}^T$ which in particular can have diagonal elements larger than one if elements of $\mathbf{H}\mathbf{B}\mathbf{H}^T$ are larger than the corresponding elements of \mathbf{R} . The number of Hessian vectors operationally computed is $M=40$ and the number of random \mathbf{B} vectors is $N=50$.

In general, in the operational system, 15% of the global influence is due to the assimilated observations in any one analysis, and the complementary 85% is the influence of the prior (background) information, a short-range forecast containing information from earlier assimilated observations. About 25% of the observational information is currently provided by surface-based observing systems, and 75% by satellite systems.

Low-influence data points usually occur in data-rich areas, while high-influence data points are in data-sparse areas or in dynamically active regions. Background error correlations also play an important role: High correlation diminishes the observation influence and amplifies the importance of the surrounding real and pseudo observations (prior information in observation space). Incorrect specifications of background and observation error covariance matrices can be identified, interpreted and better understood by the use of influence matrix diagnostics for the variety of observation types and observed variables used in the data assimilation system.

Self-sensitivities cannot be larger than one (they are bounded in the interval zero to one) but, because of the small number of eigenpair we can compute, S_{ii} can be greater than one. Approximations in both of the two terms of (8.9) contribute to the problem. In the second term the number of Hessian eigen-vectors is truncated to M . The term is therefore underestimated, and S_{ii} will tend to be over-estimated. The degree of over-estimation depends on the structure of the covariance reduction matrix $\mathbf{B}-\mathbf{A}$.

For an analysis in which observations lead to strongly localised covariance reduction (such as the humidity analysis with its short co-variance length scales ~ 180 km, and large observational impacts) a large M is required to approximate $\mathbf{B}-\mathbf{A}$ accurately. The approximate computation is mostly affecting the self-sensitivities close to the upper bound leaving the self-sensitivities <0.7 almost unaffected.

To conclude, the self-sensitivity provides a quantitative measure of the observation influence in the analysis. In robust regression, it is expected that the data have similar self-sensitivity (sometimes called leverage) - that is, they exert similar influence in estimating the regression line. Disproportionate data influence on the regression estimate can have different reasons: First, there is the inevitable occurrence of incorrect data. Second, influential data points may be legitimately occurring extreme observations. However, even if such data often contain valuable information, it is constructive to determine to which extent the estimate depends on these data. Moreover, diagnostics may reveal other patterns e.g. that the estimates are based primarily on a specific sub-set of the data rather than on the majority of the data. In the context of 4D-Var there are many components that together determine the influence given to any one particular observation. First there is the specified observation error covariance \mathbf{R} , which is usually well known and obtained simply from tabulated values. Second, there is the background error covariance \mathbf{B} , which is specified in terms of transformed variables that are most suitable to describe a large proportion of the actual background error covariance. The implied covariance in terms of the observable quantities is not immediately available for inspection, but it determines the analysis weight given to the data. Third, the dynamics and the physics of the

forecast model propagate the covariance in time, and modify it according to local error growth in the prediction. The influence is further modulated by data density. Low influence data points occur in data-rich areas while high influence data points are in data-sparse regions or in dynamically active areas. Background error correlations also play an important role. In fact, very high correlations drastically lessen the observation influence in favour of background influence and amplify the influence of the surrounding observations.

With the approximate method used here, out-of-bound self-sensitivities occur if the Hessian representation based on an eigen-vector expansion is truncated, especially when few eigen-vectors are used. However, this problem affects only a small percentage of the self-sensitivities computed in this study, and in particular those that are closer to one. Remaining values greater than one can be due to large background to observation error ratio, which is one factor that is known to contribute towards ill-conditioning and poor convergence of the 4D-Var algorithm.

8.3 THE GRADIENT TEST

If `LTEST=.true.` a gradient test will be performed both before and after minimization. This is done by the routine `GRTEST`. In the gradient test a test value t_1 is computed as the ratio between a perturbation of the cost-function and its first order Taylor expansion:

$$t_1 = \lim_{\delta\chi \rightarrow 0} \frac{J(\chi + \delta\chi) - J(\chi)}{\langle \nabla J, \delta\chi \rangle} \quad (8.10)$$

with $\delta\chi = -\alpha \nabla J$. Repeatedly increasing α by one order of magnitude, printing t_1 at each step should show t_1 approaching one, by one order of magnitude at a time, provided $J(\chi)$ is approximately quadratic over the interval $[\chi, \chi + \delta\chi]$. The near linear increase in the number of 9's in the print of t_1 over a wide range of α (initially as well as after minimization) proves that the coded adjoint is the proper adjoint for the linearization around the given state χ .

The behaviour of the cost function in the vicinity of χ in the direction of the gradient ∇J is also diagnosed by several additional quantities for each α . The results are printed out on lines in the log-file starting with the string ‘GRTEST:’. To test the continuity of J , for example, a test value t_0 is computed:

$$t_0 = \frac{J(\chi + \delta\chi)}{J(\chi)} - 1 \quad (8.11)$$

and printed. For explanation of other printed quantities see the routine `GRTEST` itself. A range of additional test was introduced in CY28r2.





Part II: DATA ASSIMILATION

CHAPTER 9 Observation processing

NOT YET AVAILABLE





Part II: DATA ASSIMILATION

CHAPTER 10 Observation screening

Table of contents

- 10.1 Introduction
- 10.2 The structure of the observation screening
 - 10.2.1 The incoming observations
 - 10.2.2 The screening run
 - 10.2.3 General rationale of the observation screening
 - 10.2.4 3D- versus 4D-Var screening
- 10.3 The independent observation screening decisions
 - 10.3.1 Preliminary check of observations
 - 10.3.2 Blacklisting
 - 10.3.3 Background quality control
- 10.4 Screening of satellite radiances
- 10.5 Scatterometer processing
 - 10.5.1 Introduction
 - 10.5.2 Background and general Scatterometer geometry
 - 10.5.3 Location of scatterometer data in the ECMWF archives
 - 10.5.4 ESA scatterometer (ERS-1 and ERS-2) processing
 - 10.5.5 NASA scatterometer (NSCAT) processing
 - 10.5.6 NASA scatterometer (QuikSCAT) processing
- 10.6 The dependent observation screening decisions
 - 10.6.1 Update of the observations
 - 10.6.2 Global time–location arrays
 - 10.6.3 Vertical consistency of multilevel reports
 - 10.6.4 Removal of duplicated reports
 - 10.6.5 Redundancy check
 - 10.6.6 Thinning
 - 10.6.7 A summary of the current use of observations
 - 10.6.8 Compression of the ODB
- 10.7 A massively-parallel computing environment

10.1 INTRODUCTION

This chapter describes the observation screening in the ECMWF 3D/4D-Var data assimilation. A more general description can be found in *Järvinen and Undén (1997)*. The purpose of the observation screening is to select a clean array of observations to be used in the data assimilation. This selection involves quality checks, removal of duplicated observations, thinning of their resolution etc.. The current selection algorithm has been operational since September 1996 and was to a large extent designed to reproduce the functionalities of the corresponding codes in the ECMWF OI analysis (*Lönnberg and Shaw 1985; 1987; Lönnberg, 1989*).

This chapter was prepared in September 1997 by Heikki Järvinen, Roger Saunders and Didier Lemeur. It was updated in February 1999 by Roger Saunders for TOVS processing, by Elias Holm and Francois Bouttier for the remainder, with further updates in October 2004 (to cy28r1) by Erik Andersson, Drasko Vasiljevic, Tony McNally (radiance data) and Hans Hersbach (scatterometer).

10.2 THE STRUCTURE OF THE OBSERVATION SCREENING

10.2.1 The incoming observations

Before the first trajectory integration of the assimilation various observation processing steps take place. The observations for the current assimilation period are extracted from the Reports Data Base (RDB) of observations, coded in BUFR. The extracted data reside in separate BUFR files for each main observing system, e.g. conventional, ATOVS, geostationary radiances, AIRS and so on. These data have already undergone some rudimentary quality control, e.g. a check for the observation format and position, for the climatological and hydrostatic limits, as well as for the internal and temporal consistency. The so-called RDB flag has been assigned according to the outcome of such checks.

The Observation Data Base (ODB, see separate documentation) is filled from the BUFR files in a sequence of jobs called BUFR2ODB. These jobs are multi-tasked running on parallel servers. Several or all observation types can run synchronously. The resulting 'raw' ODB is processed further by the IFS, in preparation for the main analysis tasks. These ODB and data manipulation tasks are referred to as 'the make CMA replacement' (for historical reasons), and are activated by the switch LMKCMARPL. MKCMARPL entails format conversions, changes of some observed variables, such as calculation of relative humidity from dry and wet bulb temperatures and wind components from speed and direction. The assignment of observation error statistics is also done at this stage, at least for conventional data.

The resulting 'extended' ODB data base (the ECMA) contains all the observational information for the data window as required for 3D/4D-Var as well as all data that are going to be monitored. The next step is that the observations are compared to the model as it is integrated for the length of the assimilation window ([Chapter 2](#)). The observation minus model differences (the departures) are computed as described in [Chapter 5](#) and stored in the ODB. These departures are an important input to the data selection procedures as many quality-control decisions depend on the magnitude of the departure. The collection of routines that perform data selection are jointly referred to as 'the screening'. The purpose of the observation screening is to select the best quality observations, to detect duplicates, and reduce data redundancy through thinning.

10.2.2 The screening run

The ECMWF 3D/4D-Var data assimilation system makes use of an incremental minimization scheme, as described in [Chapter 2](#). The sequence of jobs starts with the first (high resolution) trajectory run. During this run the model counterparts for all the observations are calculated through the non-linear observation operators, and the observa-

tion minus model difference (the departures) are calculated. As soon as these background departures are available for all observations, the screening can be performed. Prior to the screening the model fields are deallocated (dealmod) as most of the information necessary in the screening is stored in the observation data base (ODB). For the observation screening, the background errors (available as grid data in the 'errgrib' file, see [Chapter 14](#)) are interpolated to the observation locations for the observed variables ([INIFGER](#), [SUFGER](#) and [GEFGER](#)).

Technically, the final result of the observation screening is a pair of ODBs. The original 'extended' observation data base now contains observations complemented by the background departures, together with quality control information for most of the observations. This ECMA ODB remains on disc for later use in feedback creation. The compressed ODB, the CCMA, is a subset of the original observations, and is passed for the subsequent minimization job. The CCMA contains only those observations that are to be used in the minimisation.

10.2.3 General rationale of the observation screening

The general logic in the 3D/4D-Var observation screening algorithm is to make the *independent* decisions first, i.e. the ones that do not depend on any other observations or decisions ([DECIS](#)). One example is the background quality control for one observed variable. These can be carried out in any order without affecting the result of any other independent decision. The rest of the decisions are considered as mutually *dependent* on other observations or decisions, and they are taken next, following a certain logical order. For instance, the horizontal thinning of TOVS reports is only performed for the subset of reports that passed the background quality control. Finally, the CCM data base is created for the minimization in such a way that it only contains the data that will be used.

10.2.4 3D- versus 4D-Var screening

In the original 3D-Var assimilation system the screening rules were applied once, for the complete set of observations spanning a six-hour period. In the early implementation of the 4D-Var assimilation system, the same adta selection approach called '3D-screening' was applied over the 6-hour long 4D-Var time window, which resulted in essentially the same screening decisions as in 3D-Var.

In summer 1997, a new screening procedure called 4D-screening was implemented that took into account the temporal distribution of the observations. The time window is divided into time-slots of typically half-hour length (15 minutes for the first and the last time slots). The 3D-screening algorithm was then applied separately to observations within each time-slot. This allowed more data to be used by 4D-Var, for instance, all messages from an hourly reporting station can now be used, whereas only one (closest to central time) would have been allowed by the redundancy check in the 3D-screening. The 4D-screening behaviour is activated by switch LSCRE4D; it is meant to be used in conjunction with time correlation of observation errors where appropriate, as explained in [Järvinen et al \(1999\)](#) and in [Chapter 5](#). Also the current 3D-FGAT configuration ([Chapter 3](#)) relies on 4D-screening (LSCRE4D=.T.).

10.3 THE INDEPENDENT OBSERVATION SCREENING DECISIONS

10.3.1 Preliminary check of observations

The observation screening begins with a preliminary check of the completeness of the reports ([PRECH](#)). None of the following values should be missing from a report: observed value, background departure, observation error and vertical coordinate of observation. Also a check for a missing station altitude is performed for synop, temp and pilot reports. The reporting practice for synop and temp mass observations (surface pressure and geopotential height) is checked ([REPR](#)), as explained in the appendix. At this stage also, the observation error for synop geo-

potential observations is inflated if the reported level is far from the true station level (**ADDOER**). The inflation is defined as a proportion of the difference between the reported level and the true station altitude by adding 2% of the height difference to the observation error.

10.3.2 Blacklisting

Next, the observations are scanned through for blacklisting (subroutine **BLACK**). At the set-up stage the blacklist interface is initialized (**BLINIT**) to the external blacklist library. The interface between the IFS and the blacklist described in further detail in [Chapter 5](#), and in the full Blacklist documentation available elsewhere. The blacklist files ([Chapter 14](#)) consist formally of two parts. Firstly, the selection of variables for assimilation is specified in the 'data selection' part of the blacklist file. This controls which observation types, variables, vertical ranges etc. will be selected for the assimilation. Some more complicated decisions are also performed through the data selection file; for instance, an orographic rejection limit is applied in the case of the observation being too deep inside the model orography. This part of the blacklist also provides a handy tool for experimentation with the observing system, as well as with the assimilation system itself. Secondly, a 'monthly monitoring' blacklist file is provided for discarding the stations that have recently been reporting in an excessively noisy or biased manner compared with the ECMWF background field.

10.3.3 Background quality control

TABLE 10.1 THE PREDEFINED LIMITS FOR THE BACKGROUND QUALITY CONTROL, GIVEN IN TERMS OF MULTIPLES OF THE EXPECTED VARIANCE OF THE NORMALIZED BACKGROUND DEPARTURE.

Variable	Flag 1	Flag 2	Flag 3
u, v	9.00	16.00	25.00
z, ps	12.25	25.00	36.00
dz	x	x	x
T	9.00	16.00	25.00
rh, q	9.00	16.00	25.00

Flag values are denoted by 1 for a probably correct, 2 for a probably incorrect and 3 for an incorrect observation. The variables are denoted by u and v for wind components, z for geopotential height, ps for surface pressure, dz for thickness, T for temperature, rh for relative humidity and q for specific humidity, respectively.

The background quality control (**FIRST**) is performed for all the variables that are intended to be used in the assimilation. The procedure is as follows. The variance of the background departure $y - H(x_b)$ can be estimated as a sum of observation and background error variances $\sigma_o^2 + \sigma_b^2$, assuming that the observation and the background errors are uncorrelated. After normalizing with σ_b , the estimate of variance for the normalized departure is given by $1 + \sigma_o^2/\sigma_b^2$. In the background quality control, the square of the normalized background departure is considered as suspect when it exceeds its expected variance more than by a predefined multiple (**FGCHK**, **SUFGLIM**). For the wind observations, the background quality control is performed simultaneously for both wind components (**FGWND**). In practice, there is an associated background quality-control flag with four possible values, namely 0 for a correct, 1 for a probably correct, 2 for a probably incorrect and 3 for an incorrect observation, respectively (**SUSCRE0**). [Table 10.1](#) gives the predefined limits for the background quality control in terms of multiples of the expected variance of the normalized background departure. These values are set in **DEFRUN** and can be changed in namelist **NAMJO**. For satob winds the background error limits are modified as explained in [Appendix A](#)

There is also a background quality control for the observed wind direction (**FGWND**). The predefined error limits of 60°, 90° and 120° apply for flag values 1, 2 and 3, respectively. The background quality control for the wind direction is applied only above 700 hPa for upper-air observations for wind speeds larger than 15 m s⁻¹. If the wind-direction background quality-control flag has been set to a value that is greater than or equal to 2, the background quality-control flag for the wind observations is increased by 1. For scatterometer winds, a test for high wind speeds and cold SST is applied in the IFS routine **FGWND**.

10.4 SCREENING OF SATELLITE RADIANCES

This part of the documentation will be provided by the Satellite Section.

10.5 SCATTEROMETER PROCESSING

10.5.1 Introduction

This section describes the flow of ERS, NSCAT, and QuikSCAT scatterometer data through the assimilation system. The retrieval of 50 km QuikSCAT winds and some tasks for ERS are performed in the module PRESCAT, which, being part of the OBS family, are run before the screening. But it is most natural to describe the whole processing step here. This section provides a working knowledge of the software, and guidance on possible modifications and updates. It is not intended to explain the scientific background of microwave remote sensing or scatterometry and assumes some knowledge of these topics (see *Stoffelen 1999*).

Besides the introduction, this section is broken into five subsections. The next subsection gives background information on scatterometer processing at ECMWF. It includes a brief description of the various instruments, their period of functioning and operational assimilation at ECMWF. Besides it provides some history of the software, lists persons who contributed to the changes and outlines the structure and function of the whole library. [Subsection 10.5.3](#) gives concise information on the location of scatterometer data in the ECMWF archives. [Subsections 10.5.4–10.5.6](#) describe the line of processing for scatterometers (used or) currently in use at ECMWF, i.e. (ERS-1 and) ERS-2, (NSCAT) and QuikSCAT.

10.5.2 Background and general Scatterometer geometry

ESA's ERS-1 scatterometer was launched in July 1991 and stopped operating in June 2000. Its successor, ERS-2, was launched in 1995 and is still working. However, due to the loss of a proper functioning of its gyroscopes in January 2001 the yaw attitude control of the spacecraft became deteriorated. This especially affected the quality of scatterometer data, and as a result, its worldwide distribution was suspended. However, these problems were overcome by the combination of alternative on-board attitude control and the introduction of a completely revised on-ground processor. As a result, ESA resumed data distribution on 21 August 2003. Due to the loss of the on-board low-bit-rate recorders a few months earlier, global coverage was lost and data coverage is since then confined to the North-Atlantic and part of the Mediterranean. Data from ERS-2 were introduced into operations at ECMWF in January 1996, have been used until the suspension in January 2001, and were re-introduced on 9 March 2004. The NSCAT instrument was part of the payload of the ADEOS-I satellite, which was launched in August 1996. NSCAT data have been available from mid September 1996 until the spacecraft failure on June 30 1997. NSCAT data have never been part of the operational 4-D Var system. The QuikSCAT satellite, carrying the SeaWinds scatterometer instrument, was launched in June 1999. Its data was introduced in the operational 4-D Var system on 22 January 2002 and has been assimilated since that date. A second SeaWinds instrument, being on-board the Midori-II satellite, was launched in December 2002. Unfortunately, the Midori-II mission was lost in October 2003, which oc-

curred just a few weeks before the planned public release of the SeaWinds data. Consequently data from this instrument was never assimilated at ECMWF.

The scatterometers aboard the ERS-1 and ERS-2 satellites are of identical design. Operating at C-band frequency, three antennas at the right-hand side from the flight direction (45° , 90° and 135°) illuminate the ocean surface. Inside the 450 km wide swath, 19 nodes define a 25 km product. For each such node, average backscatter values for the three beams are determined from a 50 km by 50 km footprint, i.e., the 25 km product is over-sampled. More detailed information on the ERS scatterometers can be found in *Attema (1986)*, its impact on the ECMWF assimilation system in *Isaksen (1997)* and *Isaksen and Stoffelen (2000)*.

The NSCAT scatterometer that was part of the payload of the ADEOS-I satellite, consisted of three antennas on each side of the spacecraft. It operated at Ku-band frequency, and provided coverage in two simultaneous 600 km wide swaths, separated by a 350 km wide nadir gap. The resolution of the backscatter and wind product was 50 km. More detailed information on the NSCAT scatterometer can be found in the appendix of *Chelton et al. (2000)*, its impact on the ECMWF assimilation system in *Leidner et al. (2003)*.

The Seawinds scatterometer aboard the QuikSCAT and Midori-II satellites, finally, consists of two rotating beams operating at Ku-band frequency with incidence angles w.r.t. the normal of the ocean surface of 46° respectively 56° . Each beam provides a fore and an aft measurement. They cover a swath of 1,800 km in diameter, although only the inner 1,400 km is illuminated by both beams. The product is determined on a 25 km resolution, defining 76 across nodes. The first eight and last eight nodes contain two backscatter measurements (outer beam only), the other nodes can have up to 4 backscatter measurements. More detailed information on the QuikSCAT scatterometer can be found in *Leidner et al. (2000)*, its impact on the ECMWF assimilation system in *Hersbach et al. (2004)*.

Ad Stoffelen, David Anderson and Ross Hoffman were the first to work on the problem at ECMWF. Stoffelen and Anderson worked on quality control (QC) and wind retrieval issues in the OI system of these days. Hoffman looked at assimilation of backscatter information directly in 3D-Var. Once in operations, several others (Herve Roquet, Catherine Gaffard, Didier LeMeur and Lars Isaksen) took turns monitoring and improving the use of the data. Later Mark Leidner worked on the use of data from NASA scatterometers (NSCAT and QuikSCAT) and the operational implementation of the assimilation of QuikSCAT data was completed by Hans Hersbach and Lars Isaksen. The re-introduction of ERS-2 scat data in March 2004, and the formulation of an improved geophysical model function CMOD5, now being used for the inversion of ERS backscatter triplets to winds, was performed by Hans Hersbach.

Source code for scatterometer processing resides in ClearCase under the project name SCAT. The library contains the following directories:

- **etimesort/** source code for pre-processing ERS data
- **module/** shared modules
- **qbukey/** source code for adding RDB info to QuikSCAT 50km BUFR
- **qfilter/** source code for pre-processing QuikSCAT 25km BUFR
- **qretrieve/** source code for SeaWinds wind retrieval
- **dcone_qc/** source code to perform a global quality control check on QuikSCAT data with the goal to detect instrument anomalies
- **qsca_split/** source code that allows for the distribution of QuikSCAT pre-processing over several processors (not active)
- **monitoring/** empty directory in which scatterometer monitor software may reside in future
- **test/** empty directory for future test code

NSCAT-specific codes have not been put in ClearCase, because the satellite stopped operating in June 1997, i.e. its data will never be used in operations.

10.5.3 Location of scatterometer data in the ECMWF archives

TABLE 10.2 THE MARS ARCHIVE DEFINITIONS

	BUFR/MARS obstype	CMA code type	Satellite ID
ERS-1	122	122	1
ERS-2	122	122	2
NSCAT	136	210	280
QuikSCAT	137*	300	281
QuikSCAT	138*	301	281

*For QuikSCAT the BUFR format changed in February 2000 which is reflected in the change of MARS obstype from 137 to 138 and the change in the BUFR sequence descriptor.

The analysis input data for both ERS and QuikSCAT are available from MARS in BUFR format. This is not the case for NSCAT data. Data for the entire NSCAT 9-month mission are stored on ecfs in HDF format at

- ecfs:/oparch/nscat/50km/L17 - Level 1.7 files (backscatter data) and
- ecfs:/oparch/nscat/50km/L20 - Level 2.0 files (wind data), instead.

No SeaWinds data from Midori-II are present in the ECMWF archives.

The MARS archive definitions for the different wind scatterometer observations are given in [Table 10.2](#).

10.5.4 ESA scatterometer (ERS-1 and ERS-2) processing

[Fig. 10.1](#) shows a simple flow chart for ERS processing at ECMWF. Below the processing chain is described in general and the functionality of each executable in the scat library in particular.

Data for a given time window (12 hours in operations) are retrieved from MARS into patches of 6 hours, and time-wise centered around 00H, 06H, 12h and 18H. These data are then input to program TIMESORT, which sorts the observations by time and removes duplicate records. Duplicate records occur in the input data because more than one ground station may receive the same ERS data. Duplicated data are almost identical and their time stamps will differ by a small margin (< 4 seconds). The software for removing duplicates, or occasionally even triplets, resides in **etimesort**. The original algorithm was redesigned in CY28R1.

ERS winds are retrieved as part of the IFS observation pre-processor (IFS Documentation Part I “Observation processing” Chapter 10). Here, the three backscatter measurements are decoded from BUFR, and used to retrieve winds for 50 km diameter foot prints (the ERS winds are available at an over-sampled 25 km resolution). It is not possible to determine a unique wind vector solution, at least two ambiguous solutions will be found. Only the most likely wind and the first one in the opposite direction are kept and written to the observation data base (ODB) file. For this ERS winds are retrieved in-house, rather than using the unique wind distributed by ESA, to be able to supply two winds to the variational data assimilation system at ECMWF, and to be able to apply bias corrections to backscatter values before wind retrieval, and finally to be able to apply quality controls to the retrieved winds via the retrieval residual.

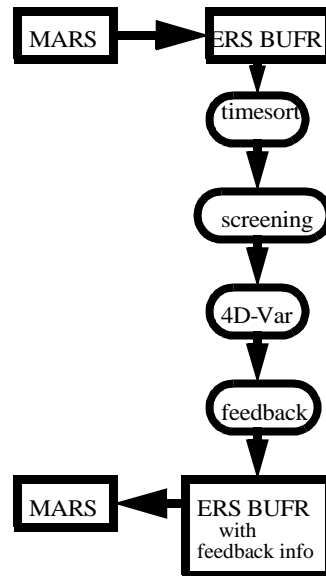


Figure 10.1 ERS processing

The in 25km-resolution available ERS data is subject to horizontal thinning, and is controlled by LSCATTHI and NTHINSCA in namelist NAMMKCMA. In the across-swath direction the inner two nodes are skipped (smallest incidence angles) because the scatterometer operates best at larger incidence angles. Then, every NTHINSCA node is used (default NTHINSCA = 4 results in use of node 3, 7, 11, 15, and 19). Along swath, the generic thinning procedure as described in Section 10.6.6 (minimum distance (NTHINSCA/4)*50km and maximum distance of (NTHINSCA/4)*100km) is applied. As a result, the data are used at a resolution of 100 km instead of the original 25 km sampling distance. It should be noted that the thinning process is actually set up in the observation pre-processing (IFS), but that only a flag is assigned at that stage, which is then applied in the screening. In that way all the data are completely pre-processed before assimilation, and the subsequent information kept in the feedback files allows to perform their monitoring at the full resolution.

In the IFS, both retrieved winds are used in the assimilation system. In 3D-Var, an observation cost function with two minima (see **pp_obs/HJO**) is used. This function is not quadratic, but depends on the fourth power and root of the product of the departures of u and v (*Stoffelen and Anderson (1997)*):

$$J(\mathbf{u}) = \frac{J_1 J_2}{(J_1^4 + J_2^4)^{0.25}}, \quad J_{1,2}(\mathbf{u}) = \frac{\|\mathbf{u} - \mathbf{u}_{1,2}\|^2}{\sigma_0^2}. \quad (10.1)$$

In the vicinity of each solution, this cost function looks quadratic. The observation error σ_0 is 2 m/s (defined in the **obs_preproc/QSCATIN** routine). Since the introduction (CY25R3) of the conjugate gradient minimisation technique, such a non-quadratic cost function is not longer allowed in 4D-Var. Instead, cost function (10.1) is replaced by:

$$J(u) = J_{1,2}(u) \quad (10.2)$$

where $J_{1,2}$ corresponds to the wind solution that is closest to the high-resolution trajectory. As a result, both retrieved wind solutions are still used. However, de-aliasing is now performed in the outer loop, enabling for a purely quadratic cost function in the inner loop. The choice between cost function (10.1) and (10.2) is determined by the logical LQSCATT (.FALSE. for cost (10.1), .TRUE. for expression(10.2)).

Quality control decisions made by the IFS screening run are:

- **High wind speed check:** Data rejected if observed or first guess wind speeds are above 35 m/s (RSCAWLI). Performed by `obs_preproc/fgwnd`
- **Sea ice check:** Data rejected if sea-ice fraction is higher than 0.01 (RSCATLI). Performed by `obs_preproc/fgwnd`
- **Global quality control:** If the average distance-to-the-cone residual for the backscatter measurements during an observation time slot (30 min.) for any of the active nodes is above the QC threshold, all ERS data for that time slot is blacklisted. This is done by the routine `obs_preproc/scaqc`.

There is no background wind check performed on ERS scatterometer data, but data may be de-weighted or effectively removed from the analysis during the minimization in 4D-Var by variational quality control (see Section 2.6 or *Andersson and Järvinen (1999)*).

Quality control decisions and departures from background and analyses are appended to each subset in the feedback BUFR message.

ERS feedback messages have a PRESCAT section sandwiched between the original ERS and the feedback data. The PRESCAT section contains outputs about the quality of the winds from the retrieval.

Here are the ERS-specific key words and bits to examine in the feedback message:

- **Winds retrieved at ESA:** BUFR descriptor 11012 for speed and 11011 for direction winds available in observation part of BUFR file.
- **Winds retrieved at ECMWF:** BUFR descriptor 11192 for u and 11193 for v winds retrieved in `obs_preproc/ERSIN`.
- **Background departures x 2 ambiguities:** BUFR descriptor 224255 for u ('U - COMPONENT AT 10 M') and for v ('V - COMPONENT AT 10 M'). BUFR descriptor 8024 = 33, BUFR descriptor 33210 = 1, BUFR descriptor 33211 = 1001.
- **Analysis departures x 2 ambiguities:** BUFR descriptor 224255 for u ('U - COMPONENT AT 10 M') and for v ('V - COMPONENT AT 10 M'). BUFR descriptor 8024 = 33, BUFR descriptor 33210 = 9, BUFR descriptor 33211 = 999.
- **Report rejected by across-swath thinning** if bit 1 of BUFR descriptor 33229 (Report Event Word 2) is set. QC decision made in `obs_preproc/SCAQC`.
- **Report rejected by along-swath thinning** if bit 10 of BUFR descriptor 33220 (Report Event Word 1) is set. QC decision made in `obs_preproc/THINNER`.
- **Report rejected if Sea Ice faction too high:** if bit 12 of BUFR descriptor 33220 (Report Event Word 1) is set. QC decision made by program IFS in subroutine `obs_preproc/fgwnd`.
- **Report rejected by high wind speed check** if bit 16 of BUFR descriptor 33220 (Report Event Word 1) is set. QC decision made in `obs_preproc/fgwnd`.
- **Report rejected if global QC fails:** if bit 16 of BUFR descriptor 33220 (Report Event Word 1) is set. QC decision made in `obs_preproc/ERSQC`. Note that currently this bit can be set for two different reasons, which is to be resolved in next model cycle.
- **Datum 4D-Var quality control status:** BUFR descriptor 33233 (Report Status Word 1) = 1/2/4/8 1 - active, 2 - passive, 4 - rejected, 8 - blacklisted Datum. 4D-Var variational quality control rejection BUFR descriptor 33236 (Datum event Word 1) bit 27 = 1.

10.5.5 NASA scatterometer (NSCAT) processing

NSCAT data has been used experimentally for impact experiments in 4D-Var as well as a surrogate for QuikSCAT data (Ku-band scatterometer as well). The processing is not automatic in IFS, as is the case for ERS and QuikSCAT. The NSCAT data quality is more consistent compared to ERS and QuikSCAT, because the archived NSCAT data are a re-processed science product, not an “as-is” real-time product.

The format and content of HDF NSCAT files are thoroughly documented in QuikSCAT Science Data Product User's Manual (available from ECMWF or JPL). Level 1.7 and 2.0 files are present for each orbit in the mission. Each backscatter file has a corresponding wind file.

Assimilation experiments with NSCAT data are only possible after offline processing of the data. Please contact the research department for further information.

10.5.6 NASA scatterometer (QuikSCAT) processing

Fig. 10.2 shows a simple flow chart for QuikSCAT processing at ECMWF. Below the processing chain is described in general. The processes QSCAT_FILTER, QSCAT25TO50KM, DCONE_QC and QSCAT_BUFR are part of the SCAT library. They are performed in the module PRESCAT, which is part of the OBS family. The processes SCREENING, and 4D-VAR, being part of the IFS library, are performed in the AN family. The FEEDBACK process, being part of the ODB library, is performed in the LAG family.

QuikSCAT data are received in the SeaWinds Real-Time BUFR Data Product (SWS_Met BUFR) format. This level 2B product contains both backscatter and wind information. The provided wind product is not used, however. Instead, wind information is retrieved directly by inversion of the backscatter product (see IFS Documentation Part I “Observation processing” Chapter10). A detailed description of the SWS_Met BUFR data content can be found in *Leidner et al. (2000)*. The SWS_Met BUFR product is archived in MARS as indicated in [Subsection 10.5.3](#).

Data for a given time window (12 hours in operations) are retrieved from MARS into six-hourly patches, time centered around 00H, 06H, 12h and 18H. These data are input to the program **qfilter**/QSCAT_FILTER, which sorts the observations by time, and removes duplicate/incomplete records. Duplicate and incomplete records are part of the QuikSCAT real-time data stream because of Seawinds' conically-scanning geometry. See *Leidner et al. (1999)* for a discussion of duplicate and incomplete records introduced by the scanning geometry.

QuikSCAT winds are inverted from the backscatter information with the program **qretrieve**/QSCAT25TO50KM. In contrast to ERS scatterometer data (see above), where the inversion from backscatter values to winds are defined in the IFS library, the wind inversion is defined in the SCAT library. Input to **qretrieve**/QSCAT25TO50KM are the sorted and undoubled 25 km QuikSCAT BUFR messages. They are decoded, consecutive rows are paired together, backscatter measurements are grouped into 50 km boxes, and winds are retrieved at this resolution. This means that from the 76 across track 25 km vector cells, 38 vector cells at 50 km resolution are created. Motivation for this transformation is that a 50 km resolution is more representative to the scales that are resolved by the increments in 4D-Var.

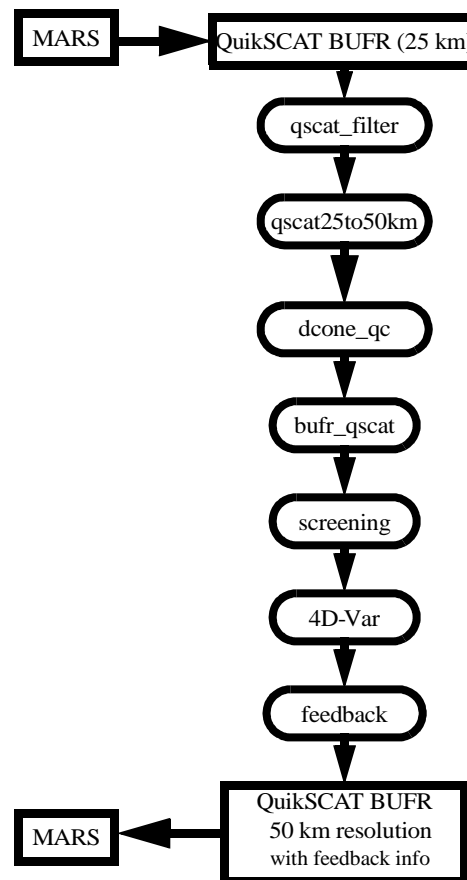


Figure 10.2 QuikSCAT processing

The 50 km wind product is based on all backscatter measurements available within that cell, i.e., four 25 km sub-cells. For this a Maximum Likelihood Estimator (MLE) is optimized expressing the misfit between observed and modelled backscatter values (based on the QSCAT-1 geophysical model function). Some details are described in the IFS Documentation (Part I “Observation processing” Section 10.2). The sum contains up to 16 backscatter measurements. In practice this number may be smaller because of:

- only outer-beam measurements are available (up to 8 values, for nodes 1–4 and 35–38),
- missing backscatter values,
- missing K_p values (see *Leidner et al., 2000*),
- the land, sea, and/or ice flag available in the product is set,
- rain contamination.

More details on the extraction of rain-contamination information can be found in the IFS Documentation (Part I: Observation Processing, chapter 10.3). Instead of the rejection on the basis of rain contamination, the code has been prepared (**qretrieve**/DIST2CONE) to reject backscatter values on the basis of a distance-to-cone method developed by *Portabella and Stoffelen (2000)*. At the moment, such a replacement requires a (small) modification of the SCAT library in ClearCase.

The inversion is performed in the routine **qretrieve**/INVERT50. On output it returns up to four ambiguous wind solutions. These winds are bias-corrected (details see IFS Documentation, Part I “Observation processing” Section 10.1.5) in such a way that on average, QuikSCAT wind speeds are in line with their ECMWF first-guess collocated

counterparts.

On output of `qretrieve/QSCAT25TO50KM`, a 50 km BUFR file is created. Among other quantities, it contains speed and direction of all wind solutions (ordered from most likely to least likely), the wind speed biases that were applied, all 16 underlying backscatter measurements, values of the resulting MLE's, rain flag and distance-to-cone information of the underlying 25 km wave vector cells.

The in this way created 50 km BUFR six-hourly files are input to the program `dcone_qc/DCONE_QC`. Goal is the detection of possible instrument anomalies. Typically when such anomalies occur, the set of backscatter values (up to 16 for the 50 km product) does not agree well with any set of backscatter values based on the geophysical model function. As a result, the MLE for the most-likely wind solution obtained in `qretrieve/INVERT50` will be too large. Occasionally large values can be caused by statistical fluctuations or by local geophysical parameters not taken into account by the model function. Consistently large values, however, indicate an instrument anomaly. In `dcone_qc/DCONE_QC` the across-node wise average MLE for each six-hour data file is compared to what should be expected on average. This average value is a factorization over expectation values as function of across node number, the wind speed of the most-likely solution and the number of backscatter values used in `qretrieve/INVERT50`. These normalizing values were determined for the period between 18 UTC 31 August 2001 and 12 UTC 31 September 2001 and are defined in `dcone_qc/INIT`. If any of the normalized averages for nodes for node 5 to 34 (i.e., where both outer and inner beam measurements are available) is larger than 1.45, the entire six-hour BUFR file is suspect. In such case bit 7 of the WVC Quality Flag (21109) is set for all observations. Otherwise, the BUFR file is not modified. This global quality control was introduced in the ECMWF assimilation system on 14 April 2002. During the three-months period before its introduction, in which QuikSCAT data was assimilated without a global QC check, it would only have been active for the six-hourly files of 12 UTC 12 March 2002 and 12 UTC 19 March 2002. For diagnostic reasons, node-wise normalized averages and all observations for which the normalized distance to the cone exceeds 25, are printed to the `obs/prescat.1` logfile. Reason why this quality control acts on six-hourly files, rather than on 30-minute time slots, as it is performed for ERS scatterometer data, is that the natural fluctuations of the MLE are larger for QuikSCAT data than they are for ERS data. As a result, 30-minute averages were found to be too short.

The `qbukey/BUFR_QSCAT` program adds RDB information to the 50 km BUFR file.

In IFS, ambiguous winds are reordered (most likely solution, solution that is most anti-parallel to the most likely, and then the remaining two in order of likeliness). Only the first two winds are input to 4D-Var using the same cost function as for ERS (i.e., the double well or purely quadratic cost function (10.1) respectively (10.2), including $\sigma_0 = 2$ m/s, see also *Stoffelen and Anderson 1997*). Only difference with ERS is, that the weight of the cost is reduced by a factor of four. In this way, QuikSCAT data is effectively assimilated on a resolution of 100 km. Calculation of the cost occurs in the IFS routine `pp_obs/hjo`.

Quality control decisions made by the IFS screening run are:

- **Sea ice check:** Data rejected if sea-ice fraction is higher than 0.01 (RSCATLI). Performed by `obs_preproc/fgwnd`
- **Sweet zone check:** Data rejected if it is in the region of the swath for which no inner beam measurement is available (node 1–4 and node 35–38). This is done by the routine `obs_preproc/scaqc`.
- **Insufficient number of ambiguities:** Data reject if less than two ambiguous wind solutions are available (`obs_preproc/scaqc`).
- **lack of azimuth diversity:** Data reject when the angle between the first and second reordered solution is less than 135 degrees. This mainly occurs for observations in the nadir part of the swath. This is done by the routine `obs_preproc/scaqc`.



- **rain contamination:** Data reject if more than one 25 km sub-cell (from which the 50 km cell is constructed) is rain contaminated (see IFS Documentation Part I: Observation Processing, chapter 10.3 for details). This is done by the routine **obs_preproc/scaqc**.
- **Global QC:** Data reject if the global-performance flag (see **dcone_qc/DCONE_QC** program above) is set. This is done by the routine **obs_preproc/scaqc**.

In addition the **obs_preproc/scaqc** code has been prepared to reject data in case for more than one 25 km sub-cell the normalized distance-to-the-cone is too large (see the program **qretrieve/QSCAT25TO50KM**, and Portabella and Stoffelen 2000 for its description). It is not active at the moment.

There is no background wind check performed on QuikSCAT scatterometer data, but data may be de-weighted or effectively removed from the analysis during the minimization in 4D-Var by variational quality control (Section 2.6 or *Andersson and Järvinen (1999)*).

After the processing in 4D-Var, a 50 km feedback file is created. Starting from the 50km BUFR file created in the **qbukey/BUFR_QSCAT** program, it adds information obtained during the 4D-Var process. Here the QuikSCAT-specific key words and bits to examine in the feedback message:

- **Background departures x 4 ambiguities:** Like for ERS described above. Only the first two departures have been used in the 4D-Var cost function.
- **Analysis departures x 4 ambiguities:** Like for ERS described above. Only the first two departures have been used in the 4D-Var cost function.
- **Report rejected if sea ice fraction is too high:** Like for ERS described above.
- **Report rejected if number of winds is < 2:** if bit 3 of BUFR descriptor 33220 (Report Event Word 1) is set. QC decision made in **obs_preproc/scaqc**..
- **Report rejected if wind directions are too close:** if bit 2 of BUFR descriptor 33229 (Report Event Word 2) is set. QC decision made in **obs_preproc/scaqc**..
- **Report rejected if data not in the sweet zone:** if bit 3 of BUFR descriptor 33229 (Report Event Word 2) is set. QC decision made in **obs_preproc/scaqc**..
- **Report rejected if data is rain contaminated:** if bit 4 of BUFR descriptor 33229 (Report Event Word 2) is set. QC decision made in **obs_preproc/scaqc**..
- **25km normalized distance-to-the cone is too large (rejection is not active):** if bit 16 of BUFR descriptor 33229 (Report Event Word 2) is set. Decision made in **obs_preproc/scaqc**..
- **Report rejected if global QC fails:** if bit 16 of BUFR descriptor 33229 (Report Event Word 1) is set. QC decision made in **obs_preproc/scaqc**..
- **Datum 4D-Var quality control:** Like for ERS described above.

10.6 THE DEPENDENT OBSERVATION SCREENING DECISIONS

10.6.1 Update of the observations

Just before performing the dependent screening decisions, the flag information gathered so far is converted into a status of the reports, namely: **active**, **passive**, **rejected** or **blacklisted**, and also into a status of the data in the reports (**FLGTST**). The reports with a RDB report flag value 2 (probably incorrect) or higher for latitude, longitude, date and time are rejected. For the observed data there are RDB datum flags for the variable and for the pressure, i.e. the pressure level of the observation. The rejection limits for these are as follows: all data are rejected for the maximum RDB datum flag value 3 (incorrect), non-standard-level data are rejected for the maximum RDB datum flag value 2, and for the pressure RDB datum flag the rejection limit is 1 (probably correct). The background quality control rejection limits are flag value 3 for all the data, and flag value 2 for the non-standard-level data.

10.6.2 Global time–location arrays

Some of the dependent decisions require a global view to the data which is not available as the memory is distributed. Therefore *ad hoc* global time–location arrays are formed and broadcast in order to provide this view (GLOBA, DISTR).

10.6.3 Vertical consistency of multilevel reports

The first dependent decisions are the vertical-consistency check of multilevel reports (**VERCO**), and the removal of duplicated levels from the reports. The vertical-consistency check of multilevel reports is applied in such a way that if four consecutive layers are found to be of suspicious quality, even having a flag value one, then these layers are rejected, and also all the layers above these four are rejected in the case of geopotential observations. These decisions clearly require the quality-control information, and they are therefore 'dependent' on the preceding decisions.

10.6.4 Removal of duplicated reports

The duplicated reports will be removed next. That is performed (**MISCE, DUPLI, REDSL**) by searching pairs of collocated reports of the same observation types, and then checking the content of these reports. It may, for instance, happen that an airep report is formally duplicated by having a slightly different station identifier but with the observed variables inside these reports being exactly the same, or partially duplicated. The pair-wise checking of duplicates results in a rejection of some or all of the content of one of the reports.

10.6.5 Redundancy check

The redundancy check of the reports, together with the level selection of multi-level reports, is performed next for the active reports that are collocated and that originate from the same station (**REDUN**). In 3D-screening, this check applies to the whole observation time window. In 4D-screening (**LSCRE4D=.true.**), this check applies separately in each timeslot.

For **land synop and paob** reports, the report closest to the analysis time with most active data is retained, whereas the other reports from that station are considered as redundant and are therefore rejected from the assimilation (**REDRP, REDMO**). For **ship synop and dribu** observations the redundancy check is done in a slightly modified fashion (**REDGL**). These observations are considered as potentially redundant if the moving platforms are within a circle with a radius of 1° latitude. Also in this case only the report closest to the analysis time with most active data is retained. All the data from the multilevel **temp and pilot** reports from same station are considered at the same time in the redundancy check (**REDOR, SELEC**). The principle is to retain the best quality data in the vicinity of standard levels and closest to the analysis time. One such datum will, however, only be retained in one of the reports. A wind observation, for instance, from a sounding station may therefore be retained either in a temp or in a pilot report, depending on which one happens to be of a better quality. A **synop mass** observation, if made at the same time and at the same station as the temp report, is redundant if there are any temp geopotential height observations that are no more than 50 hPa above the synop mass observation (**REDSM**).

10.6.6 Thinning

Finally, a horizontal thinning is performed for the AIREP, TOVS, GEOS, SSM/I, SATOB and ERS SCAT reports. The horizontal thinning of reports means that a predefined minimum horizontal distance between the nearby reports from the same platform is enforced. For AIREP reports the free distance between reports is currently enforced to about 60 km (*Cardinali et al. 2003*). The thinning of the AIREP data is performed with respect to one aircraft at a time (**MOVPL, THIAIR**). Reports from different aircraft may however be very close to each other. In this remov-



al of redundant reports the best quality data is retained as the preceding quality controls are taken into account. In vertical, the thinning is performed for layers around model levels, thus allowing more reports for ascending and descending flight paths.

TABLE 10.3 A SUMMARY OF THE CURRENT USE OF OBSERVATIONS IN THE 3D/4D-VAR DATA ASSIMILATION AT ECMWF. THESE USAGE RULES ARE SUBJECT TO CHANGE. FOR THE MOST CURRENT INFORMATION WE REFER TO THE DATA-SELECTION BLACKLIST FILES. THESE FILES ARE ARCHIVED, SO THE HISTORY IS PRESERVED.

Observation type	Variables used	Remarks
synop, ship	u, v, ps (or z), rh	u and v used only over sea, in the tropics also over low terrain (< 150 m). Orographic rejection limit 6 hPa for rh , 100 hPa for z and 800 m for ps .
airep	u, v, T	Thinned to approximately 60 km along flight tracks. Ascending and descending aircraft are thinned in the vertical to the model resolution.
satob	u, v	Selected areas and levels. Thinning of high-density winds. Strict background check to avoid slow wind-speed bias in the data.
dribu	u, v, ps	Orographic rejection limit 800m for ps
temp	u, v, T, q	Used on all reported levels. q only below 300 hPa. 10 m u and v used over land only in tropics over low terrain (< 150 m). Orographic rejection limit 10 hPa for u, v and T , and -4 hPa for q
pilot	u, v	Used on all reported levels. 10 m u and v used over land only in tropics over low terrain (< 150 m). Orographic rejection limit 10 hPa for u and v
profilers	u, v	Thinned to 5 hPa separation in the vertical. Data from American, European and Japanese networks are used.
radiance data	Tb	Info to be supplied by the Satellite Section
paob	ps	Used south of 19°S. Orographic rejection limit 800 m for ps
scatterometer	u, v	Not used in full resolution. Used if SST is warmer than 273 K or if both observed and background wind less than 35 m s^{-1}

The variables are as in Table 10.1, with the addition that Tb stands for brightness temperature. The observation types are shortened by *synop* for synoptic surface observations, *airep* for aircraft reports, *satob* for satellite cloud track winds, *dribu* for drifting buoy reports, *temp* for radiosonde soundings, *pilot* for wind soundings, *tovs* for satellite temperature soundings, *paob* for pseudo observations of surface pressure obtained from satellite images.

Thinning of TOVS, GRAD, SSM/I, SATOB and ERS SCAT reports are each done in two stages controlled by THINN. For TOVS (THINNER), a minimum distance of about 70 km is enforced and, thereafter, a repeat scan is performed to achieve the final separation of roughly 250 km or 120 km between reports from one platform. This is controlled through settings in DEFRUN, that can also be modified through namelist (NAMSCC). The thinning algorithm is the same as used for AIREPs except that for TOVS a different preference order is applied: a sea sounding is preferred over a land one, a clear sounding is preferred over a cloudy one and, finally, the closest observation time to the analysis time is preferred. For geostationary water vapour radiances, a similar thinning in two stages is applied with currently about 70 km minimum distance and about 125 km final separation (THINNER). During the thinning, preference is given to data having the largest fraction of clear sky in the clear-sky radiance average, high infrared brightness temperature (for GOES data) and, finally, a small standard deviation of brightness temperatures within the CSR mean. A similar thinning technique is applied to SSM/I data and SATOB high-density data (THINNER). Note that prior to assimilation a coarser pre-thinning may take place already during observation pre-process-

ing in order to reduce otherwise excessive data volumes.

The screening of SATOB data has been extended for atmospheric motion wind observations, including individual quality estimate. The quality information from the quality control performed by the producer at extraction time is appended to each wind observation. This Quality Indicator (QI) is introduced as an additional criterion in the thinning step; priority is given to the observation with the highest QI value.

Apart from this thinning, the other observation dependent decisions involved by the screening of the scatterometer data come essentially from the application of a sea-ice contamination test from the model sea-surface-temperature analysis, using a minimum threshold of 273 K, and a high-wind rejection test with an upper-wind speed limit set to 35 m s^{-1} for the higher of the scatterometer and background winds (FGWND).

10.6.7 A summary of the current use of observations

A summary of the current status of use of observations in the 3D-Var data assimilation is given in [Table 10.3](#). For most current information we refer to the data-selection balcklist files themselves. The history of such files as used in ECMWF operations is also available.

10.6.8 Compression of the ODB

After the observation screening roughly a fraction of 1/10 of all the observed data are active and so the compressed observation ODB (the CCMA) for the minimization run only contains those data. The large compression rate is mainly driven by the number of TOVS data, since after the screening there are only 10–20% of the TOVS reports left, whereas for the conventional observations the figure is around 40%. As a part of the compression, the observations are re-sorted amongst the processors for the minimization job in order to achieve a more optimal load balancing of the parallel computer.

10.7 A MASSIVELY-PARALLEL COMPUTING ENVIRONMENT

The migration of operational codes at the ECMWF to support a massively-parallel computing environment has set a requirement for reproducibility. The observation screening needs to result in exactly the same selection of observations when different numbers of processors are used for the computations. As mentioned earlier, in the observation screening there are the two basic types of decision to be made. Independent decisions, on one hand, are those where no information concerning any other observation or decision is needed. In a parallel-computing environment these decisions can be happily made by different processors fully in parallel. For dependent decisions, on the other hand, a global view of the observations is needed which implies that some communication between the processors is required. The observation array is, however, far too large to be copied for each individual processor. Therefore, the implementation of observation screening at the ECMWF is such that only the minimum necessary information concerning the reports is communicated globally.

The global view of the observations is provided in the form of a global 'time–location' array for selected observation types. That array contains compact information concerning the reports that are still active at this stage. For instance, the observation time, location and station identifier as well as the owner processor of that report are included. The time–location array is composed at each processor locally and then collected for merging and redistribution to each processor. After the redistribution, the array is sorted locally within the processors according to the unique sequence number. Thus, every processor has exactly the same information to start with, and the dependent decisions can be performed in a reproducible manner independently of the computer configuration.

The time–location array is just large enough for all the dependent decisions, except for the redundancy checking

of the multilevel temp and pilot reports. This is a special case, in the sense that the information concerning each and every observed variable from each level is needed. Hence, the whole multilevel report has to be communicated. The alternative to this would be to force the observation clusters of the multilevel reports always into one processor without splitting them. In that case the codes responsible for the creation of the observation arrays for assimilation would need to ensure the geographical integrity of the observation arrays distributed amongst the processors. This is, however, not possible in all the cases, and the observation screening has to be able to cope with this. Currently, it is coded in such a way that only a limited number of multilevel temp and pilot reports, based on the time–location array, are communicated between the appropriate processors as copies of these common stations.

APPENDIX A

A.1 BAD REPORTING PRACTICE OF SYNOP AND TEMP REPORTS

The way the synoptic surface stations report mass observations (pressure or geopotential height) is considered as bad if the

- station altitude is above 800 m and station reports mean sea level pressure
- station altitude is above 800 m and station reports 1000 hpa level
- station altitude is above 1700 m and station reports 900 hpa level
- station altitude is below 300 m and station reports 900 hpa level
- station altitude is above 2300 m and station reports 850 hpa level
- station altitude is below 800 m and station reports 850 hpa level
- station altitude is above 3700 m and station reports 700 hpa level
- station altitude is below 2300 m and station reports 700 hpa level
- station altitude is below 3700 m and station reports 500 hpa level

The reporting practice is also considered as bad if the station reports 500 gpm, 1000 gpm, 2000 gpm, 3000 gpm or 4000 gpm level pressure, respectively, and station altitude is more than 800 m different from the reported level.

For temp geopotentials the reporting practice is considered as bad if the

- station altitude is above 800 m and station reports 1000 hpa level
- station altitude is above 2300 m and station reports 850 hpa level
- station altitude is above 3700 m and station reports 700 hpa level

A.2 REVISED BACKGROUND QUALITY CONTROL FOR SELECTED OBSERVATIONS

The background quality-control rejection limits are applied more strictly for some observation types than stated in [Table 10.1](#). The special cases are the following ones

- airep wind observations with zero wind speed are rejected if the background wind exceeds 5 m/s
- for airep and dribu wind observations the rejection limit is multiplied by 0.5, and for pilot wind by 0.8
- for satob wind observations the rejection limit is multiplied by 0.1, except below 700 hPa level where it is multiplied by 0.2
- no background quality control is applied for scatt winds
- for dribu surface pressure observations the rejection limit is multiplied by 0.9, and for paob surface pressure by 0.7
- for airep temperature observations the rejection limit is multiplied by 1.6

A.3 USE OF ATMOSPHERIC MOTION WINDS

This appendix describes those parts of the ECMWF assimilation system which involves some special code for the AMW case, i.e. the data selection and the FG quality check. It refers to the operational status as from December 1996. A thinning procedure was introduced for high-density winds in Spring 1998.

A.3.1 Data selection

There are several model independent checks which AMW data have to pass in order to be considered for the assimilation process:

Check on longitude/latitude

- AMW must be within a circle of 55° from the sub-satellite point

Check on levels depending on the computational method

- WW CMW and WVMW must be above 400 hPa
- VIS CMW must be below 700 hPa
- IR CMW can be used at all levels.

Check on land/sea

- All AMW over sea are used
- AMW over land is not used north of 20°N .
- For Meteosat (0° mission) instead of 20°N this threshold is 35°N to allow usage of AMW over north Africa.
- For Meteosat (63° mission) the use of AMW has been extended over Asia if above 500 hPa. This is restricted for longitudes east of 30°E .
- AMW are blacklisted over the Himalayas as a precautionary measure.
- AMW over land south of 20°N (35°N for Meteosat) is used if above 500 hPa.

Check on satellite (35°N for Meteosat) is used if above 500 hPa.

This is a temporary selection on certain channels or satellites. At present channels and satellite used are:

- METEOSAT cloud tracked winds with 90 min temporal sampling
- METEOSAT IR (not at medium level), VIS, WV
- METEOSAT HVIS, also at asynoptic times, only if $QI_2 \equiv 0$
(Automatic Quality Control \equiv PASSED)
- GOES IR & WV (NOT at asynoptic times)
- GMS IR & VIS

A.3.2 Background quality check

The background quality check is based on a comparison of the AMW deviation from the background. Observed wind components are checked together. The AMW is flagged with $j = 1$ or 2 or 3 if this deviation squared is greater than a predetermined multiple $ERRLIM_j * ZREJMOD$ of its estimated variance, as given by the following expression:

if $[D_2 > (sfg^2 + sobs^2) * ERRLIM_j * ZREJMOD]$ then flag = j where $D^2 = 1/2 (Du^2 + Dv^2)$ with Du, Dv wind component deviations from background; sfg std of the background wind component error (mean for u and v); sobs std of the observation wind component error, 2 m s^{-1} for levels below 700 hPa included, 3.5 m s^{-1} at 500 hPa, 4.3 m s^{-1} at 400 hPa and 5 m s^{-1} for all levels above; $ERRLIM_j$ is 8 for $j = 1$, 18 for $j = 2$ and 20 for $j = 3$. The value of $ZREJMOD$ depends on the level of AMW and normally its value is:

- $ZREJMOD = 0.2$ for low level



- ZREJMOD = 0.1 for all others levels

A special check or asymmetric check is applied when the observed speed is more than 4 m s^{-1} slower than the background speed SPDfg. This check has a more restrictive rejection limit:

- ZREJMOD = 0.15 at low level
- ZREJMOD = 0.07 in the tropics
- ZREJMOD = $0.075 - 0.00125 * \text{SPDfg}$ all others
- ZREJMOD = 0.0 if $\text{SPDfg} > 60 \text{ m s}^{-1}$ (observation gets always flag $j = 3$)

When the data is passed to the following variational quality control its probability of being used depend on the flag j . With flag $j = 1$ the data will be assimilated, with flag $j = 2$ it will be given an intermediate probability and might be used or not and finally the analysis will reject all data with $j = 3$





Part II: DATA ASSIMILATION

CHAPTER 11 Analysis of snow

Snow depth is a model prognostic variable that needs to be analysed. Its analysis is performed in a module that is currently separated from the analysis of the atmosphere and of the soil wetness. This module includes also the sea-surface temperature, sea-ice fraction and screen-level temperature and relative humidity.

Table of contents

[11.1 Organization](#)

[11.2 Snow-depth analysis](#)

[11.3 Technical aspects](#)

11.1 ORGANIZATION

The snow analysis is a 3-D sequential analysis performed every 6 hours using a successive correction method. The snow-depth background S^b (units: m) is estimated from the short-range forecast of snow water equivalent W_s^b (units: m of water equivalent) and snow density ρ_s^b (units : kg m⁻³):

$$S^b = \frac{1000 \times W_s^b}{\rho_s^b} \quad (11.1)$$

The snow analysis S^a is performed using snow-depth observations, the snow-depth background field, and NOAA / NESDIS snow extent. If snow-depth observations are not available, the snow accumulation / melting is simulated from the model six-hour forecast. The use of the satellite derived snow extent is optional. As an alternative, snow climate can be used to ensure the stability of the scheme and to give a seasonal snow trend in areas without any observations.

11.2 SNOW-DEPTH ANALYSIS

The snow analysis is a two-step algorithm (*Drusch et al. 2004*). In the first step, the background field S^b (as defined above) is compared with the NOAA / NESDIS snow extent product. Grid boxes, which are snow free in the first guess but snow covered in the satellite derived product are updated with a constant snow depth of 10 cm. In the second step, the actual Cressman analysis is performed based on observations S^o from SYNOP reports and snow free satellite observations, which enter the analysis with a snow depth of 0 cm. The actual interpolation is given through:

$$S^a = S^b + \frac{\sum_{n=1}^N w_n (S_n^o - S^b)}{\sum_{n=1}^N w_n} \quad (11.2)$$

The weight function w_n is the product of functions of the horizontal distance r and vertical displacement h (model minus obs height) between the observation and analysis points:

$$w = H(r)v(h), \quad (11.3)$$

where

$$H(r) = \max\left(\frac{r_{\max}^2 - r^2}{r_{\max}^2 + r^2}, 0\right) \quad (11.4)$$

and

$$\begin{aligned} v(h) &= 1 && \text{if } 0 < h \\ v(h) &= \frac{h_{\max}^2 - h^2}{h_{\max}^2 + h^2} && \text{if } -h_{\max} < h < 0 \\ v(h) &= 0 && \text{if } h < -h_{\max} \end{aligned}$$

The snow depth is preserved when the model height is above the observing station, but it is severely reduced below. The observation height for the satellite data is obtained from model orography at T511 spectral resolution. The influence distances are set to $r_{\max} = 250$ km and $h_{\max} = 300$ m.

In addition to the preliminary quality control in the observation data base, the following checks are applied for each grid point :

- if $T_{2m}^b < 8^\circ\text{C}$ only snow depth observations below 140 cm are accepted.
- this limit is reduced to 70 cm if $T_{2m}^b > 8^\circ\text{C}$.
- snow-depth observations are rejected if they differ by more than 50 cm from the background.
- when only one snow-depth observation is available within the influence radius r_{\max} , the snow depth increments are set to zero.
- snow-depth analysis is limited to 140 cm.
- snow-depth increments are set to zero when larger than $(160 - 16T_{2m}^b)$ mm (where T_{2m}^b is expressed in Celsius)
- snow-depth analysis is set to zero if below 0.04 cm
- if there is no snow in the background and in more than half of the observations within a circle of radius r_{\max} , the snow-depth increment is kept to zero.

It is expected that the satellite derived snow extent can be used in the analysis to replace the role of snow depth climatology in correcting for the model bias. However, there is the option to weight the analysis of snow depth with the climatological value S^{clim} to provide the final analysis:

$$S^a = (1 - \alpha)S^a + \alpha S^{\text{clim}}$$

The relaxation coefficient α can be changed through the namelist (see [Section 11.3](#)). Its default value is set to 0.02, which corresponds to a time scale of 12.5 days at six-hourly cycling.

$$W_s^a = \frac{\rho_s^b \times S^a}{1000}$$

The snow density is unchanged in the analysis process : $\rho_s^a = \rho_s^b$

Areas with permanent snow and ice (defined using the Global Land Cover Characterization product) are set to an arbitrary high value at each analysis cycle ($W_s^a = 10\text{m}$).

11.3 TECHNICAL ASPECTS

The snow analysis software is implemented as a branch of the more comprehensive surface and screen-level analysis (SSA) package. The other branches currently include two-metre temperature and relative humidity analysis, and also sea surface temperature and sea-ice fraction analyses. The program organization when performing snow analysis is roughly as follows:

- SSA
 - CONTROL_SSA
 - INISNW
 - SCAN_DDR
 - COORDINATES
 - GETFIELDS
 - *sub_prep_ues.F90*
 - SCAN_CMA
 - SCAN_OBS
 - LAND_OBS
 - INITIAL_REJECTION
 - REDUNDANT_OBS
 - SNOW_ANALYSIS
 - CRES_FILL
 - *sub_prep_nes.F90*
 - SUCSNW
 - SCAN_OBS
 - FG2OBS
 - *SUCSNW*
 - *SNOW_FG*
 - FDB_OUTPUT
 - PRINT_SUMMARY
 - PLOTDATA
 - FEEDBACK

The main program SSA calls CONTROL_SSA where most of the setup and namelist handling are done. Routine INISNW performs initialization of the actual snow analysis by sensing the size of the observation array file (CMA-file) in SCAN_DDR and generating latitudinal coordinates that stem from the model resolution in concern and zeros of the Bessel function.

After this, all input fields are read into memory in GETFIELDS. They consist of the snow water equivalent and snow density from the first-guess (6-hour forecast), 2 m temperature first guess, snow-depth climate (varies monthly with a linear temporal interpolation), land/sea mask and finally the orography in a form of the geopotential.

In *sub_prep_nes.F90* the satellite data, which contain no snow are retrieved from buffr.

In SCAN_CMA observations are read into memory and a quick validity check of the non-applicable observations for this analysis is performed. Furthermore, the land/sea mask is calculated in LAND_OBS for the retained snow

depth observation points.

Additional screening is done in `INITIAL_REJECTION` and in `REDUNDANT_OBS`. The former one sets up an internal table where all the observations which survived from the quick screening are placed with a minimum context information. This routine rejects some of the observations entered into the table due to inconsistencies.

The routine `REDUNDANT_OBS` removes time duplicates and retains the observations of the station in concern with the closest (and the most recent) to the analysis time. Since only synoptic observations are considered, slowly moving platform handling present in the `REDUNDANT_OBS` is not applicable to the snow analysis.

The actual snow analysis is performed under `SNOW_ANALYSIS`. In a first step, the first guess field is updated with the satellite observations (routine `CRES_FILL`). The satellite observations, which contain snow are retrieved from `buffr` (routine `SUB_PREP_NES`). The analysis technique is Cressman's successive correction method (routine `SUCSNW`). The structure functions are set to be separable in horizontal and vertical directions. A special mountain region handling is performed, depending whether the datum or grid points is in the valley or at high altitudes, as explained before.

The snow-depth background (i.e. first guess) field is constructed from the model first-guess snow water equivalent and snow density. Once the snow-depth first guess field is present, it is used to calculate the first guess departure at snow-depth observation points. This increment is finally added to the snow depth fields at grid points producing the final snow depth output field, which is output in routine `FDB_OUTPUT`.

The accuracy of the analysis is estimated in `PRINT_SUMMARY` where some important statistics are summarized. The internal observation table can be printed if requested from `PLOTDATA` and an updated observation file for feedback purposes can be created in routine `FEEDBACK`.

The main logicals of the namelist `NAMSSA` are:

- `L_SNOW_ANALYSIS`: When set to `TRUE`, the snow analysis is performed.
- `L_SNOW_DEPTH_ANA`: When set to `TRUE`, the snow analysis is performed in snow depth (in opposition to snow water equivalent assuming a constant value of 250 kg m^{-2} for observed snow density).
- `L_USE_SNOW_CLIMATE`: When set to `true`, a relaxation of the snow analysis towards a monthly climatology is performed with a time scale of 12.5 days (the relaxation coefficient is passed through `NAMSSA`).
- `L_USE_FG_FIELD`: When set to `TRUE` the snow analysis is set to the first-guess value (no use of observations) and there is no relaxation to climatology.
- `L_USE_SCOVER_NESDIS`: When set to `TRUE`, the NOAA / NESDIS satellite product is used.

CHAPTER 12 Land-surface analysis

Table of contents

12.1 Introduction

12.2 Screen-level analysis

12.2.1 Methodology

12.2.2 Quality controls

12.2.3 Technical aspects

12.3 Soil analysis

12.1 INTRODUCTION

Soil temperature and soil water content are prognostic variables of the forecasting system and, as a consequence, they need to be initialised at each analysis cycle. Currently the land surface analysis is performed every 6 hours and is decoupled from the atmospheric analysis. The absence of routine observations on soil moisture and soil temperature requires to use proxy data. The ECMWF soil analysis relies on SYNOP temperature and relative humidity at screen-level (2 m) available on the GTS (around 12000 reports over the globe are provided every 6 hours). Firstly, a screen-level analysis is performed for temperature and humidity. Secondly, the screen-level analysis increments are used as inputs to perform the analysis in the soil.

12.2 SCREEN-LEVEL ANALYSIS

12.2.1 Methodology

Two independent analyses are performed for 2 m temperature and 2 m relative humidity. The method used is a two-dimensional univariate statistical interpolation. In a first step, the background field (6 h or 12 h forecast) is interpolated horizontally to the observation locations using a bilinear interpolation scheme and background increments ΔX_i are estimated at each observation location i .

The analysis increments ΔX_j^a at each model grid-point j are then expressed as a linear combination of the first-guess increments (up to N values) :

$$\Delta X_j^a = \sum_{i=1}^N W_i \times \Delta X_i \quad (12.1)$$

where W_i are optimum weights given (in matrix form) by :

$$(\mathbf{B} + \mathbf{O})\mathbf{W} = \mathbf{b} \quad (12.2)$$

The column vector \mathbf{b} (dimension N) represents the background error covariance between the observation i and the model grid-point j . The $N \times N$ matrix \mathbf{B} describes the error covariances of background fields between pairs

of observations. The horizontal correlation coefficients (structure functions) of \mathbf{b} and \mathbf{B} are assumed to have the following form:

$$\mu(i, j) = \exp\left(-\frac{1}{2}\left[\frac{r_{ij}}{d}\right]^2\right) \quad (12.3)$$

where r_{ij} is the horizontal separation between points i and j and d the e-folding distance taken to 300 km (hard coded in subroutine OIINC).

Therefore :

$$B(i, j) = \sigma_b^2 \times \mu(i, j) \quad (12.4)$$

with σ_b the standard deviation of background errors.

The covariance matrix of observation errors \mathbf{O} is set to $\sigma_o^2 \times \mathbf{I}$ where σ_o is the standard deviation of observation errors and \mathbf{I} the identity matrix.

The standard deviations of background and observation errors are set respectively to 1.5 K and 2 K for temperature and 5% and 10% for relative humidity. The number of observations closest to a given grid point that are considered to solve (12.1) is $N = 50$ (scanned within a radius of 1000 km). The analysis is performed over land and ocean but only land (ocean) observations are used for model land (ocean) grid points.

12.2.2 Quality controls

Gross quality checks are first applied to the observations such as $RH \in [2, 100]$ and $T > T^d$ where T^d is the dewpoint temperature. Redundant observations are also removed by keeping only the closest (and more recent) to the analysis time.

Observation points that differ by more than 300 m from the model orography are rejected.

For each datum a check is applied based on statistical interpolation methodology. An observation is rejected if it satisfies :

$$|\Delta X_i| > \gamma \sqrt{\sigma_o^2 + \sigma_b^2} \quad (12.5)$$

where γ has been set to 3, both for temperature and humidity analyses.

The number of used observations every 6 hours varies between 4000 and 6000 corresponding to around 40% of the available observations.

The final relative humidity analysis is bounded between 2% and 100%. The final MARS archived product is dewpoint temperature that uses the 2 m temperature analysis T_a to perform the conversion :

$$T^d = \frac{17.502 \times 273.16 - 32.19 \times \Psi}{17.05 - \Psi} \quad (12.6)$$

with

$$\Psi = \log(RH_a) + 17.502 \times \frac{T_a - 273.16}{T_a - 32.19} \quad (12.7)$$

12.2.3 Technical aspects

The technical aspects are similar to the snow analysis (see Chapter 11) except for the computation of the analysis increments obtained from the subroutine **OIUPD** instead of **SUCSNW** (Cressman interpolation).

Subroutine **OISET** selects the N closest observations from a given grid-point.

Subroutine **OIINC** provides the analysis increments from Equations (12.1) and (12.2), by first computing $\mathbf{q} = (\mathbf{B} + \mathbf{O})^{-1} \Delta \mathbf{X}$ (in subroutine **EQU SOLVE** - inversion of a linear system) which does not depend upon the position of the analysis gridpoint and then estimating $\mathbf{b}^T \mathbf{q}$ (in subroutine **DOT_PRODUCT**).

Most of the control parameters of the screen-level analysis are defined in the namelist NAMSSA:

- 1) C_SSA_TYPE : 't2m' for temperature analysis and 'rh2m' for relative humidity analysis
- 2) L_OI : 'true' for statistical interpolation and 'false' for Cressman interpolation
- 3) N_OISET : number of observations (parameter N)
- 4) SIGMAB : standard deviation of background error (parameter σ_b)
- 5) SIGMAO : standard deviation of observation error (parameter σ_o)
- 6) TOL_RH : Tolerance criteria for RH observations (parameter γ in Equation (12.5))
- 7) TOL_T : Tolerance criteria for T observations (parameter γ in Equation (12.5))
- 8) SCAN_RAD_2M(1) : Scanning radius for available observations (set to 1000 km)

12.3 SOIL ANALYSIS

The soil analysis scheme is based on an "local" optimum interpolation technique as described in *Mahfouf (1991)* and *Douville et al. (2001)*. The analysis increments from the screen-level analysis are used to produce increments for the water content in the first three soil layers (corresponding to the root zone) :

$$\Delta \theta = a \times (T_a - T_b) + b \times \left[100 \frac{e_s(T_a^d) - e_s(T_b^d)}{e_s(T_a)} \right] \quad (12.8)$$

and for the first soil temperature layer :

$$\Delta T = c \times (T_a - T_b) \quad (12.9)$$

The coefficients a and b are defined as the product of optimum coefficients α and β minimising the variance of analysis error and of empirical functions F_1 , F_2 and F_3 reducing the size of the optimum coefficients when the coupling between the soil and the lower boundary layer is weak.

$$\alpha = \frac{\sigma_\theta}{\phi \sigma_b} \left\{ \left[1 + \left(\frac{\sigma_a^{RH}}{\sigma_b^{RH}} \right)^2 \right] \rho_{T\theta} - \rho_{RHT} \rho_{RH\theta} \right\} \quad (12.10)$$

and

$$\beta = \frac{\sigma_\theta}{\phi \sigma_b^{RH}} \left\{ \left[1 + \left(\frac{\sigma_a^{RH}}{\sigma_b^{RH}} \right)^2 \right] \rho_{RH\theta} - \rho_{RHT} \rho_{T\theta} \right\} \quad (12.11)$$

with

$$\phi = \left[1 + \left(\frac{\sigma_a^T}{\sigma_b^T} \right)^2 \right] \left[1 + \left(\frac{\sigma_a^{RH}}{\sigma_b^{RH}} \right)^2 \right] - \rho_{RHT}^2 \quad (12.12)$$

where ρ_{xy} represents the correlation of background errors between parameters x and y .

The statistics of background errors have been obtained from a series of Monte-Carlo experiments with a single-column version of the atmospheric model where initial conditions for soil moisture have been perturbed randomly. They were obtained for a clear-sky situation with strong solar insolation. Empirical functions are aimed to reduce soil increments when atmospheric forecast errors contain less information about soil moisture. To obtain negligible soil-moisture corrections during the night and in winter, F_1 is a function of the cosine of the mean solar zenith angle μ_M , averaged over the 6 h prior to the analysis time :

$$F_1 = \frac{1}{2} \{ 1 + \tanh[\lambda(\mu_M - 0.5)] \} \quad \lambda = 7 \quad (12.13)$$

The optimum coefficients are also reduced when the radiative forcing at the surface is weak (cloudy or rainy situations). For this purpose, the atmospheric transmittance τ_r is computed from the mean downward surface solar radiation forecasted during the previous 6 hours $\langle R_g \rangle$ as :

$$\tau_r = \left(\frac{\langle R_g \rangle}{S_o \mu_M} \right)^{\mu_M} \quad (12.14)$$

where S_o is the solar constant.

The empirical function F_2 is expressed as :

$$F_2 = \begin{cases} 0 & \tau_r < \tau_{rmin} \\ \frac{\tau_r - \tau_{rmin}}{\tau_{rmax} - \tau_{rmin}} & \tau_{rmin} < \tau_r < \tau_{rmax} \\ 1 & \tau_r > \tau_{rmax} \end{cases} \quad (12.15)$$

with $\tau_{rmin} = 0.2$ and $\tau_{rmax} = 0.9$.

The empirical function F_3 reduces soil moisture increments over mountainous areas :

$$F_3 = \begin{cases} 0 & Z > Z_{max} \\ \left(\frac{Z - Z_{max}}{Z_{min} - Z_{max}} \right)^2 & Z_{min} < Z < Z_{max} \\ 1 & Z < Z_{min} \end{cases} \quad (12.16)$$

where Z is the model orography, $Z_{min} = 500$ m and $Z_{max} = 3000$ m.

Furthermore, soil moisture increments are set to zero if one of the following conditions is fulfilled:

- 1) The last 6 h precipitation exceeds 0.6 mm
- 2) The instantaneous wind speed exceeds 10 m s^{-1}
- 3) The air temperature is below freezing

- 4) There is snow on the ground

To reduce soil moisture increments over bare soil surfaces, the standard deviations and the correlations coefficients are also weighted by the vegetation fraction $C_v = c_L + c_H$, where low and high vegetation cover are defined in Chapter 7 of the Physics Documentation.

The statistics of forecast errors necessary to compute the optimum coefficients are given in Table 12.1.

The correlations have been produced from the Monte-Carlo experiments. The standard deviation of background error for soil moisture σ_θ is set to $0.01 \text{ m}^3\text{m}^{-3}$ on the basis of ECMWF forecasts differences between day 1 and day 2 of the net surface water budget (precipitation minus evaporation minus runoff).

The standard deviation of analysis error σ_a is given by the screen-level analysis from :

$$\frac{1}{\sigma_a^2} = \frac{1}{\sigma_b^2} + \frac{1}{\sigma_o^2} \quad (12.17)$$

From the values chosen for the screen-level analysis $\sigma_a^T = 1.2\text{K}$ and $\sigma_a^{RH} = 4.47 \%$.

TABLE 12.1 STATISTICS OF BACKGROUND ERRORS FOR SOIL MOISTURE DERIVED FROM MONTE-CARLO EXPERIMENTS

Coefficient	Value
$\rho_{T\theta 1}$	-0.82
$\rho_{T\theta 2}$	-0.92
$\rho_{T\theta 3}$	-0.90
$\rho_{RH\theta 1}$	0.83
$\rho_{RH\theta 2}$	0.93
$\rho_{RH\theta 3}$	0.91
σ_b^T	1.25 K
σ_b^{RH}	9.5 %
ρ_{RHT}	-0.99

Soil moisture increments $\Delta\theta$ are such that they keep soil moisture within the wilting point θ_{pwp} and the field capacity θ_{cap} values, i.e. :

- if $\theta_b < \theta_{cap}$ then $\theta_a = \min(\theta_{cap}, \theta_b + \Delta\theta)$
- if $\theta_b > \theta_{pwp}$ then $\theta_a = \max(\theta_{pwp}, \theta_b + \Delta\theta)$

Finally the coefficients providing the analysis increments are :

$$\begin{aligned} a &= C_v \times \alpha \times F_1 F_2 F_3 \\ b &= C_v \times \beta \times F_1 F_2 F_3 \end{aligned} \quad (12.18)$$

and

$$c = (1 - F_2) F_3 \quad (12.19)$$



The coefficient c is such that soil temperature is more effective during night and in winter, when the temperature errors are less likely to be related to soil moisture. This way, 2 m temperature errors are not used to correct soil moisture and soil temperature at the same time

In the 12 h 4D-Var configuration, the soil analysis is performed twice during the assimilation window and the sum of the increments is added to the background values at analysis time.



Part II: DATA ASSIMILATION**CHAPTER 13 Analysis of sea-ice concentration and sea surface temperature****Table of contents**

13.1 Introduction

13.2 Sea-ice concentration

13.2.1 NCEP dataset

13.2.2 ECMWF re-sampling to model grid

13.3 SST analysis

13.3.1 Daily NCEP dataset

13.3.2 ECMWF re-sampling to model grid

13.4 Technical implementation

13.1 INTRODUCTION

The analyses of sea-ice concentration (CI) and sea surface temperature (SST) are based on daily global 0.5° datasets provided by NCEP. The sea-ice product from NCEP is derived from SSM/I (Special Sensor Microwave / Imager) observations. The SST product is an Optimal Interpolation (OI) analysis based on ship, buoy, and satellite measurements. At ECMWF, the NCEP fields are re-sampled to the reduced Gaussian grid used in the IFS, and are quality checked.

CI and SST are analysed six-hourly before the atmospheric variational analysis. Since sea-ice concentration and SST are kept constant during the ten-day forecast and the NCEP fields enter the analysis once a day, the analyses are updated once a day. In the current set up, the CI analysis is done before the SST analysis. The SST field from the previous analysis is used as a quality check in the ice analysis. The CI analysis is then used to determine the SST for grid boxes containing sea ice. Both analyses are performed for model sea grid boxes i.e. those, which contain less than 50% land. Only the Great Lakes and the Caspian Sea are covered in the NCEP datasets.

13.2 SEA-ICE CONCENTRATION

ECMWF's sea-ice concentration analysis is based on the corresponding daily NCEP product as described by *Grumbine (1996)*. The primary source of information is 19 GHz and 37 GHz SSM/I antenna temperatures. This document describes the processing at NCEP including the ice algorithm and the re-sampling to the reduced Gaussian grid used in the IFS.

13.2.1 NCEP dataset

This section describes the final quality controlled NCEP dataset, which is the input to the IFS, following *Grumbine (1996)*. The sea-ice concentration algorithm, which generates total, first-year, and multiyear concentration from

one set of SSM/I brightness temperatures is introduced in 13.2.1 (b).

13.2.1 (a) Brightness-temperature processing. Brightness-temperature grids are produced using a 12-hour window, before and after 0000 UTC of the current day. The data extraction program is run at 1230 or 1330 UTC (8:30 Eastern Local Time) and, in general, 12 orbits out of 14 possible orbits are included in the analysis. Brightness temperatures are then calculated from the antenna temperatures included in the Satellite Data Record (SDR) following *Hollinger et al. (1987)*. Quality checks are applied at two stages: (i) Antenna temperature scans are removed if the corresponding surface types (encoded into an 8 bit byte) do not fall in the range of 0 to 7. (ii) Brightness-temperature checks are applied using thresholds established by *Gloersen et al. (1994)*.

13.2.1 (b) Gridding and computation of sea-ice concentration. Quality-checked antenna temperatures are remapped from scan points onto a 25.4 km, true at 60°, polar stereographic grid oriented to 80° W in the northern hemisphere, and 100° E in the southern hemisphere. The northern hemisphere grid is 385 × 465 pixels with the pole at (191, 231). The southern hemisphere grid is 345 × 355 pixels with the pole at (151, 181).

After the antenna temperatures are converted to brightness temperatures, sea-ice concentrations are calculated using the algorithm described by *Cavalieri et al. (1991)*. The algorithm calculates the total (C), first-year (C_F), and multiyear (C_M) sea-ice concentrations from the microwave polarization (PR) at 19 GHz (T_{19HV}) and the spectral gradient ratio (GR), which uses the vertically polarized 37 GHz and 19 GHz brightness temperatures T_{37V} and T_{19V} , respectively (*Cavalieri et al. 1991*)

$$PR = (T_{19V} - T_{19H}) / (T_{19V} + T_{19H}) \quad (13.1)$$

$$GR = (T_{37V} - T_{19V}) / (T_{37V} + T_{19V}) \quad (13.2)$$

C , C_F , and C_M are then obtained through:

$$C_F = (a_0 + a_1 PR + a_2 GR + a_3 PR \times GR) / D \quad (13.3)$$

$$C_M = (b_0 + b_1 PR + b_2 GR + b_3 PR \times GR) / D \quad (13.4)$$

$$C = C_F + C_M \quad (13.5)$$

with

$$D = c_0 + c_1 PR + c_2 GR + c_3 PR \times GR \quad (13.6)$$

The coefficients a_i , b_i , and c_i ($i=0,3$) are functions of a set of nine brightness temperatures. These brightness temperatures referred to as algorithm tie points are observed SSM/I radiances of known ice-free ocean, first-year sea ice, and multi-year ice for each of the three SSM/I channels.

The weather filter proposed by *Gloersen and Cavalieri (1986)* is extended to adjacent pairs of points to take the coarse resolution of the 19 GHz observations, which does not match the polar stereographic grid resolution, into account. Since the satellite does not observe the poles, the disk of missing data on the northern hemisphere is filled according to a Laplacean with boundary values specified by the observations. This method gives the minimum gradient fill pattern. In addition, the Laplacean of ice concentration is small in regions away from the ice edge, which the polar data gap always is.

Values for sea-ice concentration vary between 0% and 128%. Above 128, there are flags denoting different data

conditions: Land (157), Bad Data (166), Weather (177), Coast (195), and No Data (224).

13.2.1 (c) *Final filtering and gridding for NWP*. SST is used as a final filter. If the analysed SST is greater than 2° C, sea-ice concentration is set to 0. As stated by *Grumbine (1996)*, this filter is good as long as low concentrations are not being considered important. For NWP applications the polar stereographic product is sampled to 0.5° × 0.5° resolution using the nearest-neighbour technique.

13.2.2 ECMWF re-sampling to model grid

At ECMWF, the 0.5° × 0.5° dataset (CI^{NCEP}) is currently being used operationally. A bi-linear interpolation is applied to transform the NCEP data from the regular latitude / longitude grid to the reduced Gaussian model grid. Before May 2001, the CI product in polar stereographic projection was used. In this case, a Cressman spatial interpolation is performed to transform the data to the reduced Gaussian grid:

$$CI^a = CI^b + \frac{\sum_{n=1}^N w_n (CI_n^{NCEP} - CI^{b'})}{\sum_{n=1}^N w_n} \quad (13.7)$$

with a maximum radius r_{max} of 120 km. CI^b and $CI^{b'}$ are the first guess (ice concentration from the previous day) at the model grid point and at the observation, respectively. The weighting function is given by:

$$w(r) = \frac{r_{max} - r}{r_{max} + r} \quad (13.8)$$

After the interpolation has been performed the following quality checks are applied:

- 1) Sea-ice concentration below 20% is set to 0%.
- 2) Sea-ice concentration greater 100% is set to 100%.
- 3) If the SST is higher than 1° C sea-ice concentration is set to 0%.
- 4) Grid boxes north of 82.5° N are set to 100%.

If the total change in global ice concentration exceeds 0.2%, the CI analysis is considered to be wrong and aborted.

13.3 SST ANALYSIS

For the operational ten-day forecasts, ECMWF uses the NCEP daily real-time global SST product (RTG_SST) at 0.5° resolution. For the seasonal forecasts the weekly the 1.0° product ('Reynolds SST') is temporally interpolated to daily values.

13.3.1 Daily NCEP dataset

The information provided in this section was extracted from <http://polar.wwb.noaa.gov.sst>. The daily SST product has been developed at NCEP / MMAB (Marine Modelling and Analysis Branch). It was implemented in the production suite 30 January, 2001.

A two-dimensional variational interpolation analysis of the most recent 24-hour buoy and ship data, satellite retrieved SST data, and SSTs derived from satellite observed sea-ice coverage is used to generate the 0.5° dataset.

The algorithm employs the following data-handling and analysis techniques:

- 1) Satellite retrieved SST values are averaged within 0.5° grid boxes with day and night 'superobs' created separately for each satellite.
- 2) Bias calculation and removal, for satellite retrieved SST, is the technique employed in the seven-day Reynolds–Smith climatological analysis.
- 3) SST report from individual ships and buoys are separately averaged within grid boxes.
- 4) The first guess is the prior (un-smoothed) analysis with one-day's climate adjustment added.
- 5) Late arriving data, which did not make it into the previous SST analysis, are accepted if they are less than 36 hours old.
- 6) Where ice cover exceeds 50%, surface temperature is calculated using salinity climatology in Millero's formula for the freezing point of salt water:

$$t(S) = -0.0575S + 0.0017S^{3/2} - 0.0002S^2$$

with S in psu.

- 7) An inhomogeneous correlation-scale-parameter l , for the correlation function $\exp(-d/2l)$ is calculated from a climatological temperature gradient, as:

$$l = \min(450, \max(2.25/|\nabla T|, 100))$$

with d and l in km and ∇T in $^\circ\text{C}/\text{km}$.

The RTG_SST analysis is done over all ocean areas, the Great Lakes, and the Caspian Sea. The spatial grid (720×360) is defined with indices starting just east of the Greenwich Meridian and near the South Pole.

13.3.2 ECMWF re-sampling to model grid

The interpolation from the regular latitude / longitude grid to the reduced Gaussian model grid is done by bi-linear interpolation. Ice-free grid boxes are up dated with the latest SST value retrieved from the archive. For grid boxes characterized by sea-ice concentrations exceeding 20% the SST is set to -1.7°C .

13.4 TECHNICAL IMPLEMENTATION

Technically, CI and SST analyses are controlled using the logical expressions *L_sst_analysis*, *lssmidata*, *licenmc*, and *lsstnmc*. If *L_sst_analysis* is 'true', the analyses are performed (control_ssa.F90). *lssmidata*, *licenmc*, and *lsstnmc* address the input data handling. In the current set up, *lssmidata* and *lsstnmc* are set to 'true' and *licenmc* is set to 'false' (setcomssa.F90). Whenever there are no ice data in polar stereographic projection available (which is the case from 9/05/2001 onwards) *lssmidata* is set to 'false' and *licenmc* is set to 'true' in sstana where the namelist for the analyses is created. The actual CI and SST fields on the regular 0.5° grid are retrieved from the MARS archive (fetchmars). The CI product on polar stereographic projection, which was used before May 2001, is stored in buffr format and can be obtained through the fetchobs script.

The SST and CI analyses software is implemented as a branch of the more comprehensive surface and screen-level analysis (SSA) package. The other branches currently include two-meter temperature and relative humidity analysis, and also snow water equivalent analysis. The main program ssa.F90 calls control_ssa.F90. Within control_ssa.F90 variables are initialized (through setcomssa.F90), the namelist is read, and the ODB and the analyses are initialized (through inisst.F90). Major components of the initialization are the interpolation of the regular latitude / longitude fields to the reduced Gaussian model grid and the conversion from the resulting field to a one-



dimensional array. The key components for this process are coordinates.F90, reg_to_gg.F90, reg2gg.F90, get-fields.F90 and field_to_array.F90.

The actual CI analysis is then performed in ice_analysis.F90. In case the polar stereographic product is used, the buffr file is processed in getsatbuff.F90 and the interpolation to the reduced Gaussian grid is done in ice_cressman.F90. The first guess CI field is updated through the NCEP interpolated product and the quality checks given in 13.2.3 are applied. Output statistics are prepared and printed in the corresponding log file (sst.1).

The SST analysis is done within sst_analysis.F90. The first guess field is updated through the interpolated NCEP field. Correction based on the actual CI analysis are applied as outlined in 13.3.2. The log file for the output is sst.1. The calling tree for the CI / SST analyses is given below.

- CONTROL_SSA
 - SETCOMSSA
 - INISST
 - COORDINATES
 - REG_TO_GG
 - REG2GG
 - GETFIELDS
 - FIELD2ARRAY
 - ICE_ANALYSIS
 - GETSATBUFF
 - ICE_CRESSMAN
 - LATBAND
 - CALC_DISTANCE
 - CORWHD
 - SST_ANALYSIS
 - FDB_OUTPUT
 - PRINT_SUMMARYsea-ice
 - PLOTDATA





Part II: DATA ASSIMILATION

CHAPTER 14 Data Flow

Table of contents

14.1 Notation

14.2 Data assimilation cycling

14.3 Overview of 4D-Var data flow

14.4 Input GRIB fields

- 14.4.1 reftrajshml
- 14.4.2 reftrajggml
- 14.4.3 reftrajafc
- 14.4.4 errgrib
- 14.4.5 SSTDATA\${starttime}
- 14.4.6 SGS\${starttime}
- 14.4.7 CD\${starttime}
- 14.4.8 UWAVES\${starttime}
- 14.4.9 WINDS\${starttime}

14.5 Input observation data

14.6 Input data files

- 14.6.1 Invariant data files
- 14.6.2 Date-dependent data files

14.7 Output GRIB fields

- 14.7.1 Output type ‘an’ model level spectral fields
- 14.7.2 Output type ‘an’ model level Gaussian grid-point fields
- 14.7.3 Output type ‘an’ surface Gaussian grid-point fields
- 14.7.4 Output type ‘an’ wave model fields
- 14.7.5 Output error fields

14.8 Output observation data

14.9 Sea surface temperature analysis

- 14.9.1 Input GRIB fields on model grid
- 14.9.2 Input NCEP fields
- 14.9.3 Input data files

- 14.9.4 Output GRIB fields on model grid
- 14.10 2 metre temperature analysis
 - 14.10.1 Input GRIB fields on model grid
 - 14.10.2 Input observation data
 - 14.10.3 Output GRIB field on model grid
- 14.11 2 metre relative humidity analysis
 - 14.11.1 Input GRIB fields on model grid
 - 14.11.2 Input observation data
 - 14.11.3 Output GRIB field on model grid
- 14.12 Snow analysis
 - 14.12.1 Input GRIB fields on model grid
 - 14.12.2 Input data files
 - 14.12.3 Input observation data
 - 14.12.4 Output GRIB field on model grid
- 14.13 Soil moisture analysis
 - 14.13.1 Input GRIB fields on model grid
 - 14.13.2 Output GRIB fields on model grid
 - 14.13.3 Invariant climatological fields

14.1 NOTATION

The following environment variables, which are used in the same way in the data assimilation scripts, are referred to in this chapter.

TABLE 14.1 DEFINITION OF ENVIRONMENT VARIABLES

Variable	Meaning	Default value
\${DATA}	Data directory for invariant files	
\${GTYPE}	Gaussian grid type	l_2 (ie linear reduced Gaussian grid)
\${IFS_CYCLE}	IFS cycle name	CY28R1
\${LEVELS}	Number of vertical model levels	60
\${MM}	Month	
\${RESOL}	Spectral truncation	511
\${starttime}	Start of 4D-Var window as yyyyymmddhh	
\${WDIR}	Work directory (1 for each cycle)	

In this chapter, the notation illustrated in Fig. 14.1 is used in diagrams to distinguish between computation steps and data sets.

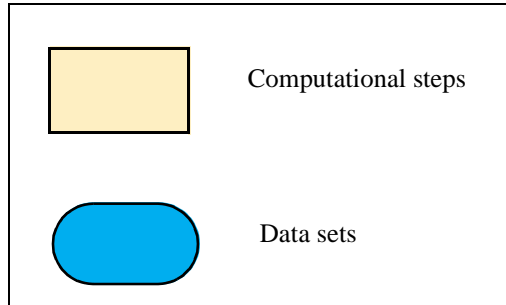


Figure 14.1 Notation

14.2 DATA ASSIMILATION CYCLING

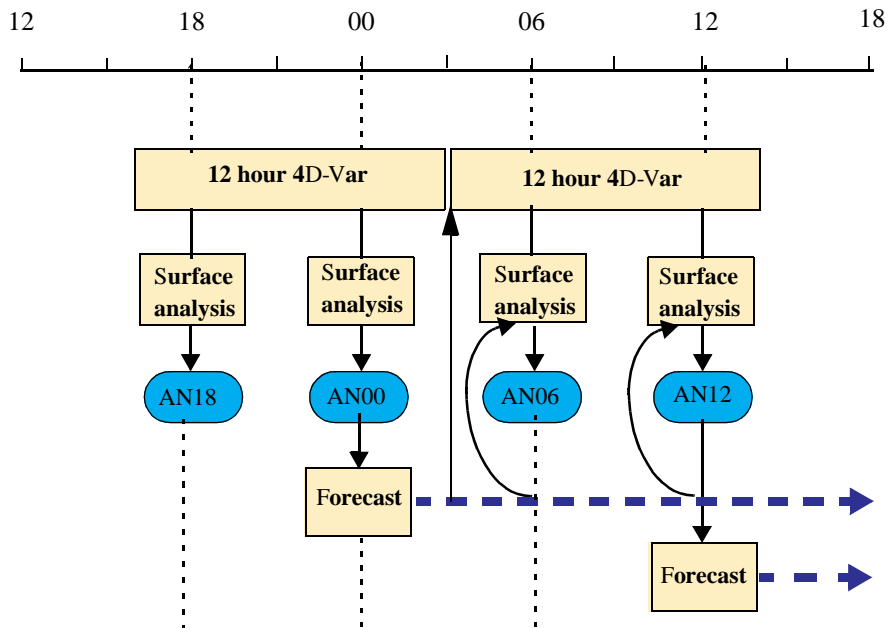


Figure 14.2 Data assimilation cycling with 12 hour 4D-Var

Fig. 14.2 gives an overview of the data flow through the data assimilation system. It shows the operational configuration, with two cycles per day of 12-hour 4D-Var. The 0000 UTC assimilation uses observations from the time window 1501 - 0300 UTC. Its first guess is the three-hour forecast from the previous day's 1200 UTC analysis. It generates two sets of analysed fields, at 1800 and 0000 UTC. A separate surface analysis is run every six hours. The final analysis is a combination of the fields from 4D-Var and from the surface analysis.

The 1200 UTC analysis uses observations from the time window 0301 - 1500 UTC. Its first guess is the three hour forecast from the 0000 UTC analysis. It generates analysed fields at 0600 and 1200 UTC, and these are combined with the appropriate surface analysis fields to give the full analyses. Ten day forecasts are run from the analyses at 0000 and 1200 UTC.

14.3 OVERVIEW OF 4D-VAR DATA FLOW

Figure 14.3 gives an overview of the data input to and output from 4D-Var. There are three types of input data:

- (i) GRIB fields from the Fields Data Base (FDB). GRIB is a World Meteorological Organisation (WMO) standard format for the representation of General Regularly-distributed Information in Binary. The GRIB code is described at <http://www.ecmwf.int/products/data/software/grib.html>. The background fields and forecast errors are read from the Fields Data Base.
- (ii) observations from the Observation Data Base (ODB)
- (iii) other data files

Output data from 4D-Var is in two forms:

- (i) GRIB fields in the Fields Data Base, eg analysis fields, error fields
- (ii) updates to the ODB, including departures of observations from the background and the analysis and quality control information

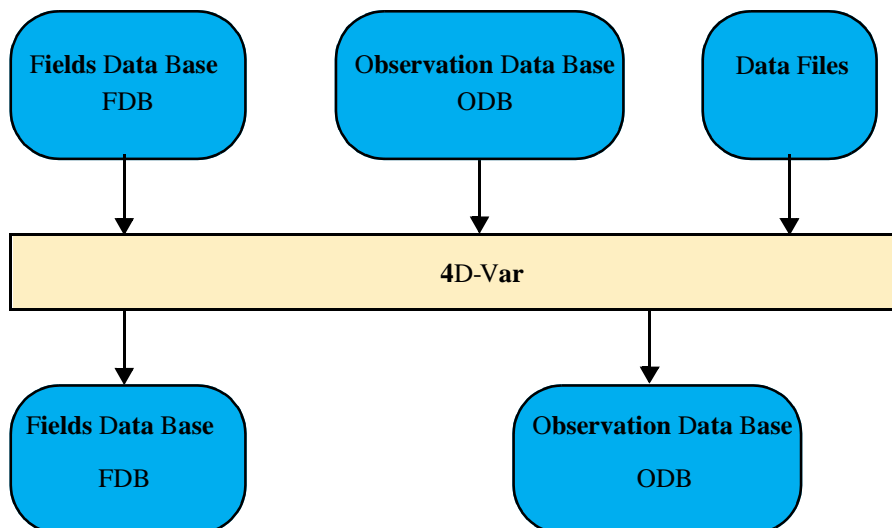


Figure 14.3 4D-Var data flow



14.4 INPUT GRIB FIELDS

The following files in the work directory, \$WDIR, contain GRIB format fields which have been extracted from the Fields Data Base. Fields of type 'fc' are taken from the forecast from the previous cycle's analysis, and are valid at the start of the 4D-Var window. Fields of type 'an' are taken from the previous analysis. The spectral orography is taken from the climatology file of the appropriate resolution, to ensure that the orography is not changed by encoding into and decoding from GRIB. Fields of type 'ef', forecast error, were output from the previous cycle's 4D-Var analysis.

Files which are needed as input to the coupled wave model also have the stream defined. If stream=DA, then the fields were output from the atmospheric model, and the GRIB codes are defined in (ECMWF local table 2, Version 128). If stream=WAVE, then the fields were output from the wave model and the GRIB codes are defined in (ECMWF local table 2, Version 140).

14.4.1 reftrajshml

TABLE 14.2 BACKGROUND, SPHERICAL HARMONICS, MODEL LEVELS

Code	Name	Description	Units	Levels	Type
129	Z	Orography (geopotential)	m ² s ⁻²	1	climate
133	Q	Specific humidity	kg kg ⁻¹	1-\$LEVELS	fc
130	T	Temperature	K	1-\$LEVELS	fc
138	VO	Vorticity	s ⁻¹	1-\$LEVELS	fc
152	LNSP	Logarithm of surface pressure		1	fc
155	D	Divergence	s ⁻¹	1-\$LEVELS	fc
203	O3	Ozone mass mixing ratio	kg kg ⁻¹	1-\$LEVELS	fc

14.4.2 reftrajggml

1

TABLE 14.3 BACKGROUND, GAUSSIAN GRID, MODEL LEVELS

Code	Name	Description	Units	Levels	Type
133	Q	Specific humidity	kg kg ⁻¹	1-\$LEVELS	fc
203	O3	Ozone mass mixing ratio	kg kg ⁻¹	1-\$LEVELS	fc
246	CLWC	Cloud liquid water content	kg kg ⁻¹	1-\$LEVELS	fc
247	CIWC	Cloud ice water content	kg kg ⁻¹	1-\$LEVELS	fc
248	CC	Cloud cover	(0-1)	1-\$LEVELS	fc

14.4.3 reftrajscf

TABLE 14.4 SURFACE FIELDS, GAUSSIAN GRID, BACKGROUND (VARIABLE FIELDS) AND ANALYSIS (INVARIANT FIELDS)

Code	Name	Description	Units	Type
031	CI	Sea-ice cover	(0-1)	fc
032	ASN	Snow albedo	(0-1)	fc
033	RSN	Snow density	kg m ⁻³	fc
034	SST	Sea surface temperature	K	fc
035	ISTL1	Ice surface temperature, layer 1	K	fc
036	ISTL2	Ice surface temperature, layer 2	K	fc
037	ISTL3	Ice surface temperature, layer 3	K	fc
038	ISTL4	Ice surface temperature, layer 4	K	fc
039	SWVL1	Volumetric soil water, layer 1	m ³ m ⁻³	fc
040	SWVL2	Volumetric soil water, layer 2	m ³ m ⁻³	fc
041	SWVL3	Volumetric soil water, layer 3	m ³ m ⁻³	fc
042	SWVL4	Volumetric soil water, layer 4	m ³ m ⁻³	fc
139	STL1	Soil temperature level 1	K	fc
141	SD	Snow depth	m of water equivalent	fc
148	CHNK	Charnock parameter		fc
170	STL2	Soil temperature level 2	K	fc
183	STL3	Soil temperature level 3	K	fc
198	SRC	Skin reservoir content	m of water	fc
235	SKT	Skin temperature	K	fc
236	STL4	Soil temperature level 4	K	fc
238	TSN	Temperature of snow layer	K	fc
027	CVL	Low vegetation cover	(0-1)	an
028	CVH	High vegetation cover	(0-1)	an
029	TVL	Type of low vegetation	Table index	an
030	TVH	Type of high vegetation	Table index	an
160	SDOR	Standard deviation of orography		an
161	ISOR	Anisotropy of sub-gridscale orography		an
162	ANOR	Angle of sub-gridscale orography	rad	an
163	SLOR	Slope of sub-gridscale orography		an
172	LSM	Land-sea mask	(0,1)	an
173	SR	Surface roughness	m	an
174	ALB	Albedo	(0-1)	an
234	LSRH	Logarithm of surface roughness		an



14.4.4 errgrib

TABLE 14.5 BACKGROUND ERRORS, MODEL LEVELS, GAUSSIAN GRID

Code	Name	Description	Units	Levels	Type
130	T	Temperature	K	1-\$LEVELS	ef
131	U	u velocity	m s^{-1}	1-\$LEVELS	ef
132	V	v velocity	m s^{-1}	1-\$LEVELS	ef
133	Q	Specific humidity	kg kg^{-1}	1-\$LEVELS	ef
138	VO	Vorticity	s^{-1}	1-\$LEVELS	ef
152	LNSP	Logarithm of surface pressure		1	ef
156	GH	Geopotential height	m	1-\$LEVELS	ef
157	R	Relative humidity	%	1-\$LEVELS	ef
194	BTMP	Brightness temperature	K	channels 1-54	ef
203	O3	Ozone mass mixing ratio	kg kg^{-1}	1-\$LEVELS	ef

14.4.5 SSTDATA\${starttime}

TABLE 14.6 BACKGROUND, SURFACE, GAUSSIAN GRID, INPUT FOR WAVE MODEL

Code	Name	Description	Units	Type	Stream
031	CI	Sea-ice cover (0-1)	fc	DA	

14.4.6 SGSS\${starttime}

TABLE 14.7 BACKGROUND, SURFACE, REGULAR LATITUDE/LONGITUDE GRID, INPUT FOR WAVE MODEL

Code	Name	Description	Units	Type	Stream
251	2DFD	2D wave spectra	$\text{m}^2 \text{s radian}^{-1}$	fc	WAVE

14.4.7 CD\${starttime}

TABLE 14.8 BACKGROUND, SURFACE, REGULAR LATITUDE/LONGITUDE GRID, INPUT FOR WAVE MODEL

Code	Name	Description	Units	Type	Stream
233	CDWW	Coefficient of drag with waves		fc	WAVE

14.4.8 UWAVE\${starttime}

TABLE 14.9 BACKGROUND, SURFACE, REGULAR LATITUDE/LONGITUDE GRID, INPUT FOR WAVE MODEL

Code	Name	Description	Units	Type	Stream
245	WIND	10 metre wind speed	m s ⁻¹	fc	WAVE

14.4.9 WIND\${starttime}

TABLE 14.10 BACKGROUND, SURFACE, GAUSSIAN GRID, INPUT FOR WAVE MODEL

Code	Name	Description	Units	Type	Stream
165	10U	10 metre U wind component	m s ⁻¹	fc	DA
166	10V	10 metre U wind component	m s ⁻¹	fc	DA

14.5 INPUT OBSERVATION DATA

Observations are read into 4D-Var from the Observation Data Base (ODB). The observation processing is described in more detail in the ODB documentation (file:///home/rd/mps/public/ugodb.pdf).

14.6 INPUT DATA FILES

Input data files can be split into two categories, invariant and date-dependent. For the invariant files, a single copy is used for the lifetime of the experiment or the operational suite. The file is copied or linked into the experiment's \${DATA} directory at start-up time in task datalinks.

Some files, such as blacklists and bias files, are date-dependent. In the operational suite, the blacklist can be changed at short notice if, for example, a satellite channel fails or a new data source arrives which has to be passively monitored to assess its quality before it can be used actively. Date-dependent files are copied to the \${WDIR} directory in task vardata at the beginning of each data assimilation cycle.

14.6.1 Invariant data files

- (i) \${DATA}/an/cmod.table.ieee - scatterometer coefficients
- (ii) \${DATA}/an/external_bl_mon_monit.b - external blacklist file
- (iii) \${DATA}/an/neuroflux_1\${LEVELS} - extended linearized longwave radiation
- (iv) \${DATA}/an/radjacobian_1\${LEVELS} - extended linearized longwave radiation
- (v) \${DATA}/an/rs_bias_T_table1 - radiosonde temperature bias correction coefficients
- (vi) \${DATA}/an/rs_bias_T_table2 - radiosonde temperature bias correction coefficients
- (vii) \${DATA}/an/rs_bias_T_table3 - radiosonde temperature bias correction coefficients
- (viii) \${DATA}/an/stabal96.bal - background error balance parameters
- (ix) \${DATA}/an/stabal96.cv - background error correlations
- (x) \${DATA}/climate/\${RESOL}/\${GTYPE}/O3CHEM\${MM} - monthly ozone chemistry climate files

- (xi) $\{\text{DATA}\}/\text{ifs}/\text{namelist}_{\{\text{IFS_CYCLE}\}}$ - an empty copy of all the IFS namelists
- (xii) $\{\text{DATA}\}/\text{ifs}/\text{rtable}_{\{\text{GTYPE}\}}_{\{\text{RESOL}\}}$ - namelist NAMRGRI, defining the number of points on each row of the Gaussian grid
- (xiii) $\{\text{DATA}\}/\text{ifs}/\text{vtable}_{\text{L}}_{\{\text{LEVELS}\}}$ - namelist NAMVV1, defining the hybrid vertical coordinate level coefficients
- (xiv) $\{\text{DATA}\}/\text{sat}/\text{rt_coef_airs_newpred_ieee}$ - AIRS radiative transfer coefficient file
- (xv) $\{\text{DATA}\}/\text{sat}/\text{rt_coef_atovs_newpred_ieee}$ - ATOVS radiative transfer coefficient file
- (xvi) $\{\text{DATA}\}/\text{sat}/\text{rt_coef_goesimg_newpred}$ - GOES radiative transfer coefficient file
- (xvii) $\{\text{DATA}\}/\text{sat}/\text{rt_coef_meteosat_newpred}$ - METEOSAT radiative transfer coefficient file

14.6.2 Date-dependent data files

- (i) $\{\text{WDIR}\}/\text{bl_data_sel}$ - data selection blacklist
- (ii) $\{\text{WDIR}\}/\text{monthly_bl_mon_monit.b}$ - monthly monitoring blacklist
- (iii) $\{\text{WDIR}\}/\text{var}/\text{bcor_airs.dat}$ - AIRS bias correction
- (iv) $\{\text{WDIR}\}/\text{var}/\text{bcor_goes.dat}$ - GOES bias correction
- (v) $\{\text{WDIR}\}/\text{var}/\text{bcor_meto.dat}$ - METEOSAT bias correction
- (vi) $\{\text{WDIR}\}/\text{var}/\text{bcor_noaa.dat}$ - ATOVS bias correction
- (vii) $\{\text{WDIR}\}/\text{var}/\text{bcor_s}$
- (viii) smi.dat - SSM/I bias correction

14.7 OUTPUT GRIB FIELDS

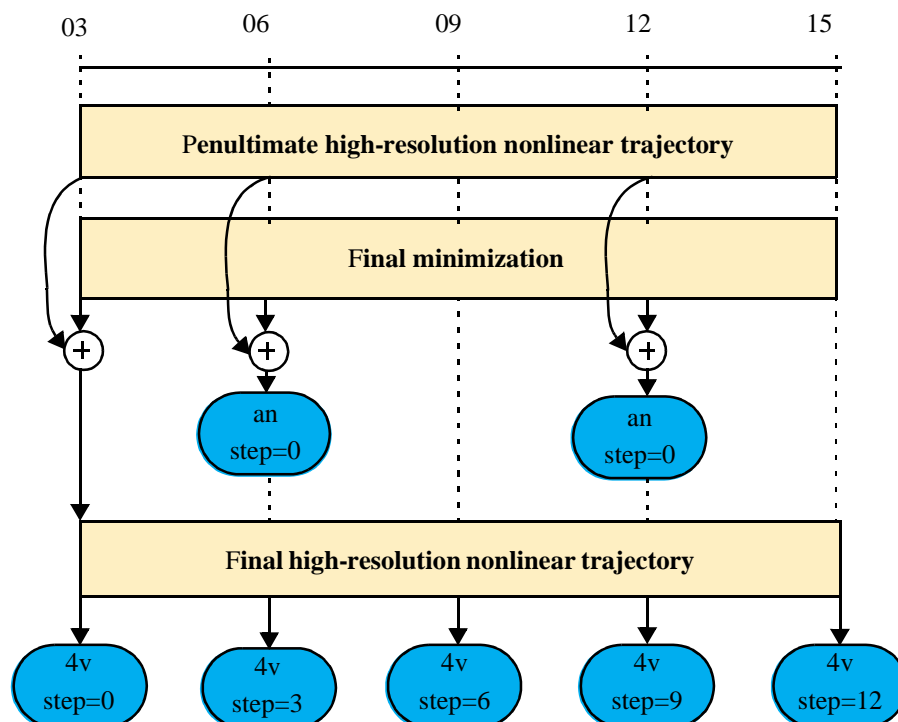


Figure 14.4 Type 'an' and type '4v' fields written from 4D-Var to the Fields Data Base

Fields of type '4v' (4D-Var analysis), 'an' (analysis), 'ea' (analysis errors) and 'ef' (forecast errors) are written in GRIB code to the Fields Data Base from 4D-Var. Fig. 14.4 illustrates the difference between type '4v' and type 'an' analysis fields. For type '4v' fields, the analysis increment from the final minimization is interpolated back to high resolution and added to the penultimate high resolution trajectory at its starting point. Analysis fields output from the final high resolution non-linear trajectory are of type '4v', with a base time at the start of the trajectory and a step corresponding to the number of hours into the trajectory. So, for example, for the 1200 UTC 12 hour 4D-Var for date `yyyymmdd`, with an observation window from 0300 to 1500 UTC, the 4D-Var analysis at 1200 UTC is stored in the Fields Data Base and MARS with parameters:

```
date=yyyymmdd, hour=03, step=9, type=4v
```

For type 'an' fields, the increment from the final minimization is added to the penultimate high resolution trajectory at the actual analysis time. Fields from the surface analysis are combined with fields from 4D-Var to give the full analysis. For the 1200 UTC 12 hour 4D-Var for date `yyyymmdd`, with an observation window from 0300 to 1500 UTC, the type 'an' analysis at 1200 UTC is stored in the Fields Data Base and MARS with parameters:

```
date=yyyymmdd, hour=12, step=0, type=an
```

Output analysis fields, of type '4v' and 'an', can be generated on model levels, pressure levels and isentropic surfaces. Namelist `NAMFPC` controls the content of the post-processing, and there is a wide selection of fields that can be produced. The IFS determines internally whether fields should be generated in spectral or grid-point form. Described below is only the list of fields that are needed as input for the next forecast in order to cycle the data assimilation forward in time. The forecast starts from fields of type 'an'. Some of the surface fields are generated by the surface analysis jobs, which run at the same time as 4D-Var. It is important that these fields are excluded from the type 'an' post-processing of 4D-Var, so that they cannot overwrite the surface analysis fields.

14.7.1 Output type 'an' model level spectral fields

TABLE 14.11 OUTPUT TYPE 'AN' MODEL LEVEL SPECTRAL FIELDS

Code	Name	Description	Units	Levels
130	T	Temperature	K	1-\$LEVELS
138	VO	Vorticity	s ⁻¹	1-\$LEVELS
152	LNSP	Logarithm of surface pressure		1
155	D	Divergence	s ⁻¹	1-\$LEVELS

14.7.2 Output type 'an' model level Gaussian grid-point fields

TABLE 14.12 OUTPUT TYPE 'AN' MODEL LEVEL GAUSSIAN GRID-POINT FIELDS

Code	Name	Description	Units	Levels
133	Q	Specific humidity	kg kg ⁻¹	1-\$LEVELS
203	O3	Ozone mass mixing ratio	kg kg ⁻¹	1-\$LEVELS
246	CLW C	Cloud liquid water content	kg kg ⁻¹	1-\$LEVELS



TABLE 14.12 OUTPUT TYPE 'AN' MODEL LEVEL GAUSSIAN GRID-POINT FIELDS

247	CIW C	Cloud ice water content	kg kg ⁻¹	1-\$LEVELS
248	CC	Cloud cover	(0-1)	1-\$LEVELS

14.7.3 Output type 'an' surface Gaussian grid-point fields

TABLE 14.13 OUTPUT TYPE 'AN' SURFACE GAUSSIAN GRID-POINT FIELDS

Code	Name	Description	Units
027	CVL	Low vegetation cover	(0-1)
028	CVH	High vegetation cover	(0-1)
029	TVL	Type of low vegetation	Table index
030	TVH	Type of high vegetation	Table index
032	ASN	Snow albedo	(0-1)
035	ISTL1	Ice surface temperature, layer 1	K
036	ISTL2	Ice surface temperature, layer 2	K
037	ISTL3	Ice surface temperature, layer 3	K
038	ISTL4	Ice surface temperature, layer 4	K
042	SWVL4	Volumetric soil water, layer 4	m ³ m ⁻³
129	Z	Orography (geopotential)	m ² s ⁻²
148	CHNK	Charnock parameter	
160	SDOR	Standard deviation of orography	
161	ISOR	Anisotropy of sub-gridscale orography	
162	ANOR	Angle of sub-gridscale orography	rad
163	SLOR	Slope of sub-gridscale orography	
165	10U	10 metre U wind component	m s ⁻¹
166	10V	10 metre V wind component	m s ⁻¹
172	LSM	Land-sea mask	(0,1)
173	SR	Surface roughness	m
174	ALB	Albedo	(0-1)
198	SRC	Skin reservoir content	m of water
234	LSRH	Logarithm of surface roughness	
235	SKT	Skin temperature	K
236	STL4	Soil temperature level 4	K

14.7.4 Output type 'an' wave model fields

The output wave model fields are on a regular latitude/longitude grid. They are identified by stream 'WAVE' and are encoded with GRIB codes defined in [ECMWF local table 2, Version 140](#).

TABLE 14.14 OUTPUT TYPE 'AN' WAVE MODEL FIELDS

Code	Name	Description	Units
251	2DFD	2D wave spectra	m ² s radian ⁻¹
233	CDWW	Coefficient of drag with waves	
245	WIND	10 metre wind speed	m s ⁻¹

14.7.5 Output error fields

The forecast errors output from one cycle are used as the background errors input to the next cycle, and their content is described in Section x.4.4 above. The analysis errors contain similar fields, but are of type 'ea'. The analysis errors are used to calculate the perturbations for the Ensemble Prediction System.

14.8 OUTPUT OBSERVATION DATA

Departures of observations from the background and the analysis, and quality information are written to the Observation Data Base (ODB). The observation processing is described in more detail in Part I.

14.9 SEA SURFACE TEMPERATURE ANALYSIS

The sea surface temperature analysis is done every 6 hours.

14.9.1 Input GRIB fields on model grid

These are extracted from the Fields Data Base. The background fields, of type 'fc', are taken from the forecast from the previous 4D-Var analysis time. The persistence analysis, of type 'an', is taken from the previous sea surface temperature analysis time, 6 hours earlier (which is not necessarily a 4D-Var analysis time). In the table below, 'T' is used to denote the analysis time, and 'T-6' is used to denote the persistence analysis time.

TABLE 14.15 INPUT GRIB FIELDS ON MODEL GRID

Code	Name	Description	Units	Type	Time
031	CI	Sea-ice cover	(0-1)	fc	T
034	SST	Sea surface temperature	K	fc	T
034	SST	Sea surface temperature	K	an	T-6

14.9.2 Input NCEP fields

The sea surface temperature analysis and sea ice analysis from NCEP (National Center for Environmental Prediction, Washington) are input on a 0.5×0.5 degree regular latitude / longitude grid. These fields are extracted from MARS with parameters:

expver=1, origin=kwbc



14.9.3 Input data files

- (i) \$DATA/sst/lstfil - land/sea mask for NCEP data, 0.5x0.5 degree regular latitude/longitude grid, 720x360 points
- (ii) \$DATA/sst/sst_clim - surface air temperature monthly climatology, reduced to mean-sea level (0.5x0.5 degree regular latitude/longitude grid, 720x361 points)
- (iii) \${DATA}/climate/\${RESOL}/\${GTYPE}/lsmoro - land/sea mask and orography on model Gaussian grid
- (iv) \${DATA}/climate/\${RESOL}/\${GTYPE}/clake - lake mask

14.9.4 Output GRIB fields on model grid

The following fields are written to the Fields Data Base:

TABLE 14.16 OUTPUT GRIB FIELDS ON MODEL GRID

Code	Name	Description	Units	Type
031	CI	Sea-ice cover	(0-1)	an
034	SST	Sea surface temperature	K	an

14.10 2 METRE TEMPERATURE ANALYSIS

The 2 metre temperature analysis is done every 6 hours.

14.10.1 Input GRIB fields on model grid

These are extracted from the Fields Data Base. The background fields, of type 'fc', are taken from the forecast from the previous 4D-Var analysis time. The invariant fields, of type 'an', are taken from the previous 4D-Var analysis.

TABLE 14.17 INPUT GRIB FIELDS ON MODEL GRID

Code	Name	Description	Units	Type
129	Z	Orography	m ² s ⁻²	an
172	LSM	Land/sea mask	(0-1)	an
139	STL1	Soil temperature level 1	K	fc
167	2T	2 metre temperature	K	fc
168	2D	2 metre dewpoint temperature	K	fc

14.10.2 Input observation data

Observations are read from the Observation Data Base.

14.10.3 Output GRIB field on model grid

The analysed 2 metre temperature field is written to the Fields Data Base.

TABLE 14.18 OUTPUT GRIB FIELD ON MODEL GRID

Code	Name	Description	Units	Type
167	2T	2 metre temperature	K	an

14.11 2 METRE RELATIVE HUMIDITY ANALYSIS

The 2 metre relative humidity analysis is done every 6 hours. Although the analysed field is 2 metre relative humidity, the final output product is 2 metre dewpoint temperature. The 2 metre relative humidity analysis cannot start until the 2 metre temperature analysis has completed, since the output from the 2 metre temperature analysis is needed in the computation of the 2 metre dewpoint temperature.

14.11.1 Input GRIB fields on model grid

These are extracted from the Fields Data Base. The background fields, of type 'fc', are taken from the forecast from the previous 4D-Var analysis time. The invariant fields, of type 'an', are taken from the previous 4D-Var analysis.

TABLE 14.19 INPUT GRIB FIELDS ON MODEL GRID

Code	Name	Description	Units	Type
129	Z	Orography	m ² s ⁻²	an
172	LSM	Land/sea mask	(0-1)	an
139	STL1	Soil temperature level 1	K	fc
167	2T	2 metre temperature	K	fc
168	2D	2 metre dewpoint temperature	K	fc

14.11.2 Input observation data

Observations are read from the Observation Data Base.

14.11.3 Output GRIB field on model grid

The derived 2 metre dewpoint temperature field is written to the Fields Data Base.

TABLE 14.20 OUTPUT GRIB FIELD ON MODEL GRID

Code	Name	Description	Units	Type
168	2D	2 metre dewpoint temperature	K	an

14.12 SNOW ANALYSIS

The snow analysis is done every 6 hours. It cannot start until the 2 metre temperature analysis has completed, since the 2 metre temperature analysis field is one of the inputs to the snow analysis.



14.12.1 Input GRIB fields on model grid

These are extracted from the Fields Data Base. The background fields, of type 'fc', are taken from the forecast from the previous 4D-Var analysis time. The invariant fields of type 'an', orography and land/sea mask, are taken from the previous 4D-Var analysis. This is denoted T4V in the table below. The persistence snow depth analysis, of type 'an', is taken from the previous snow analysis time, 6 hours earlier (which is not necessarily a 4D-Var analysis time). In the table below, 'T' is used to denote the snow analysis time, and 'T-6' is used to denote the persistence snow analysis time.

TABLE 14.21 INPUT GRIB FIELDS ON MODEL GRID

Code	Name	Description	Units	Type	Time
129	Z	Orography	$\text{m}^2 \text{s}^{-2}$	an	T4V
172	LSM	Land/sea mask	(0-1)	an	T4V
033	RSN	Snow density	kg m^{-3}	fc	T
141	SD	Snow depth	m of water equivalent	fc	T
141	SD	Snow depth	m of water equivalent	an	T-6
167	2T	2 metre temperature	K	an	T

14.12.2 Input data files

- (i) $\{\text{DATA}\}/\text{climate}/\{\text{RESOL}\}\{\text{GTYPE}\}/\text{snow}$ - snow depth climatology (m of water equivalent) on model Gaussian grid
- (ii) $\{\text{DATA}\}/\text{climate}/\{\text{RESOL}\}\{\text{GTYPE}\}/\text{cicecap}$ - on model Gaussian grid
- (iii) $\$\text{WDIR}/\text{imssnow}$ - NESDIS snow cover field (0,1) on polar stereographic grid of approximately 25 km resolution. The data is in BUFR format, with triplets of latitude / longitude / snow cover. The NESDIS snow cover field is only used once per day, for the 06Z snow analysis.

14.12.3 Input observation data

Observations are read from the Observation Data Base.

14.12.4 Output GRIB field on model grid

The following fields are written to the Fields Data Base:

TABLE 14.22 OUTPUT GRIB FIELD ON MODEL GRID

Code	Name	Description	Units	Type
033	RSN	Snow density	kg m^{-3}	an
141	SD	Snow depth	m of water equivalent	an

14.13 SOIL MOISTURE ANALYSIS

The soil moisture analysis is done every 6 hours. It cannot start until the sea surface temperature analysis, the snow analysis and 4D-Var have completed.

14.13.1 Input GRIB fields on model grid

These are extracted from the Fields Data Base. The background fields, of type 'fc', are taken from the forecast from the previous 4D-Var analysis time. The analysed fields, of type 'an', are output from the current 4D-Var analysis, the sea surface temperature analysis, the 2 metre temperature analysis, the 2 metre relative humidity analysis or the snow analysis.

TABLE 14.23 INPUT GRIB FIELDS ON MODEL GRID

Code	Name	Description	Units	Type	Origin
039	SWVL1	Volumetric soil water, layer 1	m ³ m ⁻³	fc	Forecast
040	SWVL2	Volumetric soil water, layer 2	m ³ m ⁻³	fc	Forecast
041	SWVL3	Volumetric soil water, layer 3	m ³ m ⁻³	fc	Forecast
133	Q	Specific humidity on lowest model level	kg kg ⁻¹	fc	Forecast
139	STL1	Soil temperature, level 1	K	fc	Forecast
142	LSP	Large scale precipitation	m	fc	Forecast
143	CP	Convective precipitation	m	fc	Forecast
167	2T	2 metre temperature	K	fc	Forecast
168	2D	2 metre dewpoint temperature	K	fc	Forecast
170	STL2	Soil temperature, level 2	K	fc	Forecast
176	SSR	Surface solar radiation	W m ⁻² s	fc	Forecast
183	STL3	Soil temperature level 3	K	fc	Forecast
238	TSN	Temperature of snow layer	K	fc	Forecast
027	CVL	Low vegetation cover	(0-1)	an	4D-Var
028	CVH	High vegetation cover	(0-1)	an	4D-Var
029	TVL	Type of low vegetation	Table index	an	4D-Var
030	TVH	Type of high vegetation	Table index	an	4D-Var
129	Z	Orography	m ² s ⁻²	an	4D-Var
133	Q	Specific humidity on lowest model level	kg kg ⁻¹	an	4D-Var
141	SD	Snow depth	m of water equivalent	an	Snow analysis
165	10U	10 metre U wind component	m s ⁻¹	an	4D-Var
166	10V	10 metre V wind component	m s ⁻¹	an	4D-Var
167	2T	2 metre temperature	K	an	2 metre temp. anal.
168	2D	2 metre dewpoint temperature	K	an	2 metre rel. hum. anal.
172	LSM	Land-sea mask	(0,1)	an	4D-Var
174	AL	Albedo	(0-1)	an	4D-Var

14.13.2 Output GRIB fields on model grid

The following fields are output from the soil moisture analysis and written to the Fields Data Base. Before being written, the STL1 (soil temperature level 1) field is manipulated as follows:

- (i) land values are unchanged

(ii) over sea,

$$STL1 = SST \times (1 - CI) + ISTLA \times CI$$

where

SST = analysed sea surface temperature

CI = analysed sea ice field, which varies between 0 (open water)
and 1 (full ice cover)

$ISTL1$ = background soil temperature level1

TABLE 14.24 OUTPUT GRIB FIELDS ON MODEL GRID

Code	Name	Description	Units
039	SWVL1	Volumetric soil water, layer 1	m ³ m ⁻³
040	SWVL2	Volumetric soil water, layer 2	m ³ m ⁻³
041	SWVL3	Volumetric soil water, layer 3	m ³ m ⁻³
139	STL1	Soil temperature, level 1	K
170	STL2	Soil temperature, level 2	K
183	STL3	Soil temperature, level 3	K
238	TSN	Temperature of snow layer	K

14.13.3 Invariant climatological fields

The final step of the soil moisture analysis task is to copy the invariant fields from the climatology files to the analysis, after first manipulating the GRIB headers to give values appropriate for the current data assimilation cycle. In this way, it is ensured that invariant fields remain unchanged, without any loss of precision due to repeatedly encoding and decoding GRIB fields.

TABLE 14.25 INVARIANT CLIMATOLOGICAL FIELDS

Code	Name	Description	Units
027	CVL	Low vegetation cover	(0-1)
028	CVH	High vegetation cover	(0-1)
029	TVL	Type of low vegetation	Table index
030	TVH	Type of high vegetation	Table index
129	Z	Orography	m ² s ⁻²
160	SDOR	Standard deviation of orography	
161	ISOR	Anisotropy of sub-gridscale orography	
162	ANOR	Angle of sub-gridscale orography	rad
163	SLOR	Slope of sub-gridscale orography	
172	LSM	Land-sea mask	(0,1)



TABLE 14.25 INVARIANT CLIMATOLOGICAL FIELDS

173	SR	Surface roughness	m
174	ALB	Albedo	(0-1)
234	LSRH	Logarithm of surface roughness	

Part II: DATA ASSIMILATION

REFERENCES

- Alduchov, O. A. and Eskridge, R.E., 1996:* Improved Magnus form approximation of saturation vapor pressure. *J. Appl. Met.*, **35**, 601–609.
- Andersson, E., Pailleux, J., Thépaut, J.–N., Eyre, J. R., McNally, A. P., Kelly, G. A. and Courtier, P., 1994:* Use of cloud–cleared radiances in three/four–dimensional variational data assimilation. *Q. J. R. Meteorol. Soc.*, **120**, 627–653
- Andersson, E., Haseler, J., Undén, P., Courtier, P., Kelly, G., Vasiljevic, D., Brankovic, C., Cardinali, C., Gaffard, C., Hollingsworth, A., Jakob, C., Janssen, P., Klinker, E., Lanzinger, A., Miller, M., Rabier, F., Simmons, A., Strauss, B., Thépaut, J.–N. and Viterbo, P., 1998:* The ECMWF implementation of three dimensional variational assimilation (3D–Var). Part III: Experimental results. *Q. J. R. Meteorol. Soc.*, **124**, 1831–1860.
- Andersson, E. and Järvinen, H., 1999:* Variational quality control. *Q. J. R. Meteorol. Soc.*, **125**, 697–722
- Andersson, E., Fisher, M., Munro, R. and McNally, A., 2000:* Diagnosis of background errors for radiances and other observable quantities in a variational data assimilation scheme, and the explanation of a case of poor convergence. *Q. J. R. Meteorol. Soc.* **126**, 1455–1472.
- Andersson, E., C. Cardinali, L. Isaksen and A. Garcia-Mendez, 2001:* ‘On the impact of frequent data in ECMWF’s 4D–Var scheme: Hourly surface pressure data, European profilers and profiling aircraft data’. Pp. 179–183 in Proceedings of the 8th ECMWF workshop on meteorological operational systems.
- Andersson, E. and A. Garcia-Mendez, 2002:* Assessment of European wind profiler data, in an NWP context. *ECMWF Tech. Memo.*, **372**, pp 14.
- Andersson, E., A. Beljaars, J. Bidlot, M. Miller, A. Simmons and J.N. Thépaut, 2003:* A major new cycle of the IFS: Cycle 25r4. *ECMWF Newsletter*, **97**, 12–20.
- Andersson, E., E. Hölm and J. N. Thépaut, 2004:* Impact studies of main types of conventional and satellite humidity data. Proc. 3rd WMO Workshop on “The Impact of Various Observing Systems on NWP”, Alpbach, Austria, 9–12 March 2004. pp XX. (In press).
- Attema, E., P. W., 1986:* An experimental campaign for the determination of the radar signature of the ocean at C–band. *Proc. Third International Colloquium on Spectral Signatures of Objects in Remote Sensing*, Les Arcs, France, ESA, **SP-247**, 791–799.
- Bauer, P., G. Kelly and E. Andersson, 2002:* SSM/I radiance assimilation at ECMWF. Proc ECMWF/GEWEX workshop on “Humidity Analysis”, Reading, 8–11 July 2002, 167–175.
- Betts, A., 1997:* The parametrization of deep convection: A review. Pp. 166–188 in Proceedings of the ECMWF workshop on new insights and approaches to convective parametrization, 4–7 November 1996.
- Blackadar, A. K., 1962:* The vertical distribution of wind and turbulent exchange in a neutral atmosphere. *J. Geophys. Res.*, **67**, 3095–3102
- Blondin, C., 1991:* ‘Parametrization of land surface processes in numerical weather prediction’. Pp. 31–54 in *Land surface evaporation: measurement and parametrization*, T. J. Schmugge and J.–C. André, Eds., Springer–Verlag
- Bormann, N., S. Saarinen, G. Kelly and J.N. Thépaut, 2003:* The spatial structure of observation errors in atmospheric motion vectors from geostationary satellite data. *Mon. Wea. Rev.*, **131**, 706–718.

- Bouttier, F., 2001a*: The development of 12-hourly 4D-Var. *ECMWF Tech. Memo.* **348**, pp 21.
- Bouttier, F., 2001b*: The use of profiler data at ECMWF. *Meteorologische Zeitschrift*, **10**, 497—510.
- Bouttier, F., Derber, J. and Fisher, M., 1997*: The 1997 revision of the Jb term in 3D/4D-Var. ECMWF Tech. Memo. 238.
- Buck, A.L., 1981*: New equations for computing vapor pressure and enhancement factor. *J. Appl. Met.*, **20**, 1527–1532.
- Buizza, R., 1994*: Sensitivity of optimal unstable structures. *Q. J. R. Meteorol. Soc.*, **120**, 429–451
- Cardinali, C., Andersson, E., Viterbo, P., Thépaut, J.-N. and Vasiljevic, D., 1994*: Use of conventional surface observations in three-dimensional variational data assimilation. ECMWF Tech. Memo. 205.
- Cardinali, C., L. Isaksen and E. Andersson, 2003*: Use and impact of automated aircraft data in a global 4D-Var data assimilation system. *Mon. Wea. Rev.*, **131**, 1865—1877.
- Cardinali, C., S. Pezzulli and E. Andersson, 2004*: Influence matrix diagnostic of a data assimilation system. *Q. J. R. Meteorol. Soc.* **130**, (in press).
- Cavaliere, D.J. et al., 1991*: Aircraft active and passive microwave validation of sea-ice concentration from the Defense Meteorological Satellite Program (DMSP) Special Sensor Microwave Imager. *J. G. R. Oceans*, **96** (C12), 21989-22008
- Chelton, D., B., Freilich, M. H., and S. K. Esbensen. 2000*: Satellite observations of the wind jets off the Pacific coast of Central America. Part I: Case studies and statistical characteristics. *Mon. Wea. Rev.*, **128**, 1,993-2,018.
- Chevallier, F. and J.-F. Mahfouf, 2001*: Evaluation of the Jacobians of infrared radiation models for variational data assimilation. *J. Appl. Meteorol.*, **40**, 1445-1461
- Chevallier, F., J.-J. Norcrette, F. Chéruy, and N. A. Scott, 2000*: Use of a neural network-based longwave radiative transfer scheme in the ECMWF atmospheric model. *Q. J. R. Meteorol. Soc.*, **126**, 761-776
- Courtier, P., Thépaut, J.-N. and Hollingsworth, A., 1994*: A strategy for operational implementation of 4D-Var, using an incremental approach. *Q. J. R. Meteorol. Soc.*, **120**, 1367–1388
- Courtier, P., Andersson, E., Heckley, W., Pailleux, J., Vasiljevic, D., Hamrud, M., Hollingsworth, A., Rabier, F. and Fisher, M., 1998*: The ECMWF implementation of three dimensional variational assimilation (3D-Var). I: Formulation. *Q. J. R. Meteorol. Soc.*, **124**, 1783-1807.
- Derber, J.C. and F. Bouttier, 1999*: A reformulation of the background error covariance in the ECMWF global data assimilation system. *Tellus*, **51A**, 195—221.
- Dethof, A. and E. Holm, 2004*: Ozone assimilation in the ERA-40 reanalysis project. *Q. J. R. Meteorol. Soc.*, 131, In press.
- Douville, H., Viterbo, P., Mahfouf, J.-F. and Beljaars, A. C. M. (2001)*: “Evaluation of the optimum interpolation and nudging techniques for soil moisture analysis using FIFE data” *Mon. Wea. Rev.*, **128**, 1733-1756.
- Drusch, M., D. Vasiljevic and P. Viterbo, 2004*: ECMWF’s global snow analysis: Assessment and revision based on satellite observations. *J. Appl. Met.*, **43(9)**, 1282-1294
- Dubuisson, P. J., J. Buriez, and Y. Fouquart, 1996*: High spectral solar radiative transfer in absorbing and scattering media: Application to the satellite simulation. *J. Quant. Spectrosc. Radiat. Transfer*, **55**, 103-126
- Ebert, E. E. and J. A. Curry, 1992*: A parametrization of ice optical properties for climate models. *J. Geophys. Res.*, **97D**



- Engelen, R. J., E. Andersson, F. Chevallier, A. Hollingsworth, M. Matricardi, A. McNally, J. N. Thépaut and P. Watts, 2004: Estimating atmospheric CO₂ from advanced infrared satellite radiances within an operational 4D-Var data assimilation system: Methodology and first results. *J. Geophys. Res.*, **109**, D19309, xxx—xxx.
- Eyre, J. R., 1991: A fast radiative transfer model for satellite sounding systems. ECMWF Tech. Memo. 176.
- Fisher, M., 1996: The specification of background error variances in the ECMWF variational analysis system. Proc. ECMWF workshop on “Non-linear aspects of data assimilation”, Reading, 9-11 September 1996, 645—652.
- Fisher, M. and Courtier, P., 1995: Estimating the covariance matrices of analysis and forecast error in variational data assimilation, ECMWF Tech. Memo. 220.
- Fisher, M. 1998: Minimization algorithms for variational data assimilation, Proc. ECMWF Seminar on "Recent developments in numerical methods for atmospheric modelling", Reading, U.K. 7-11 September 1998, 364-385.
- Fisher, M. and Andersson, E., 2001: Developments in 4D-Var and Kalman Filtering. *ECMWF Tech Memo.*, 347, pp 36.
- Fisher, M., 2003: Background error covariance modeling. Proc. ECMWF Seminar on “Recent Developments in Data Assimilation for Atmosphere and Ocean”, 8—12 Sept 2003, Reading, U.K., 45—63.
- Foster, D.J. and R.D. Davy, 1988 : Global snow depth climatology. U.S. Air Force Environmental Tech. Applications Center/TN-88/006, 48 pp. [Available from National Climate Data Center, 151 Patton Avenue, Asheville, NC 28801]
- Fouquart, Y., 1987: Radiative transfer in climate models. Pp. 223-284 in *Physically based modelling and simulation of climate and climate changes*, Ed. M. E. Schlesinger, Kluwer Acad. Publ.
- Fouquart, Y. and B. Bonnel, 1980: Computations of solar heating of the earth’s atmosphere: A new parametrization. *Beitr. Phys. Atmos.*, **53**, 35-62
- Gauthier, P. and Thépaut, J.-N., 2001: Impact of the digital filter as a weak constraint in the preoperational 4DVAR assimilation system of Meteo-France. *Mon. Wea. Rev.*, 129, 2089-2102.
- Geleyn, J.-F., 1988: Interpolation of wind, temperature and humidity values from the model levels to the height of measurement. *Tellus*, **40**, 347–351
- Geleyn, J. F. and A. Hollingsworth, 1997: An economical and analytical method for the interactions between scattering and line absorption of radiation. *Contrib. to Atmos. Phys.*, **52**, 1-16
- Gilbert, J. C. and Lemaréchal, C., 1989: Some numerical experiments with variable storage quasi-Newton algorithms. *Math. Prog.*, **B25**, 407–435
- Gloersen, P. and D. J. Cavalieri, 1986: Reduction of weather effects in the calculation of sea-ice concentration from microwave radiances. *J. G. R. Oceans*, 91 (C3), 3913-3919
- Gloersen, P., et al., 1994: ‘Arctic and Antarctic sea ice, 1978-1987: Satellite passive microwave observations and analysis’. NASA SP-511, Greenbelt, MD, NASAGustafsson, N., 1992: Use of a digital filter as a weak constraint in variational data assimilation. Proc. ECMWF Workshop on "Variational Data Assimilation with Special Emphasis on 3-dimensional aspects.", Reading, U.K., 327-338.
- Gregory, D. and M. Miller, 1989: A numerical study of the parametrization of deep tropical convection. *Q. J. R. Meteorol. Soc.*, **115**, 1209-1241
- Grumbine, R.W., 1996: ‘Automated passive microwave sea-ice concentration analysis at NCEP’. NOAA NCEP Tech Note, 13 pp Harris, B., and G. Kelly, 2001: A satellite radiance bias correction scheme for radiance assimila-

tion. *Q. J. R. Meteorol. Soc.*, **127**, 1453—1468.

Hersbach, H., Isaksen, L, Leidner, S. M. and P. A. E. M. Janssen 2004: The impact of SeaWinds scatterometer data in the ECMWF 4D-Var assimilation system. In preparation.

Hoaglin, D. C., Mosteller, F. and Tukey J.W., 1982. Understanding Robust and Exploratory Data Analysis. *Wiley Series in Probability and Statistics*

Hoaglin, D. C., and Welsch, R. E. 1978: The hat matrix in regression and ANOVA. *The American Statisticians*, 32, 17—22 and *Corrigenda* 32, 146.

Hollinger, J. et al., 1987: Special Sensor Microwave / Imager user's guide, report, *Nav. Res. Lab., Washington D.C.*

Hollingsworth, A. and Lönnberg, P., 1986: The statistical structure of short-range forecast errors as determined from radiosonde data. Part I: The wind field. *Tellus*, **38A**, 111–136

Hólm, E., E. Andersson, A. Beljaars, P. Lopez, J-F. Mahfouf, A.J. Simmons and J.N. Thépaut, 2002: Assimilation and modeling of the hydrological cycle: ECMWF's status and plans. *ECMWF Tech. Memo.*, **383**, pp 55.

Ingleby, N. B. and Lorenc, A. C., 1993: Bayesian quality control using multivariate normal distributions. *Q. J. R. Meteorol. Soc.*, **119**, 1195–1225.

Isaksen, L, (1997). Impact of ERS scatterometer data in the ECMWF 4D-Var assimilation system. Preliminary studies. In *Space at the Service of our Environment*, 1,829-1,851, Florence, Italy, May 1997, ESTEC, European Space Agency [SP-414]. Available from ESA Publications Division, ESTEC Noordwijk, The Netherlands.

Isaksen, L. and A. C. M. Stoffelen, 2000: ERS scatterometer wind data impact on ECMWF's tropical cyclone forecasts. *IEEE Trans. Geosci. Remote Sens.*, **38** (4), 1885-1892.

Isaksen, L. and P. A. E. M. Janssen, 2004: Impact of ERS scatterometer winds in ECMWF's assimilation. *Q. J. R. Meteorol. Soc.*, 130, 1793-1814.

Janisková, M., J.-F. Mahfouf, J.-J. Morcrette and F. Chevallier, 2000: 'Development of linearized radiation and cloud schemes for the assimilation of cloud properties'. ECMWF Tech. Memo. 301

Janisková, M., J.-F. Mahfouf, J.-J. Morcrette and F. Chevallier, 2002: Linearized radiation and cloud schemes in the ECMWF model: Development and evaluation. *Q. J. R. Meteorol. Soc.*, **128**, 1505—1527.

Järvinen, H. and Undén, P., 1997: 'Observation screening and first guess quality control in the ECMWF 3D-Var data assimilation system'. ECMWF Tech. Memo. 236.

Järvinen, H, S Saarinen and P Undén, 1996: User's guide for blacklisting. 51pp. Available on request from ECMWF, Shinfield Park, RG2 9AX, Reading, Berkshire, England.

Järvinen, H., E. Andersson and F. Bouttier, 1999: Variational assimilation of time sequences of surface observations with serially correlated errors. submitted to *Tellus*, 28pp. also, RD Tech Memo no.266.

Kelly, G. and Pailleux, J., 1988: Use of satellite vertical sounder data in the ECMWF analysis system. ECMWF Tech. Memo. 143.

Kelly, G., Andersson, E., Hollingsworth, A., Lönnberg, P., Pailleux, J. and Zhang, Z., 1991: Quality control of operational physical retrievals of satellite sounding data. *Mon. Weather Rev.*, **119**, 1866–1880.

Klinker, E., F. Rabier, G. Kelly and J. F. Mahfouf, 2000: The ECMWF operational implementation of four-dimensional variational assimilation. Part I: experimental results and diagnostics with operational configuration. *Q. J. R. Meteorol. Soc.* **126**, 1191—1215.



- Köpken, C., G. Kelly, and J.-N. Thépaut, 2004:* Assimilation of METEOSAT radiance data within the 4D-Var system at ECMWF. Part II. *Q. J. R. Meteorol. Soc.*, (To appear July 2004).
- Leidner, S. M., Hofman, R. N. and Augenbaum, J., 1999:* SeaWinds Scatterometer Real-Time BUFR Geophysical Data Product User's Guide Version 1.0, available from ECMWF and AER
- Leidner, S. M., R.N. Hoffman and J. Augenbaum, 2000:* SeaWinds Scatterometer Real-Time BUFR Geophysical Data Product, User's Guide Version 2.3.0, NOAA/NESDIS.
- Leidner, S. M, Isaksen, L, and R. N. Hoffman, 2003:* Impact of NSCAT winds on tropical cyclones in the ECMWF 4D-Var assimilation system, *Mon. Wea. Rev.*, **131**, In press.
- Lönnberg, P, 1989:* Developments in the ECMWF analysis system. ECMWF Seminar on Data assimilation and the use of satellite data. 5-9 September 1988, 75-119.
- Lönnberg, P. and Hollingsworth, A., 1986:* The statistical structure of short-range forecast errors as determined from radiosonde data. Part II: The covariance of height and wind errors. *Tellus*, **38A**, 137–161.
- Lönnberg, P and D Shaw, 1985:* Data selection and quality control in the ECMWF analysis system. ECMWF Workshop on The Use And Quality Control of Meteorological Observations, 6-9 November 1984, 225-254.
- Lönnberg, P and D Shaw (Eds.), 1987:* ECMWF Data Assimilation Scientific Documentation. Research Manual 1.
- Lorenc, A. C., 1986:* Analysis methods for numerical weather prediction. *Q. J. R. Meteorol. Soc.*, **112**, 1177–1194.
- Lorenc, A. C., 1988:* Optimal nonlinear objective analysis. *Q. J. R. Meteorol. Soc.*, **114**, 205–240.
- Lott, F. and Miller M.J., 1997 :* A new subgrid-scale orographic drag parametrization : its formulation and testing. *Q.J.R. Meteorol. Soc.*, **123**, 101-127.
- Louis, J.-F., 1979:* A parametric model of vertical eddy fluxes in the atmosphere. *Boundary-Layer Meteorol.*, **17**, 187–202.
- Louis, J.-F., Tiedtke, M. and Geleyn, J.-F., 1982:* 'A short history of the PBL parametrization at ECMWF'. Pp. 59–80 in Proc. ECMWF Workshop on Planetary boundary layer parameterization, Reading, 25–27 November, 1981
- Lynch, P., 1993:* Digital Filters for Numerical Weather Prediction. HIRLAM Technical Report No 10.
- Lynch, P., 1997:* The Dolph-Chebyshev Window: A Simple Optimal Filter. *Mon. Weather Rev.*, **125**, 655–660
- Machenhauer, B., 1977:* On the dynamics of gravity oscillations in a shallow water model, with application to normal mode initialization. *Contrib. Atmos. Phys.*, **50**, 253-271.
- McNally, A. P. and Vesperini, M., 1996:* Variational analysis of humidity information from TOVS radiances. *Q. J. R. Meteorol. Soc.*, **122**, 1521–1544.
- McNally, A.P., E. Andersson, G. Kelly and R. W. Saunders, 1999:* The use of raw TOVS/ATOVS radiances in the ECMWF 4D-Var assimilation system. *ECMWF Newsletter*, **83**, 2–7.
- McNally, A.P., and P.D. Watts, 2003:* A cloud detection algorithm for high spectral resolution infrared sounders. *Q. J. R. Meteorol. Soc.*, **129**, 3411–3423.
- Mahfouf, J.-F., 1991:* Analysis of soil moisture from near surface parameters : a feasibility study. *J. Appl. Meteor.*, **30**, 1534-1547
- Mahfouf, J.-F., Buizza, R., and Errico, R. M., 1997:* Strategy for including physical processes in the ECMWF data assimilation system. In Proceedings of the ECMWF Workshop on non-linear aspects of data assimilation, Shinfield

Park, Reading, RG2 9AX, 9–11 September 1996

Mahfouf, J.-F., 1999: Influence of physical processes on the tangent-linear approximation. *Tellus*, **51A**, 147-166

Mahfouf, J.-F., R. Buizza and R. M. Errico, 1997: 'Strategy for including physical processes in the ECMWF variational data assimilation system'. Pp. 595-632 in Proceedings of the ECMWF seminar on data assimilation, 2-6 September 1996

Mahfouf, J. F. and F. Rabier, 2000: The ECMWF operational implementation of four-dimensional variational assimilation. Part I: experimental results with improved physics. *Q. J. R. Meteorol. Soc.* **126**, 1171—1190.

Matricardi, M., Chevallier, F. and Tjemkes, S., 2001: An improved fast radiative transfer model for the assimilation of radiance observations. Tech. Memo. No 345, Available from ECMWF, Shinfield Park, Reading, Berkshire RG2 9AX, UK.

Mlawer, E, S. J. Taubman, P. D. Brown, M. Iano and S. A. Clough, 1997: Radiative transfer for inhomogeneous atmospheres: RRTM a validated correlated-k model for the longwave. *J. Geophys. Res.*, **102**, 16663-16682

Morcrette, J.-J., 1989: 'Description of the radiation scheme in the ECMWF operational weather forecast model'. ECMWF Tech. Memo. 165

Morcrette, J.-J., 1991: Radiation and cloud radiative properties in the ECMWF operational forecast model. *J. Geophys. Res.*, **96D**, 9121-9132

Morcrette, J.-J., 1998: 'Description of the radiation scheme in the ECMWF operational weather forecast model.' ECMWF Tech. Memo. 252

Morcrette, J.-J., 2000: On the effects of the temporal and spatial sampling of radiation fields on the ECMWF forecasts and analyses. *Mon. Weather Rev.*, **128**, 876-887

Munro, R., C. Köpken, G. Kelly, J.-N. Thépaut, and R. Saunders, 2004: Assimilation of METEOSAT radiance data within the 4D-Var system at ECMWF, Part I. *Q. J. R. Meteorol. Soc.*, To appear July 2004.

Pailleux, J., 1990: 'A global variational assimilation scheme and its application for using TOVS radiances'. Pp. 325–328 in Proc. WMO International Symposium on Assimilation of observations in meteorology and oceanography", Clermont-Ferrand, France

Parrish, D. F. and Derber, J. C., 1992: The National Meteorological Center's spectral statistical interpolation analysis system. *Mon. Weather Rev.*, **120**, 1747–1763.

Portabella, M., and A. Stoffelen, 2000: Quality control and wind retrieval for SeaWinds. *Scientific report WR-2002-01*, Koninklijk Nederlands Meteorologisch Instituut, The Netherlands.

Rabier, F. and McNally, A., 1993: 'Evaluation of forecast error covariance matrix'. ECMWF Tech. Memo. 195.

Rabier, F., McNally, A., Andersson, E., Courtier, P., Undén, P., Eyre, J., Hollingsworth, A. and Bouttier, F., 1998: The ECMWF implementation of three dimensional variational assimilation (3D-Var). II: Structure functions. To appear in *Q. J. R. Meteorol. Soc.*

Rabier, F., Mahfouf, J.-F., Fisher, M., Järvinen, H., Simmons, A., Andersson, E., Bouttier, F., Courtier, P., Hamrud, M., Haseler, J., Hollingsworth, A., Isaksen, L., Klinker, E., Saarinen, S., Temperton, C., Thépaut, J.-N., Undén, P., and Vasiljevic, D., 1997a: Recent experimentation on 4D-Var and first results from a simplified Kalman filter. ECMWF Tech. Memo. 240.

Rabier, F., Thépaut, J.-N. and Courtier, P., 1997b: Four-dimensional variational assimilation at ECMWF. In Pro-

ceedings of the ECMWF Seminar on data assimilation, Shinfield Park, Reading, RG2 9AX, September 1996.

Rabier, F. and Courtier, P., 1992: Four-dimensional assimilation in the presence of baroclinic instability. *Q. J. R. Meteorol. Soc.*, **118**, 649–672.

Rabier, F., H. Järvinen, E. Klinker, J.F. Mahfouf and A. Simmons, 2000: The ECMWF operational implementation of four-dimensional variational assimilation. Part I: experimental results with simplified physics. *Q. J. R. Meteorol. Soc.* **126**, 1143–1170.

Saunders, R. W. and Matricardi, M., 1998: ‘A fast forward model for ATOVS (RTATOV)’. Tech. Proc. 9th International TOVS Study Conf., Igls, Austria, 20–26 February, 1997. 11 pp.

Savijärvi, H., 1995: Error growth in a large numerical forecast system. *Mon. Wea. Rev.*, **123**, 212–221.

Simmons, A. J. and Burridge, D., 1981: An energy and angular momentum conserving vertical finite difference scheme and hybrid coordinate. *Mon. Weather Rev.*, **109**, 758–766.

Simmons, A. J. and Chen, J., 1991: The calculation of geopotential and the pressure gradient in the ECMWF atmospheric model: Influence on the simulation of the polar atmosphere and on temperature analyses. *Q. J. R. Meteorol. Soc.*, **117**, 29–58.

Sherlock, V. J., 1999: ISEM-6: Infrared Surface Emissivity Model for RRTOV-6. Forecasting Research Technical Report No 299, Available from Met Office, London Road, Bracknell, Berkshire RG12 2SZ, UK

Slingo, J. M., 1997: The development and verification of the cloud prediction scheme in the ECMWF model. *Q. J. R. Meteorol. Soc.*, **113**, 899-927

Smith, E. A. and L. Shi, 1992: Surface forcing of the infrared cooling profile over the Tibetan plateau. Part I: Influence of relative longwave radiative heating at high altitude. *J. Atmos. Sci.*, **49**, 805-822

Stoffelen, A. 1999: Scatterometry. PhD Thesis, available from KNMI

Stoffelen, A. and Anderson, D., 1997: Ambiguity removal and assimilation of scatterometer data. *Q. J. R. Meteorol. Soc.*, **123**, 491–518.

Talagrand, O., 1997: Assimilation of observations, an Introduction. *J. Meteorol. Soc. Japan*, Vol 75, N.1B,191—209.

Temperton, C., 1988: Implicit normal mode initialization. *Mon. Weather Rev.*, **116**, 1013-1031.

Temperton, C., 1989: Implicit normal mode initialization for spectral models. *Mon. Weather Rev.*, **117**, 436-451.

Thépaut, J.N. and E. Andersson, 2003: Assimilation of high-resolution satellite data. *ECMWF Newsletter*, **97**, 6—12.

Tiedtke, M., 1989 : A comprehensive massflux scheme for cumulus parametrization in large-scale models. *Mon. Weather Rev.*, **117**, 1779–1800.

Tiedtke, M., 1993: Representation of clouds in large-scale models. *Mon. Weather Rev.*, **121**, 3040-3061

Tiedtke, M., 1996: An extension of cloud-radiation parametrization in the ECMWF model: The representation of subgrid-scale variations of optical depth. *Mon. Weather Rev.*, **124**, 745-750

Tomassini, M., LeMeur, D. and Saunders, R., 1997: Satellite wind observations of hurricanes and their impact on NWP model analyses and forecasts. To appear in *Mon. Weather Rev.*

Trémolet, Y., 2003: Model error in variational data assimilation. Proc. ECMWF Seminar on “Recent Developments in Data Assimilation for Atmosphere and Ocean”, 8—12 Sept 2003, Reading, U.K., 361—367.

Trémolet, Y., 2004: Diagnostics of linear and incremental approximations in 4D-Var. *Q. J. R. Meteorol. Soc.* **130**, (in press)

Uppala, S.M., and Co-authors, 2005: The ERA-40 re-analysis. *Q. J. R. Meteorol. Soc.* **131**, (in press)

Vasiljevic, D., Cardinali, C. and Undén, P., 1992: 'ECMWF 3D-Variational assimilation of conventional observations'. In Proc. ECMWF workshop on Variational assimilation with emphasis on three-dimensional aspects. Reading, 9–12 November 1992.

Veerse, F. and J.N. Thépaut, 1998: Multiple-truncation incremental approach for four-dimensional variational data assimilation. *Q. J. R. Meteorol. Soc.* 124, 1889-1908

Wergen, W., 1987: Diabatic nonlinear normal mode initialisation for a spectral model with a hybrid vertical coordinate. ECMWF Tech. Report 59.



